THE EFFECT OF SHEARING IN THE MELT ON THE MORPHOLOGY AND MECHANICAL BEHAVIOUR OF KRATON 1101

A

THESIS

BY

A.G. DICKSON

DEPARTMENT OF CHEMICAL ENGINEERING - McGILL UNIVERSITY
UNDER SUPERVISION OF DR. J.M. CHARRIER

SUBMITTED TO THE FACULTY OF GRADUATE STUDIES
AND RESEARCH OF McGILL UNIVERSITY IN PARTIAL
FULFILMENT OF THE REQUIREMENTS FOR THE DEGREE OF
MASTER OF ENGINEERING

McGILL UNIVERSITY JANUARY 1972

M. Eng. Chemical Engineering

Alex Dickson

EFFECT ON SHEARING IN THE MELT ON THE MECHANICAL BEHAVIOUR AND MORPHOLOGY OF KRATON 1101

ABSTRACT

Kraton 1101 is a polystyrene-polybutadiene-polystyrene copolymer. Polystyrene and polybutadiene blocks are incompatible and separate into two phases. In solvent cast or compression molded material the polystyrene is in the form of spheres approximately 250 A in diameter in a matrix of polybutadiene. Kraton 1101 behaves as an elastomer at room temperature, yet, because it is not crosslinked it can be "melted" and processed like a thermoplastic.

In this work the effect of shearing in the melt on the shape and size of the polystyrene domains in Kraton 1101 was investigated. The morphology of the samples was studied using low angle X-ray scattering and electron microscopy. Shearing was found to change the shape of the polystyrene domains from spheres to long cylinders, and created a marked anisotropy in the mechanical behaviour. A model was developed to represent the initial Young's modulus of molded and sheared Kraton 1101.

ACKNOWLEDGEMENTS

The author wishes to express his gratitude to the following people who made completion of this work possible:

To his director, Dr. J.M. Charrier, for his assistance and guidance on this project.

To Dr. R. St. John Manley for the use of his low angle X-ray camera, and to Mike Cooper for his help with the same.

To Dr. N.V. Hien and Mark Firth for their help in obtaining the electron microscope pictures.

To Andy Krish and his staff for their help in the design and construction of the experimental apparatus.

To Shell Canada Ltd. for supplying the Kraton 1101 used in the experiments.

To his wife Jane for her aid and moral support.

TABLE OF CONTENTS

LIST OF ILLUSTRATIONS

LIST OF TABLES

I. INTRODUCTION

Thermoplastic elastomers are a new and unique class of materials which combine the end use properties of vulcanized rubbers and the processing advantages of thermoplastics. The relationship of these materials to existing plastics is shown on Figure 1. The Figure also compares the stress-strain properties of natural rubber vulcanizates and Kraton 1101, a typical thermoplastic elastomer. These new materials are truly elastomeric in behaviour.

Before discussing the structure of thermoplastic elastomers a brief discussion of rubber elasticity as we normally think of it is in order. Treloar (1) gives the following three conditions for the occurrence of rubber elasticity:

1. long chain molecules possessing freely rotating links,
2. weak secondary forces between molecules permitting random rotation, and
3. an interlocking of the molecules at a few places along their length to form a three dimensional structure.

The fundamental concept of the theory of rubber elasticity is based on the tendency of a chain to take up a random configuration which has the maximum possible entropy. By pulling on a

	THERMO-SETTING	THERMO-PLASTICS
RIGID	epoxies	polystyrene
FLEXIBLE	highly vulcanized rubber	polyethylene
RUBBERY	vulcanized rubber	

thermoplastic elastomers

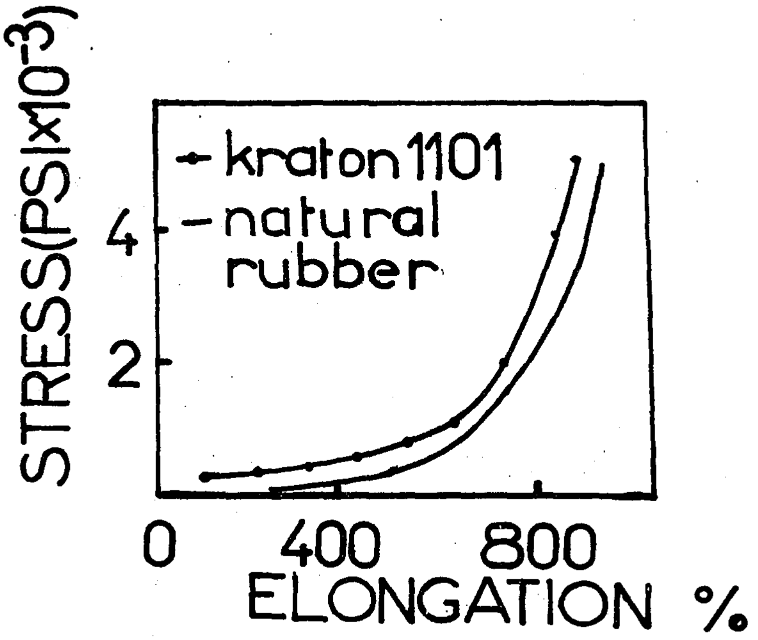

FIGURE 1-RELATIONSHIP OF THERMOPLASTIC ELASTOMERS TO OTHER PLASTICS

rubber a restoring force that is entropic in origin is created. The crosslinks serve to stop the molecules from slipping past one another and to transmit the force. Even uncrosslinked (unvulcanized) rubber shows a considerable degree of elasticity due to physical entanglements of the chains. However, prolonged stressing in this causes flow.

Raw rubber, for example natural rubber or polyisoprene, is vulcanized with sulphur or a peroxide at a temperature of about 150°C and under pressure in a **mold**. The process is continued until the required degree of crosslinking is attained. This vulcanization step is eliminated with thermoplastic elastomers which can be processed in extruders and injection molding equipment.

How can these thermoplastic elastomers behave like crosslinked rubber although they are not vulcanized, and have flow properties similar to thermoplastics? The answer lies in the molecular structure. Thermoplastic elastomers are tri-block copolymers with two terminal blocks that are in the glassy state at room temperature and a middle block in the rubbery state. For example the rubbery block could be polybutadiene with a glass transition at about -70°C, while the glassy blocks might be polystyrene with a glass transition at about 100°C. In the rest of the text polystyrene will be referred to as PS, polybutadiene as PB, and polystyrene-polybutadiene-polystyrene tri-block copolymers as S-B-S block copolymers.

The advent of anionic polymerization techniques made possible the preparation of S-B-S block copolymers. Zelinski and Childers (2) describe how the polymerization can be carried out. Organic derivatives of lithium or sodium are used as initiators, and sequence addition of the different monomers is used to make up the blocks.

Most polymers are incompatible with one another and if two homopolymers are mixed together they will separate into two phases, Bohn (3). Molecular mixing is only possible for a few polymers. Compatibility is improved by decreasing molecular weight, dilution with solvents, and increasing temperature.

This incompatibility is also present in block copolymers. Kraus et al (4) have studied the dynamic mechanical properties and glass transition temperatures of random and block copolymers. Random copolymers exhibit one glass transition temperature intermediate between the two homopolymers composing it. Block copolymers show a glass transition temperature for each of the blocks. This indicates that similar blocks are associated in homogeneous regions. Direct electron microscope examination has proved this to be the case. Morton et al (5) and Beecher et al (6) have shown that the PS blocks in S-B-S block copolymers form roughly spherical domains from 100 to 400 angstroms in diameter depending on the molecular weight of the PS block. The PB block forms a continuous rubbery matrix still attached to the glassy domains of PS.

These glassy domains behave as the crosslinks in the vulcanized rubber. They also act as fillers in raising the stress values and ultimate strength. When the temperature is raised, however, the glassy blocks gradually soften permitting flow above their glass transition temperature.

Charrier and Ranchoux (7) studied the effects of shearing above the glass transition temperature of PS on an S-B-S block copolymer. The materials they used were Kraton 1101 which has block molecular weights PS(11,000), PB(53,000), and PS(11,000), and Kraton 3226 which is Kraton 1101 with about 30% plasticizer and other ingredients. They found that by shearing both Kraton 1101 and Kraton 3226 could be made highly anisotropic. Mechanical testing in simple tension of sheared samples gave stress values 1.5 times greater in the direction of flow than stress values at the same extension in the direction perpendicular to the flow. Low angle X-ray scattering showed that the anisotropy was due to an orientation of the glassy domains of polystyrene in the flow direction.

Charrier and Ranchoux (7) carried out a systematic study of the effect of shearing on Kraton 3226, but only preliminary experiments were done using Kraton 1101. This work is a continuation of their preliminary study. Four steps are involved.

1. Determination of the mechanical properties of compression molded Kraton 1101.
2. Design of an apparatus to shear Kraton 1101 above the glass transition temperature of PS.
3. Detailed determination of the stress-strain properties of the sheared material with an Instron tester.
4. Investigation of the morphology of the sheared material using low angle X-ray scattering and electron microscopy.

A knowledge of the relationships between processing parameters, resulting morphology, and mechanical behaviour can be very useful. It can permit, by controlling the processing of the material, the obtaining of the desired morphology and mechanical properties in the product.

The literature survey which follows discusses the morphology of compression molded and cast films of S-B-S block copolymers. The resulting mechanical behaviour of these materials has been the object of many studies and a few are reported. Finally an outline of the research done up until now on the flow behaviour of S-B-S block copolymers and the effects of this flow on the structure and properties is given. Wherever possible results from studies using Kraton 1101 are reported since it was the copolymer used in this work.

II. LITERATURE SURVEY

1. Morphology of S-B-S Block Copolymers

S-B-S block copolymers form two phase structures. The middle block phase forms a continuous rubbery matrix, and the dispersed end block phase serves as junction points. The evidence for this structure is experimental and theoretical.

Many workers have studied the morphology of solvent cast and compression molded Kraton 1101. Beecher et al (6) studied compression molded sheets and films cast from two solvent systems. These were 90% THF/10% MEK and 90% benzene/10% heptane. Samples from films cast from THF/MEK yielded and necked in a small region which grew until the specimen was uniform; deformation then proceeded homogeneously. Samples from films cast from benzene/heptane showed no evidence of necking. Compression molded samples showed no yield point, but were otherwise similar to THF/MEK cast films.

The yielding and necking of THF/MEK cast films indicated that a continuous PS structure had been destroyed by the deformation. This interconnected PS network was formed because of the solvents used. The THF, a better solvent for the PB, evaporates first. PS domains are left swollen with MEK and more easily in contact with each other. As the MEK evaporates thin paths of PS remain to interconnect the PS domains. If destroyed by deformation the interconnections could be reformed by annealing at a temperature close to the glass transition temperature of PS.

Electron micrographs of thin cast films in the study showed that the PS aggregated into domains 120 ± 20A in diameter. THF/MEK cast films showed an interconnected structure in roughly cubic arrangement. Compression molded samples had the same structure with fewer interconnections. Films cast from benzene/heptane had almost no ties between the spheres of PS.

Miyamoto et al (8) obtained electron micrographs of an S-B-S block copolymer with 30% by weight PS and a PS block molecular weight of 15,000. They found more complicated structures in cast films than Beecher et al observed. Ethyl acetate and MEK cast films had a continuous phase consisting of a mixture of PS and PB, and a discrete phase of dispersed islands of PB ranging in size from 500 to 3000A. Films cast from toluene and carbon tetrachloride had large islands about one micron in diameter composed of PS and PB which were separated by canals of PB. In the islands PB was the dispersed phase. The dynamic mechanical behaviour of these two structures was quite different, but it could be made more similar if the samples were annealed for 6 hours at 120°C.

This indicates that the morphology can change to a more favoured structure if the temperature is above the glass transition of the polystyrene. This effect will be studied more in the first part of this work to see if annealing can affect the stress-strain properties of compression molded Kraton 1101.

Low angle X-ray scattering confirms this two phase morphology. Brown et al (9) obtained low angle X-ray scattering data from toluene cast samples of Kraton 1101. The scattering was consistent with a primitive cubic lattice of PS spheres. The diameter of these spheres was 240Å, and the minimum inter-domain distance between the boundaries of the PS domains was 65Å.

McIntyre et al (10) studied scattering from an S-B-S block copolymer with block molecular weights of 21,000, 63,000 and 21,000. Samples were cast from THF/MEK mixtures (90%/10%). Their scattering was most easily reconciled with a face centered orthorhombic structure. From the low angle X-ray scattering data the diameter of the PS domains was calculated as 356Å and the three unit cell distances as 676, 676 and 566Å. These dimensions gave a PS volume percent of 36,which agrees with the stoichiometric value calculated from the block molecular weights. The minimum interdomain distance between the boundaries of the domains was 54Å. Fischer (11) examined another S-B-S block copolymer with 36% by volume PS.

His samples were cast from toluene. Using electron micrographs of thin cast films he found a hexagonal arrangement of PS spheres 300A in diameter. The minimum interdomain distance between the boundaries of the domains was 200A. The periodicity found by low angle X-ray scattering was 530A which agrees well with the 500A center to center distance between domains found by electron microscopy.

The experimental data presented above show that the morphology of S-B-S block copolymers depends greatly on the type of preparation and the molecular weights of the blocks. For Kraton 1101 the domain sizes found vary from 100 to 240A. However, what is important is that the domains of compression molded or solvent cast Kraton 1101 are spherical in shape. Theoretical models which have been proposed predict a domain size in good agreement with the experimental findings.

The simplest way to estimate the domain sizes and interdomain distances is to assume that in each phase the molecules will assume their unperturbed dimensions. Then, as described by Fedors (12), the root-mean-square end-to-end distance of the polymer chains $(\overline{r_o^2})^{\frac{1}{2}}$ may be used as a measure of the size of the randomly coiled segment. For PS, $(\overline{r_o^2})^{\frac{1}{2}} = 0.65 M_{PS}^{\frac{1}{2}}$ Å and for PB, $(\overline{r_o^2})^{\frac{1}{2}} = M_{PB}^{\frac{1}{2}}$ Å(12). It has been demonstrated by Flory (13) that for a randomly coiled molecule chain segments extend over dimensions about twice $(\overline{r_o^2})^{\frac{1}{2}}$. Hence the diameter of a randomly coiled molecule is $2(\overline{r_o^2})^{\frac{1}{2}}$ and the diameter of a spherical domain should be $4(\overline{r_o^2})^{\frac{1}{2}}$. Therefore the diameter of a PS domain in Kraton 1101 with a block molecule weight 11,000 should be approximately 300Å. This value agrees closely with the experimental values. For Kraton 1101 the molecular weight of the PB block is 53,000 and from the above formula the $(\overline{r_o^2})^{\frac{1}{2}}$ for PB is 230Å. Experimentally it was found (9,10) that the minimum interdomain distance between the boundaries of the PS domains was about 60Å. This must mean that some PB chains are attached to domains further away than nearest neighbours.

Meier (14) has proposed a model based on thermodynamic arguments to predict the diameter of spherical domains in two block copolymers as a function of molecular weight and temperature. He considers each of the blocks are the same molecular weight. Random flight statistics are assumed applicable with chain perturbations allowed for by the chain expansion parameter α (13). The radius of the domains is given by the following expression:

$$R_S = \frac{4}{3} \cdot K \cdot M_{PS}^{\frac{1}{2}} \cdot \alpha \qquad \ldots\ldots\ldots\ldots\ldots\ldots(1)$$

$$\alpha^3 - \alpha = 3 \cdot M_{PS}^{\frac{1}{2}} \cdot \gamma/(K \cdot k \cdot A \cdot T) \qquad \ldots\ldots\ldots(2)$$

Here M_{PS} is the molecular weight of the PS, A is Avogadro's number, κ is Boltzmann's constant, γ is the interfacial energy, T is the absolute temperature and K is the constant in the relationship $(\overline{r_o^2})^{\frac{1}{2}} = K\ M_{PS}^{\frac{1}{2}}$.

Bianchi et al (15) derived a theoretical expression for the domain radius of an S-B-S block copolymer. Their approach is based on minimizing the free energy change from complete mixing of the blocks to a two phase system of spherical domains. The resulting equation for the radius of the PS domains is:

$$R_S = M_{PS}\ \gamma/(\rho\ RT) \qquad \dots\dots\dots\dots\dots\dots\dots(3)$$

ρ is the density of PS and the rest of the symbols have the same meaning as before.

Equations 1 and 3 are plotted on Figure 2 as a function of temperature. The plots are for Kraton 1101 using a molecular weight of 11,000 and an interfacial energy of 3 dyne/cm estimated by Bianchi et al. Both theories predict a domain diameter of approximately 280A at 25°C, and predict that the domain radius should decrease with temperature.

Based on the theoretical calculations the domain diameter of PS in Kraton 1101 is **likely** about 240Å as given by Brown et al (9). The values obtained by Beecher et al (6)

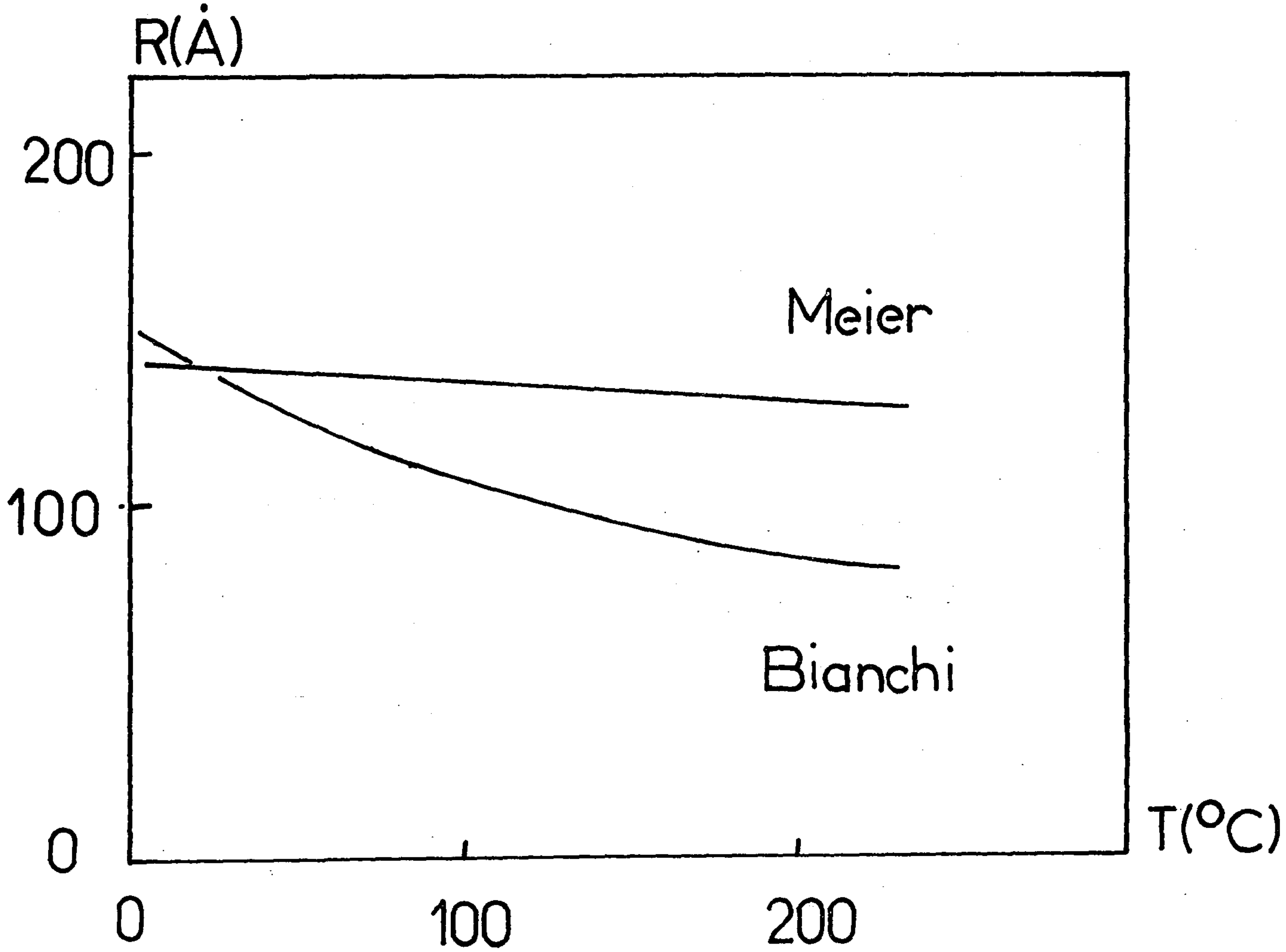

FIGURE 2 -THEORETICAL DOMAIN RADIUS IN KRATON 1101

using electron microscopy of thin cast films probably do not represent bulk values. The experimental values of the domain radius are lower than the theoretical predictions because of the presence of some connections between domains.

2. Mechanical Behaviour of S-B-S Block Copolymers

The mechanical behaviour of S-B-S block copolymers is interesting in its own right, but this behaviour can also yield information about the structure and mechanisms of deformation of these materials. Many workers have taken this approach.

First let us examine what block sizes could be expected to give useful mechanical properties. Fedors (12) has done this. The lower the molecular weight of the polymer the easier the processability of the melt. However, the molecular weight must be high enough for the PS to give a reasonably high glass transition temperature, T_g, for good mechanical properties in the solid state. For PS the T_g increases from 75 to 89°C as the molecular weight increases from 5000 to 12,000, but very little after that. Accordingly 12,000 is a good molecular weight for the PS block. Fedor calculates that a 1% strain could decrease the glass transition temperature of the PS block by 8°C, and that with actual strains the T_g could decrease by up to 30°C. Thus Fedors predicts that S-B-S elastomers would have good properties up to 60°C. As we shall see this is the case.

Studies on filled rubbers have shown that the optimum filler volume fraction is 0.25 (12). From this Fedors calculates the optimum PB molecular weight as 83,000. These block molecular weights of 12,000, 83,000 and 12,000 are very similar to Kraton 1101.

Morton (5) demonstrated that, provided that it is not too small, block size does not influence the stress-strain behaviour of S-B-S block copolymers. What matters is the volume fraction of PS; thus samples with PS block molecular weights of 13,000 and 20,000 and the same volume fraction of PS have identical stress-strain curves. Because changes in PB molecular weight at constant volume fraction PS do not change the stress-strain curve either, Morton concludes that the centre block molecular weight cannot be considered as the "molecular weight between crosslinks of the kinetic theory of rubber elasticity" (1).

Brunwin et al (16) investigated the effect of temperature on the physical crosslinks in S-B-S block copolymers. They found the network was stable up to about 60°C. The stress-stiffening or upturn in the stress-strain curve (see Figure 1) below this temperature is due to the finite extensibility of the PB chains. These chains fully extend because of the high viscous forces opposing the motion of the glassy

PS regions. With increasing temperature the PS segments become more mobile and stress values at the same elongation become lower. Above 60°C the domains soften and flow, and no upturn occurs in the stress-strain curve. This effect of temperature on the stress is opposite to that observed for vulcanized rubbers (1). For vulcanized rubbers a temperature rise causes an increase in the segmental motion which in turn causes an increase in the restoring force.

Brunwin et al found that samples stressed below the glass transition temperature of the PS undergo some stress softening, but they recover completely if placed in boiling water. They concluded from this that the PS domains deformed but did not flow during deformation, and that recovery at room temperature was only slowed by hindered segmental motion of the PS segments. Beecher et al (6) followed the behaviour of PS domains by observing them under the electron microscope. They cast thin films of Kraton 1101 on water and stretched them using a pair of dividers. Examination of films stretched to various degrees showed that first the interdomains connections of PS that were oriented in the direction of stretching ruptured. This left strings of interconnected PS spheres aligned perpendicular to the force. With higher elongation these rows became V shaped patterns and the domains separated from each other to become ellipsoids. These ellipsoids remained much the same from an elongation of 200% to 800%, but at higher elongations again deformed. Failure always occurred by a gross deformation of the PS domains. Beecher et al confirmed by electron microscopy that broken interconnections could be reformed by annealing above the glass transition temperature of the PS.

The domains of PS were found to be very deformable by Beecher et al (6). They explained this by postulating a transition zone between the PB and the PS. The evidence for this was a third transition temperature for Kraton 1101, midway between the glass transition temperatures of the two homopolymers. This transition phase is likely softer than the PS and permits the domains to deform easily and reform upon heating. It is this transition zone which is affected most by increases in temperature and responsible for the effects found by Brunwin et al.(16).

Smith and Dickie (17) studied the viscoelastic properties of compression molded Kraton 1101. They obtained isochronal one minute stress-strain curves (i.e. the stress read after one minute for various elongations). These isochrones were obtained from -40 to 40°C, and time temperature superposition was successfully accomplished. The shift factor was found to vary linearly with temperature, and was independent of extension from an extension ratio of 1.2 to 5. Smith and Dickie suggest this linear behaviour of the shift factor, log a_T, with temperature as indicative of the influence of the glassy domains. They give the following figures to support this:

Kraton 1101 $\frac{d \log a_T}{dT} = -0.116$ from -40 to $40^{\circ}C$ (4)

Polystyrene $\frac{d \log a_T}{dT} = -0.11$ 50 to $80^{\circ}C$ (5)

Polybutadiene (Crosslinked) $\frac{d \log a_T}{dT} = 0.004$ -30 to $60^{\circ}C$ (6)

From these figures they conclude that the PB in Kraton 1101 acts in an elastic manner and does not affect the viscoelastic behaviour of the material from -40 to $40^{\circ}C$. This is in agreement with the electron microscope studies by Beecher et al (6), and the effect of temperature on the stress-strain curves found by Brunwin et al (16).

Shen and Kaelble (18) studied the viscoelastic behaviour of Kraton 1101 over a wider range of temperature. They found that the shift factor is predicted well by one WLF equation at low temperatures and another at high temperatures. In between, from -60 to $60^{\circ}C$, the shift factor was found to vary linearly with temperature, as found by Smith and Dickie. Shen and Kaelble conclude that the viscoelastic behaviour is dominated by PS at high temperatures and by PB at low temperature. In between the response is governed by an interfacial region. Smith and Dickie's results indicate that this region is very similar in its response to PS.

3. Flow Behaviour of S-B-S Block Copolymers in the Molten State

The picture developed up until now shows a two phase structure, with the size and arrangement of the PS regions depending on the method of preparation. The PS domains have been shown to be easily deformed by elongating the solid material. Connections between domains that broke upon stretching could easily be reformed by heating.

Flow of these S-B-S block copolymers in the melt would then be expected to have a great effect on the domains' structure, and therefore on the physical properties of the solid material. Little work has been done however.

Arnold and Meier (19) studied the rheological behaviour of several S-B-S block copolymers. From their results they concluded that S-B-S had three types of behaviour depending on the shear rate. At low shear rates the three dimensional network of PB chains between PS domains persists. At intermediate shear rates some PS blocks are pulled from the domains, but aggregates of PS still remain. In this region the viscosity would be higher than that expected for molecules of the same molecular weight. This is because of the effects of aggregates of PS. Finally, at very high shear rates the aggregates themselves become disrupted, and the system behaves as an assemblage of individual molecules. Arnold and Meier found that this flow transition at high shear rates always occurred at a critical stress of 4.5×10^5 dynes/cm^2 independent of block size. Moreover the flow behaviour above the critical stress followed a power law behaviour similar to PS.

Holden et al (20) found the same flow transition at about 10^6 dynes/cm^2. They found the flow behaviour to be very temperature sensitive. This sensitivity can be described by the energy of activation of flow ΔE given by:

$$E = \frac{R\, d(\ell n\ \eta)}{d(1/T)} \qquad \text{............(7)}$$

where η is the viscosity at some constant shear stress, R is the gas constant, and T is the absolute temperature. For S-B-S block copolymers ΔE is not a constant. At high temperatures, 200°C, it approaches that of homopolybutadiene, 4.5 kcal/mole, and at low temperatures, 100°C it approaches the ΔE of homopolystyrene, 82 kcal/mole. Because ΔE is higher than for pure PB flow of S-B-S block copolymers probably requires flow of PS blocks in the domains and through the PB, as well as flow of the PB blocks.

The work discussed above indicates that flow disrupts the PS domains. But what happens when the stress is removed?

Erdhart et al (21) have done a very interesting study of a tri-block copolymer of polyethylene oxide, polystyrene, and polyethylene oxide. For these materials a Newtonian viscosity was observed at low shear rates. They sheared a sample at a high shear rate for one minute and then monitored the viscosity at a low shear rate where the viscosity was Newtonian. The viscosity increased with time (over 45 minutes) indicating a partial recovery of structure. However, the original viscosity (the Newtonian viscosity at low shear rates) was not reached. Erdhart et al propose this could be due to an irreversible chain scission. However, it could also have been due to a different shape of aggregate reformed after the shearing at high rates where the domain structure was disrupted. What happens to the PS domains in S-B-S block copolymers after shearing is the object of this work. Previous work done on this subject will be discussed in the next section.

4. Effects of Flow in the Molten State on the Solid State Morphology and Mechanical Behaviour of S-B-S Block Copolymers

In the last section we found that the domain structure can be altered by shearing in the melt. For polyethylene oxide, polystyrene, polyethylene oxide block copolymers there are indications that the domains reform once the shear stress is removed. Do the effects of shearing remain with S-B-S block copolymers once the shear stress is removed and the material is cooled?

Harpell and Wilkes (22) used an S-B-S block copolymer of 30% PS with a PS block molecular weight of 16,500. Films of the copolymer were cast from benzene solutions and milled in a rubber mill at 140°C. The milled material was annealed in a mold. Low angle X-ray scattering showed a definite orientation of the PS domains, and the scattering became more intense the better the annealing. The scattering was explainable by a morphology of long PS cylinders in a PB matrix. Annealing did not destroy this structure, but only purified the domains. Thus the morphology of benzene cast films (spheres of interconnected PS) has been permanently changed to rods of PS by shearing in the rubber mill.

They also found some other very interesting effects. Longer annealing times or higher temperatures reduced the interdomain distance. Annealing also caused a free sample to shrink in the milled direction and increase in thickness. This fact is consistent with annealing causing the domains to become smaller (purer) and at the same time closer together. The shrinkage could be caused by PB segments that were trapped in the PS domains becoming free and returning to a random coil. This picture explained the physical properties found. Torsional modulus increased as annealing progressed because of the purer domains, but the tensile stress decreased at high elongations because annealing reduced built-in stresses by freeing trapped PB chains.

Keller et al (23) studied low angle X-ray scattering from extruded rods of an S-B-S block copolymer with block molecular weights 10,000, 55,000 and 10,000. With the beam along the extrusion direction the scattering was a hexagonal array of spots, and with the beam perpendicular to the extrusion direction the scattering was oriented arcs. This meant that the structure was one of a hexagonal arrangement of PS cylinders in the extrusion direction. The cylinder diameter was calculated as 150A with a centre to centre distance between cylinders of 300A. This was later confirmed (24) by electron microscopy using low temperature ultra-microtomy to prepare samples. From the pictures, rods were clearly evident with a centre to centre distance from 270 to 320A, and a cylinder diameter of 130 to 170A. With this morphology of oriented cylinders of PS the sheared copolymer should be highly anisotropic.

Folkes and Keller (25) in a later work measured the initial Young's modulus along the extrusion direction (longitudinal direction), and perpendicular to the extrusion direction (transverse direction). At 23°C, the longitudinal modulus, El, was found to be 4.25×10^9 dynes/cm^2, and the transverse modulus, Et, was 4.65×10^7 dynes/cm^2. They show the two modulli can be calculated by the following relations (26):

$$El = Vs\ Es + (1 - Vs)\ Eb \qquad ....(8)$$

$$Et = 4/3\ Eb/(1 - Vs) \qquad ....(9)$$

The first formula is the parallel law for two phase materials, and the latter is the series law modified to take account to the fact that the PB phase is constrained in one direction by the PS rods. Vs is the volume fraction of the PS, Es is the modulus of PS, and Eb is the modulus of PB. Using a value for Es of 2×10^{10} dynes/cm^2 and a value for Eb of 2×10^7 dynes/cm^2, El was calculated as 4×10^9 dynes/cm^2 and Et as 3.25×10^7 dynes/cm^2. Both of these agree very well with the experimental values. The success of these formulas show that the PS cylinders can be regarded as infinitely long, at least from a mechanical viewpoint. The agreement was only this good for annealed samples. Unannealed samples had lower modulli in the longitudinal direction due to the presence of defect planes perpendicular to the cylinders. Annealing reduced the number of these defect planes.

Charrier and Ranchoux (7) sheared Kraton 1101. However, their material was sheared between parallel plates making samples much easier to obtain. They too found an anisotropic material, but the morphology appeared different from Keller's, i.e. X-ray scattering along the extrusion direction produced a ring, not spots. Perpendicular to the extrusion the scattering was similar to that found by Keller et al. They went further than Keller and showed that the anisotropy persisted at extension ratios up to 4.

III. EXPERIMENTAL APPARATUS AND TECHNIQUES

The experimental work can be divided into three parts:

1. preparation of samples,
2. mechanical testing of samples, and
3. determination of the morphology of samples.

Each part involves different techniques and apparatus.

1. Preparation of Samples

a) Annealing of Compression Molded Samples

To anneal samples,four small annealing molds were made. Mild steel was used to make them so that use would not mar the mold surfaces. The size of the cavity in the molds was approximately 2½ by 1 by 1/16 inches. The molds are shown in Figure 3. To facilitate the rate of heat transfer when the molds were cooled after annealing, slots were machined in the top and bottom sections of the molds.

The experimental procedure used in annealing samples was as follows. A 4 by 4 by 5/64 inch sheet of Kraton 1101 was compression molded between cellophane covered aluminum plates. A sandwich using a suitable spacer containing nodules of Kraton 1101 was first put in the press and left to heat for 10 minutes

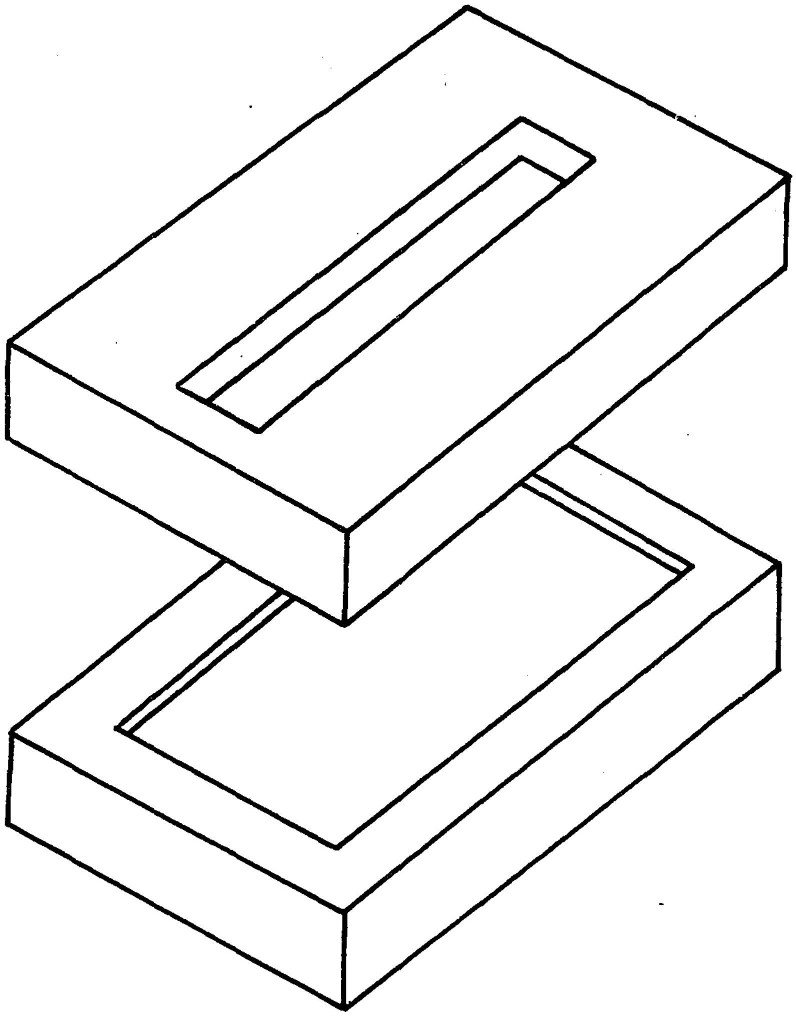

FIGURE 3 -ANNEALING MOLD

at 200°C. Pressure was then applied and finally cooling water was circulated in the platens of the press. The cellophane, when soaked with water, allowed easy removal of the Kraton 1101 from the mold. Four pieces could be cut from the compression molded sheet each just big enough to fit in the annealing molds. These were then remolded in the annealing molds. After cooling the two parts of each mold were fastened together using screws and taken to an oven for annealing at temperatures between 120 and 200°C. When the annealing was completed the annealing molds were either slowly cooled at ambient temperature or quenched rapidly by plunging them into liquid nitrogen.

b) Shearing Apparatus and Procedure

Two different types of shearing apparatus were used. For the first experiments the pressure flow device used by Charrier and Ranchoux (7) was modified and produced excellent sheared sheets. However, a parallel plate plastometer later designed also gave some very interesting results.

The pressure flow device is shown on Figure 4. It was designed to fit in an Instron environmental chamber for temperature control. Before the Kraton 1101 could be sheared an isotropic premolding had to be made which would fit snugly in the reservoir of the pressure flow device. A premold made

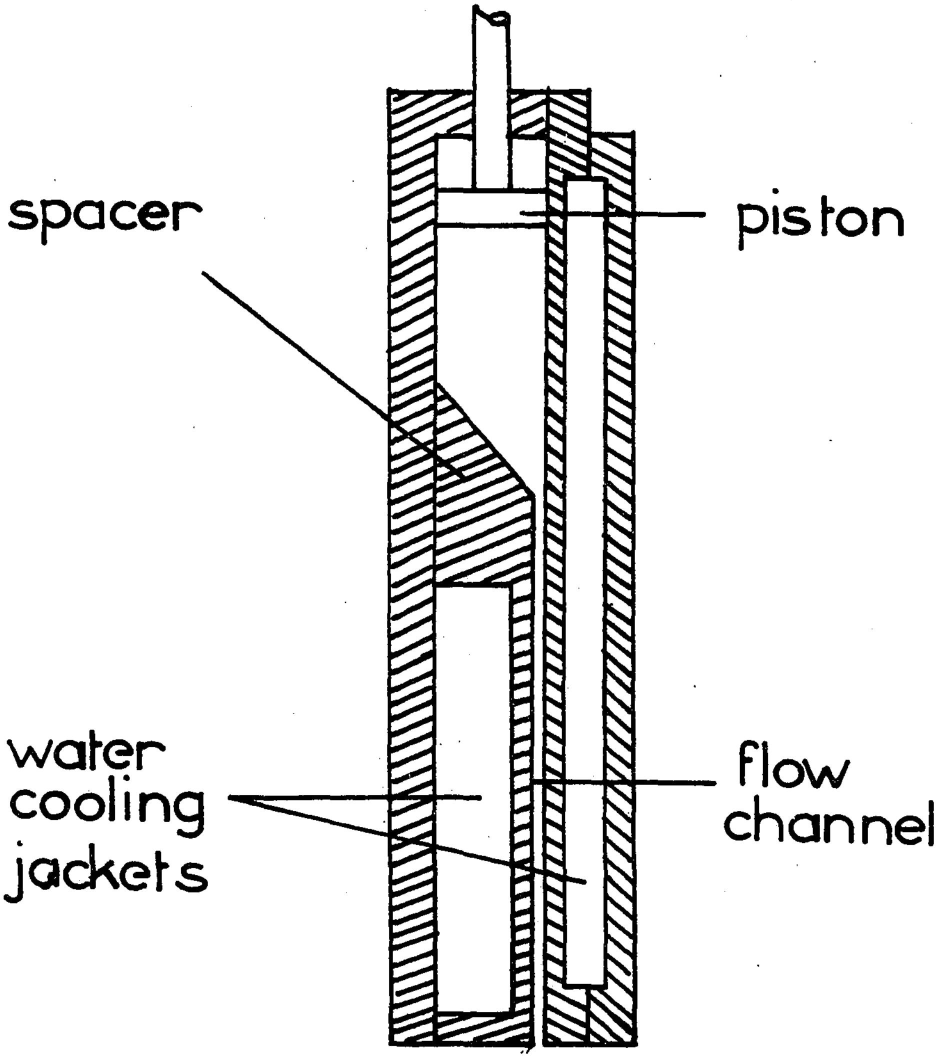

FIGURE 4-PRESSURE FLOW DEVICE

for this purpose is shown in Figure 5. Unprocessed Kraton was placed in the premold and heated under vacuum for one hour at 170°C, and then removed to a press. Here the piston of the premold was forced down and the nodules of Kraton were compressed together. The premolding was left to cool under pressure and then removed from the premold.

The premolding was placed in the pressure flow device and heated to 200°C. This took 3 hours. Shearing was then begun. As the piston of the pressure flow device moved down the molten premolding material was forced from the reservoir which is 1 inch deep through a 45 degree tapered section into a rectangular channel. The channel has a cross section 4 x 1/16 inches with a length of 4 inches. When the shearing experiment was completed water could be circulated in 2 cooling jackets. The pressure flow device was easy to dismantle, and the gap thickness could be adjusted by using spacers of varying thickness.

Charrier and Ranchoux experimented mainly with Kraton 3226 which is Kraton 1101 with 30% plasticizer and other ingredients. Since the pure material has a much higher viscosity than the modified Kraton, several modifications had to be made to the existing pressure flow device. The gas pressure system first used to move a floating piston proved unsuitable because the higher pressures required caused leakage around the piston.

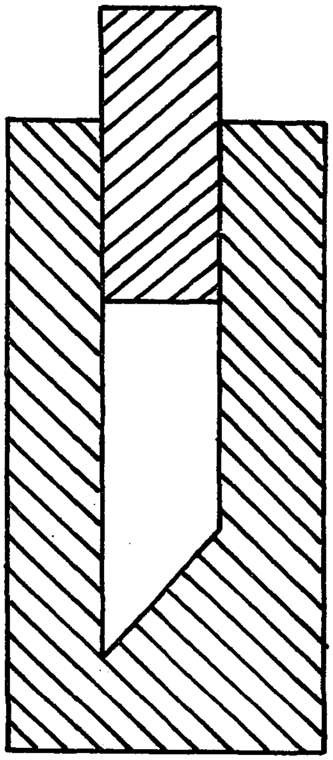

FIGURE 5 -PREMOLD

So a guided piston arrangement was built which could be driven using the Instron crosshead. See Figure 6. A support base and columns fastened the pressure flow device to the base of the Instron. Even with the guided piston the smallest gap that could be used was 5/64 inch otherwise the pressure and corresponding force became too high. Removal of the sheared sheets of Kraton 1101 from the device proved to be a real problem. After being subjected to heat and pressure during shearing the Kraton 1101 stuck tenaciously to the aluminum plates of the pressure flow device. Any stress applied to the sheared sheet while removing it would have made measurement of the initial modulus meaningless. Silicon mold release did not help much, and neither did polishing the flow surfaces of the device. The best solution was to bond Teflon to the surfaces. A 1/64 inch sheet of Teflon stayed in place very well.

The parallel plate plastometer is shown on Figure 7. It was also designed to be used in the Instron environmental chamber, and uses the same support base as the pressure flow device. The apparatus was used in the following manner; a sample of Kraton 2 by 2 by 1/8 inches was placed in the centre, and heated to 200°C. The top plate was then moved down at a constant speed and the sample of Kraton 1101 was sheared into a sheet 2 by 4 by 1/16 inches. From Figure 7 it can be seen that the flow is constrained in one direction by the channel.

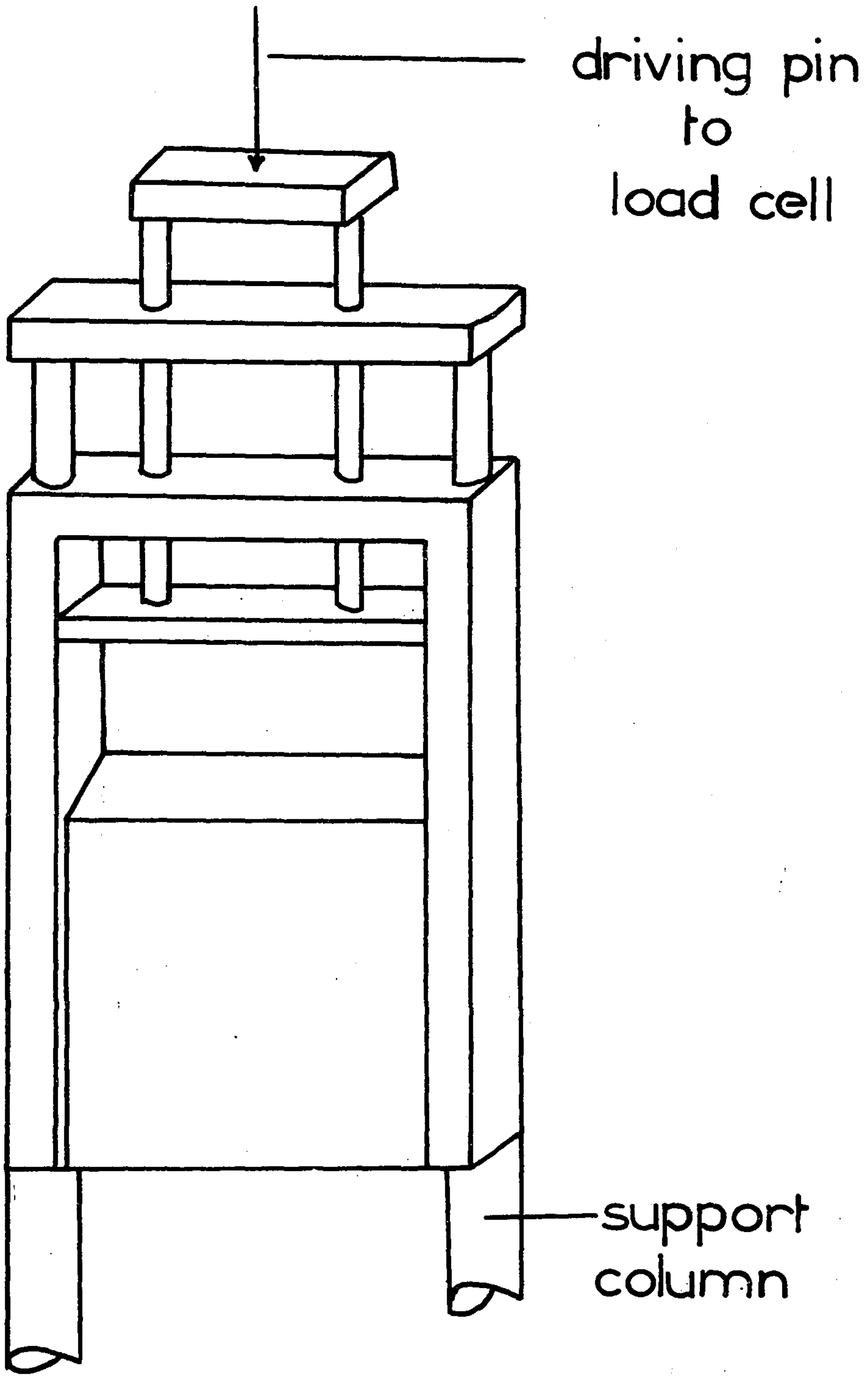

FIGURE 6 - PISTON GUIDE AND SUPPORT

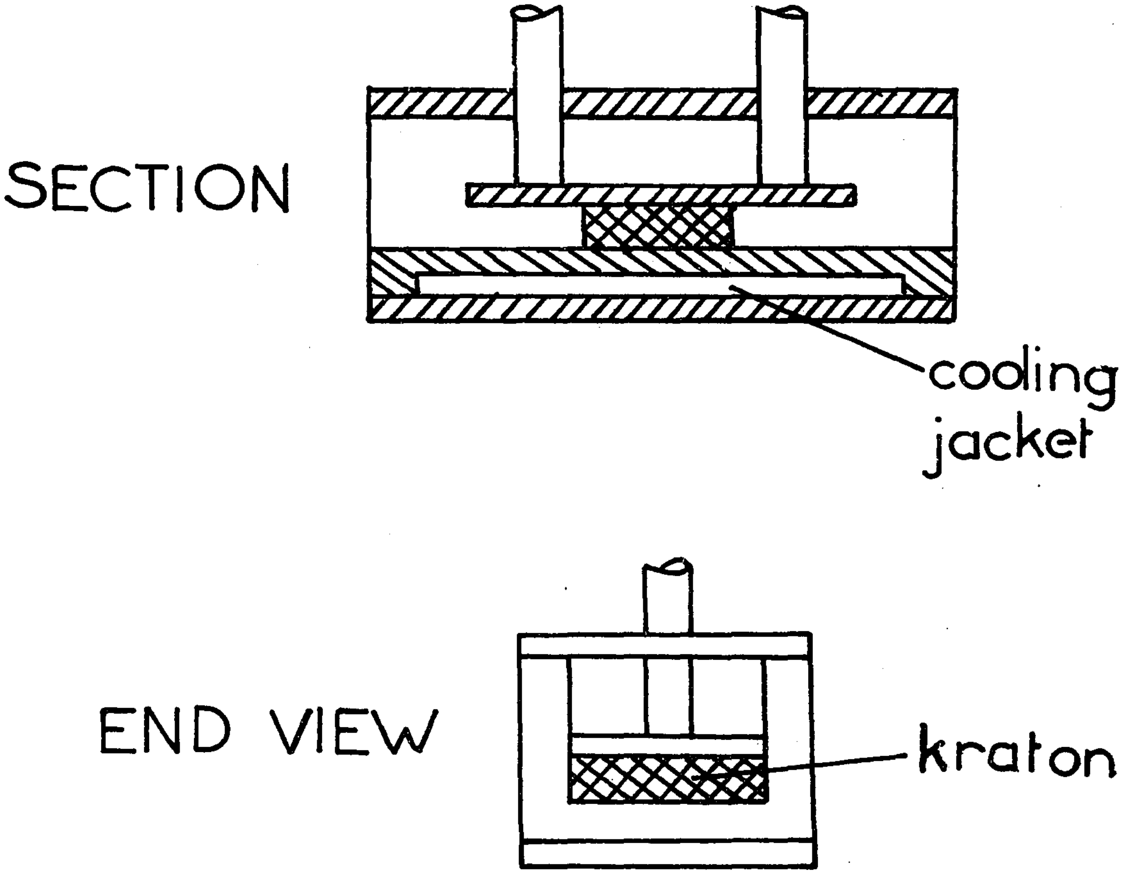

FIGURE 7-PARALLEL PLATE PLASTOMETER

The major reason for building the parallel plate plastometer was that it permitted sheets of Kraton 1101 previously sheared in the pressure flow device to be sheared again. This could be done either in the previous flow direction or perpendicular to it. The theory behind this apparatus is developed in Appendix A. As we shall see use of this theory allows a better measurement of the flow behaviour of Kraton than is possible with the pressure flow device.

2. Mechanical Testing

Mechanical testing for annealed and sheared samples was done in simple tension using an Instron tensile tester. Tesing was done using an Instron crosshead speed of 10 cm/min and at ambient temperature, $24^{o}C$, for all samples. The quantities desired were the initial Young's modulus and the stress-strain curve up to an elongation ratio of approximately 8, and if possible the ultimate tensile properties. To obtain these quantities a dumbell sample of well defined geometry had to be used for the testing.

Different shapes and sizes were tried to try and keep the sample size small, avoid rupture at the clamps, and have a long enough uniform region for accuracy. The shape and size of the dumbell sample cutter finally selected is shown in Appendix B. The length of the sample is such that four samples could be cut from each sheared sheet. The width at the clamps is four times the width of the uniform region of the sample; earlier tests had shown that this is a minimum ratio on samples approximately 1/16 inch to keep the sample from slipping out of the clamps or rupturing there prematurely. Work by Outa (27) on tensile testing of rubber dumbell samples had shown that fracture would always occur where the sample started to increase in width if the angle exceeded five degrees, therefore, to increase the width, two angles were used instead of one, a five degree angle to increase the width enough to avoid breaks because of stress concentration, and a 30 degree angle to increase the width of the sample enough to avoid it slipping from the clamps. The cutter has a uniform region 0.5 cm wide and 1.0 cm long, which are minimum value to obtain decent accuracy in the elongation measurements. The width has to be greater than the thickness of the samples (sheared samples were about 0.2 cm thick) so that when a sample is cut out from a sheet it will be rectangular in cross section.

The initial modulus of such a sample can be calculated from the initial slope of the Instron chart. The chart records the force on the sample versus the distance moved by the Instron crosshead. The calculation is shown in Appendix B. The rest of the stress-strain curve is obtained by photographing the sample while it is being elongated (two reference marks were drawn in the uniform region with Indian ink). Every time a photograph was taken a mark was recorded on the Instron chart to indicate the force on the sample. The elongation of the sample can be determined from the photographs, and the nominal stress from the Instron chart. Nominal stress, F/A_o, is based on the initial cross sectional area, A_o, of the uniform region. When the sample breaks in the uniform region the ultimate elongation can be determined by extrapolation of the stress-strain curve to the ultimate stress.

3. Determination of the Morphology of Samples

a) Low Angle X-Ray Scattering

Low angle X-ray scattering was done on Seiffert X-ray machine, described by Keissig (28). The radiation used was nickel filtered copper Kα,with a wavelength of 1.54 A. The X-rays were pin-hole collimated and the scattering was recorded on a flat film with a sample to film distance of 40 cm. A schematic drawing of the camera is shown on Figure 8(a). During exposure of the film the camera was operated under vacuum to eliminate background scattering from the air which could obscure the pattern of interest in the low angle region. For the purposes of this work an exposure time of 12 hours was adequate. Such long exposures are common in low angle X-ray scattering

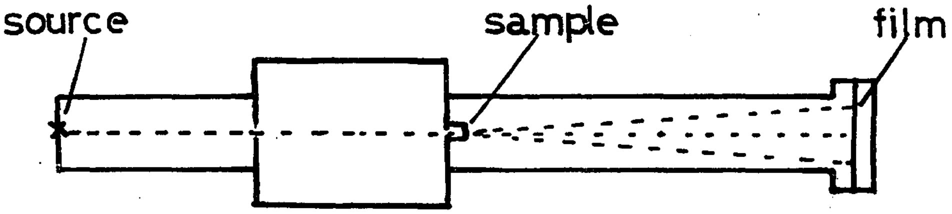

FIGURE 8a
LOW ANGLE CAMERA

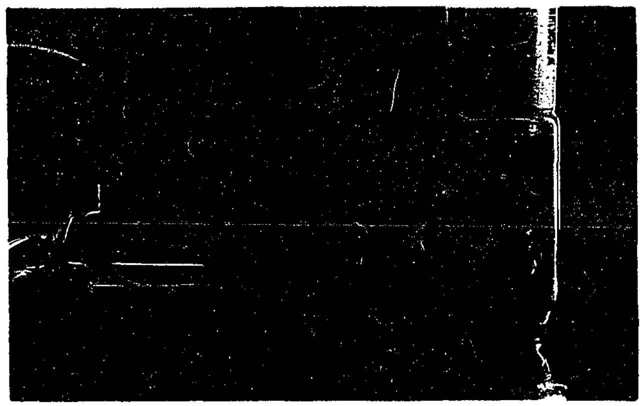

FIGURE 8b
DEVICE TO MAKE SAMPLES FOR ELECTRON MICROSCOPY

because of the low radiation intensities resulting from the collimation required and the long sample to film distance.

b) Electron Microscopy

There are many methods discussed in the literature for obtaining samples of rubbers suitable for examination under the electron microscope. One method is to harden the rubber and produce ultra-thin films by ultra-microtomy. The rubber can be hardened by cooling with liquid nitrogen, or by swelling with a suitable monomer and polymerizing in situ, or by treating with osmium tetroxide as discussed by Kato (29). The latter was the method first tried. The osmium tetroxide reacts with the unsaturated double bond of the PB and hardens it enough for ultra-microtomy. Being a heavy metal osmium does not let electrons pass through it easily and the PB regions appear dark under the electron microscope. The osmium tetroxide does not react with the PS phase, and thus it is possible to distinguish the two phases of Kraton 1101 under the electron microscope. However, the osmium tetroxide only penetrates Kraton 1101 to a depth of several microns so a section approximately 3 microns thick must be first cut and stained with the osmium tetroxide. The stained section has to be mounted in a resin and then cut in the ultra-microtome. The technique was tried, but was not successful. The problem was that the initial slice was too thick, and the osmium tetroxide did not harden the section sufficiently.

Another method for obtaining samples suitable for examination under the electron microscope is by two step replication. The technique of Bradford and Vanderhoff (30) was tried. Sheared Kraton 1101 was fractured in liquid nitrogen and a primary replica made with poly vinyl alcohol. This replica was then coated with a thin film of carbon, and the primary replica dissolved away in water. The carbon replicas were then picked up on electron microscope grids. However the attempt was unsuccessful due to fragmentation of the carbon films on the water.

The third method tried was developed by Katsky et al (31). This method consists of dissolving away the surface of a sample until it is thin enough for examination under the electron microscope. The apparatus used to prepare the samples is shown in Figure 8(b). The sample of Kraton 1101 to be treated is placed on an electron microscope grid which is placed on the wire mesh in the apparatus. A glass bulb which is cooled by water is used to support this mesh. THF is then refluxed down over the sample. In about an hour the sample thins enough for transmission electron microscopy. Ten grids can be prepared at one time. When thin enough the films of Kraton 1101 are stained for 2 hours in osmium tetroxide vapour. This method proved very successful and did not appear to destroy any of the original structure.

IV. RESULTS

1. Annealing of Compression Molded Sheets

Bianchi et al (10) showed theoretically that the PS domains in S-B-S block copolymers should decrease in size as temperature is increased. The following experiments were carried out to see if this effect could be observed by annealing samples at different temperatures. The experiments were done also to establish the mechanical properties of compression molded Kraton 1101 for comparison with the properties of sheared material.

a) four sheets were annealed for two hours at 200°C. Two of these were quenched in liquid nitrogen, and two were left to cool slowly at ambient temperature. This experiment was performed to see if the domain size would have time to change from the size at 200°C while cooling slowly.

b) two sheets were annealed for one hour at 200°C, and two more were annealed for two hours, also at 200°C. All were slowly cooled. This experiment was performed to see if the longer annealing time degraded the material enough to affect the mechanical behaviour.

c) in the final experiment two sheets were annealed for twenty-four hours at 120°C and two sheets were annealed for six hours at 160°C. All were slowly cooled. Longer times were used for lower temperatures to give the structure time to rearrange.

Samples were cut from the annealed sheets and tested. The initial Young's moduli of the samples are given in Table 1.

TABLE 1

INITIAL YOUNG'S MODULI OF ANNEALED KRATON 1101

Annealing Time Hrs.	Annealing Temp C	Cooling Rate	Young's Mod. Dumbell Sample KGF/cm2	Young's Mod. Rect. Sample KGF/cm2
2	200	slow	625	---
2	200	fast	600	---
2	200	slow	610	640
1	200	slow	610	600
6	160	slow	690	---
24	120	slow	670	640

The table also shows the Young's modulus determined using a rectangular section 0.5 cm wide and 3.0 cm long for three of the samples. The agreement between this modulus and that determined from the initial slope of the Instron chart for the dumbell sample is satisfactory. From the table it appears that annealing temperature and the rate of cooling do not affect the Young's modulus significantly. Also doubling the annealing time at 200°C does not appear to degrade the material enough to affect the modulus. However, the method itself is subject to an inaccuracy of approximately 10% due to the fact that a slope must be taken from a graph. In addition the samples themselves may vary slightly in the unavoidable flow orientation they experience during **molding**.

The rest of the stress strain curves are shown in Figures 9 and 10. The nominal stress, F/A_o, is plotted versus the extension ratio, λ. Figure 9 shows that the rate of quenching has no significant effect on the stress-strain curves for samples annealed at 200°C. Figure 10 shows that the annealing temperature has no significant effect on the stress-strain curves up to an extension ratio of about 6. Deviations past this extension can be explained by small differences in the slight flow orientation experienced during molding.

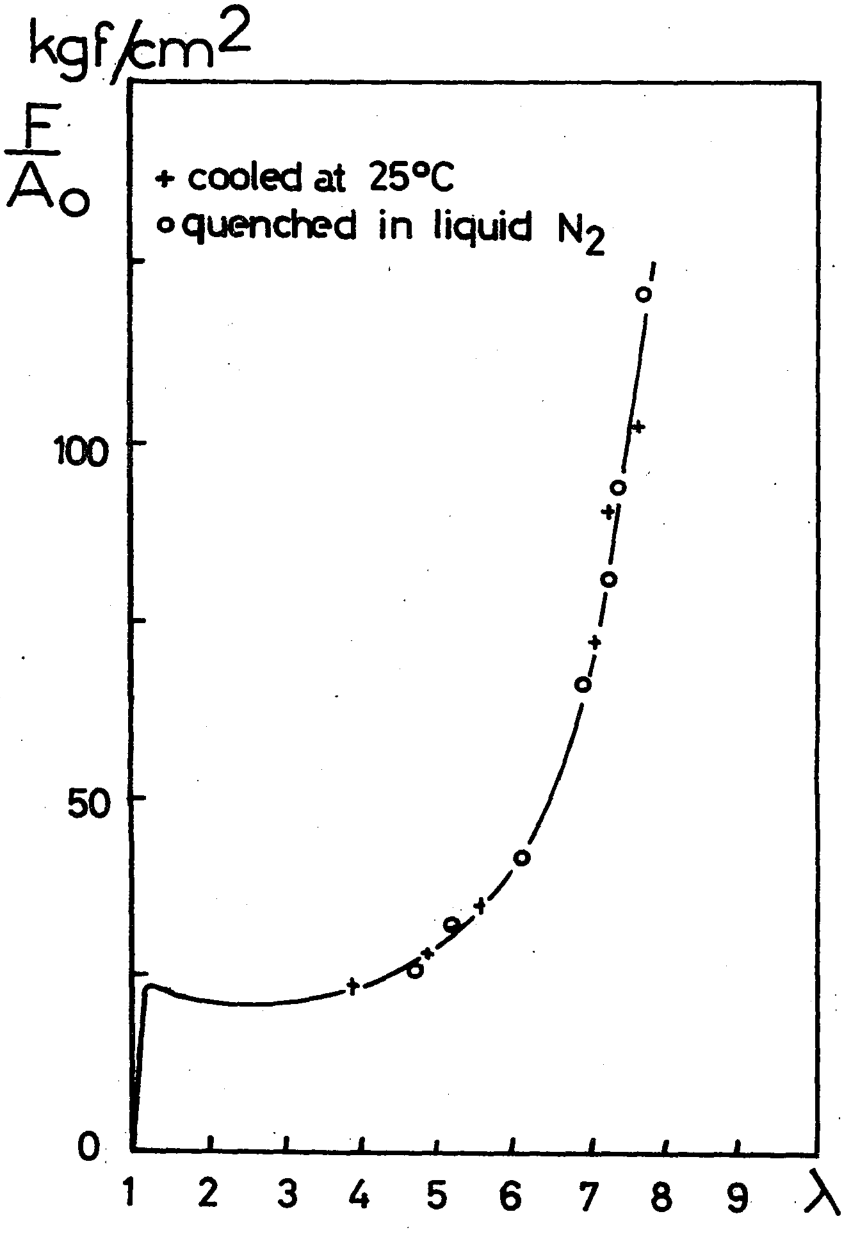

FIGURE 9

EFFECT OF QUENCHING ON KRATON 1101 ANNEALED AT 200°C

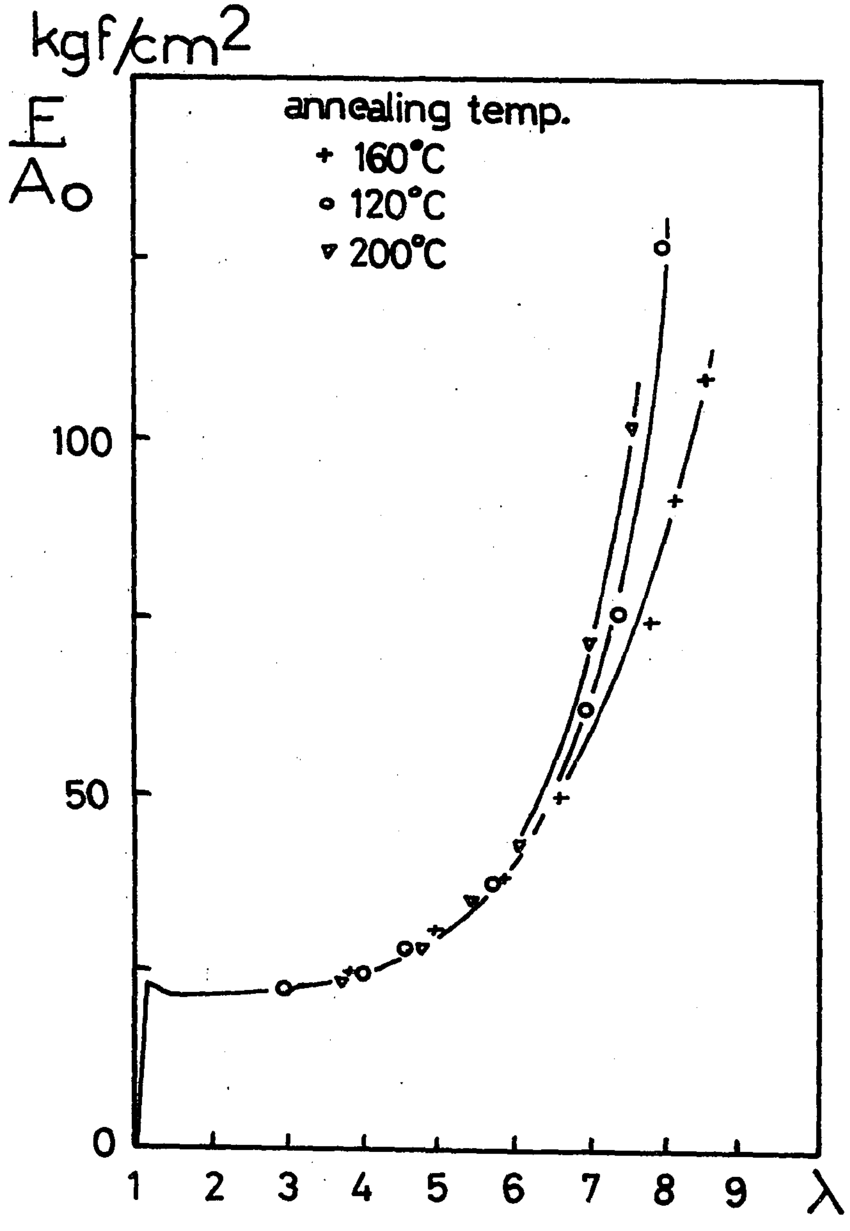

FIGURE 10
EFFECT OF ANNEALING TEMPERATURE ON KRATON 1101 COOLED AT 25 °C

Figure 11 shows a typical Instron recording for a compression molded sample and two of the photographs used to record the extension. The yield stress, which occurred at a nominal stress of 23 kgf/cm^2, is evident from the recording. This yield stress was common to all compression molded samples. The photographs show clearly that the samples neck in a region which grows until the whole sample is once again homogeneous.

Unfortunately ultimate properties could not be measured for compression molded samples. They slipped from the clamps at a nominal stress of 250 kgf/cm^2 and an extension ratio of about 8.5. It was very difficult to prevent this happening with samples that were of the order of 1/16 inch thick. The region of the sample clamped necked as well, and when this was complete tended to slip. The clamps were fastened together using screws, but even using strong springs to maintain a constant pressure on the sample did not help much. Going to thinner samples for compression molded samples was impractical as too much flow orientation would have occurred in molding the Kraton 1101 nodules which were of the order of 1/16 inch.

2. Shearing in the Pressure Flow Device

a) Flow Behaviour

Shearing experiments were all done at 200°C and when complete cooling water was circulated immediately in the cooling jackets of the pressure flow device. In the flow in the narrow

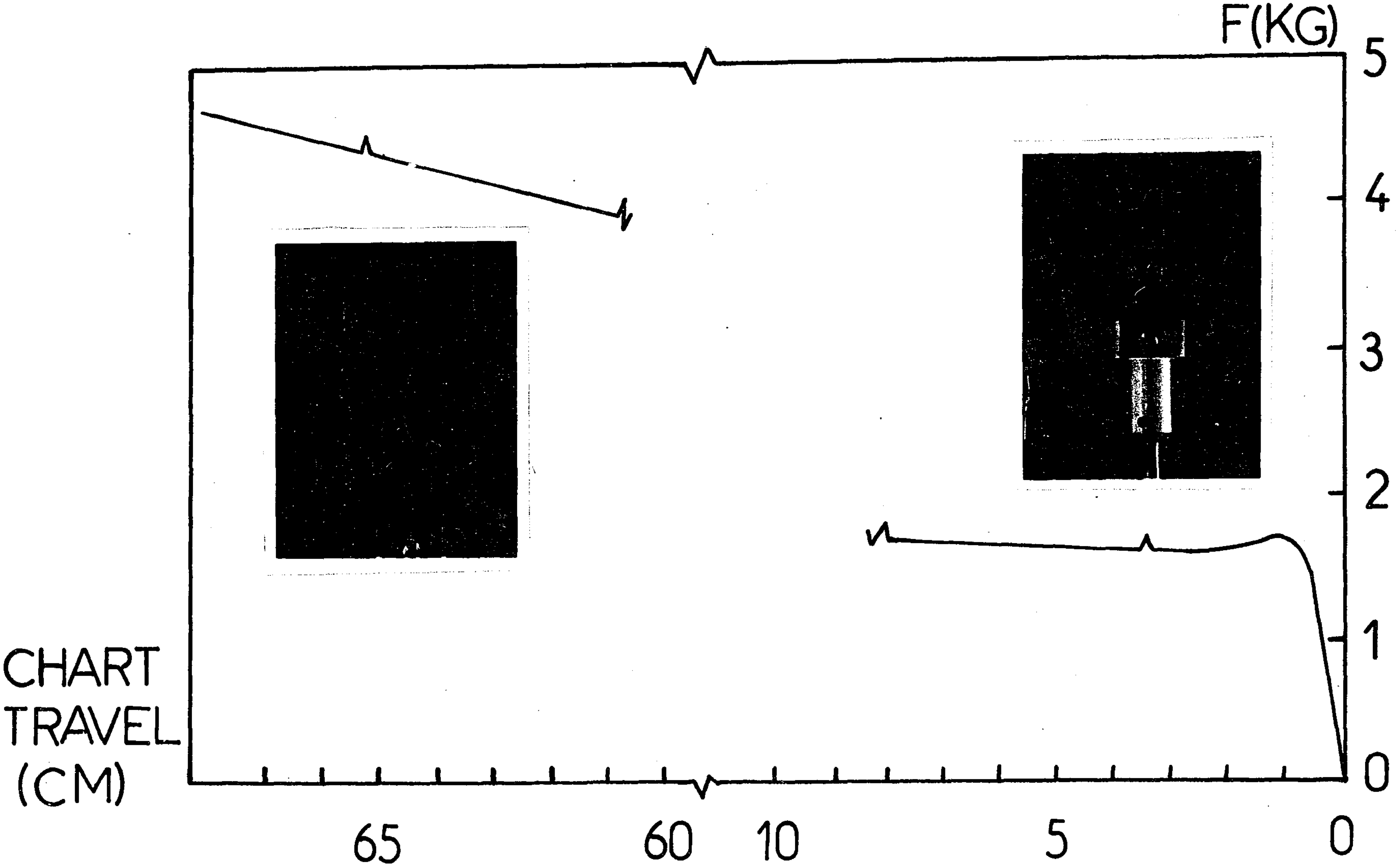

FIGURE 11 -TYPICAL INSTRON RECORDING

gap it is assumed that once the entrance region is passed the flow is a pressure type flow between parallel plates. Four plots of the force on the piston as a function of time for the pressure flow device are given in Figure 12. Three of these are for flow between Teflon surfaces with Instron crosshead speeds of 0.02, 0.05 and 0.2 cm/min., and the fourth one is for flow between aluminum surfaces with a crosshead speed of 0.05 cm/min. Eventually the force becomes constant when the gap becomes full of polymer. The final force to cause flow is the same at 0.05 cm/min for aluminum surfaces and for Teflon surfaces. This means that the same type of flow occurs in each case, and the Kraton 1101 is not slipping at the wall on the Teflon. Assuming fully developed parabolic flow between parallel plates, the wall shear stress, τ_w, and the apparent viscosity can be calculated for each experiment. This has been done and the values are plotted in Table 2.

The Kraton 1101 has a very high viscosity: as a comparison, the Newtonian viscosity of a monodisperse polystyrene with a molecular weight of 97,000 is approximately 10^4 poise (19). The viscosity of Kraton 1101 is very shear dependent, and the viscosity has only been listed here for later comparison with more data obtained from the parallel plate plastometer. It is important to note that the shear stress at the wall is above or very close to the critical

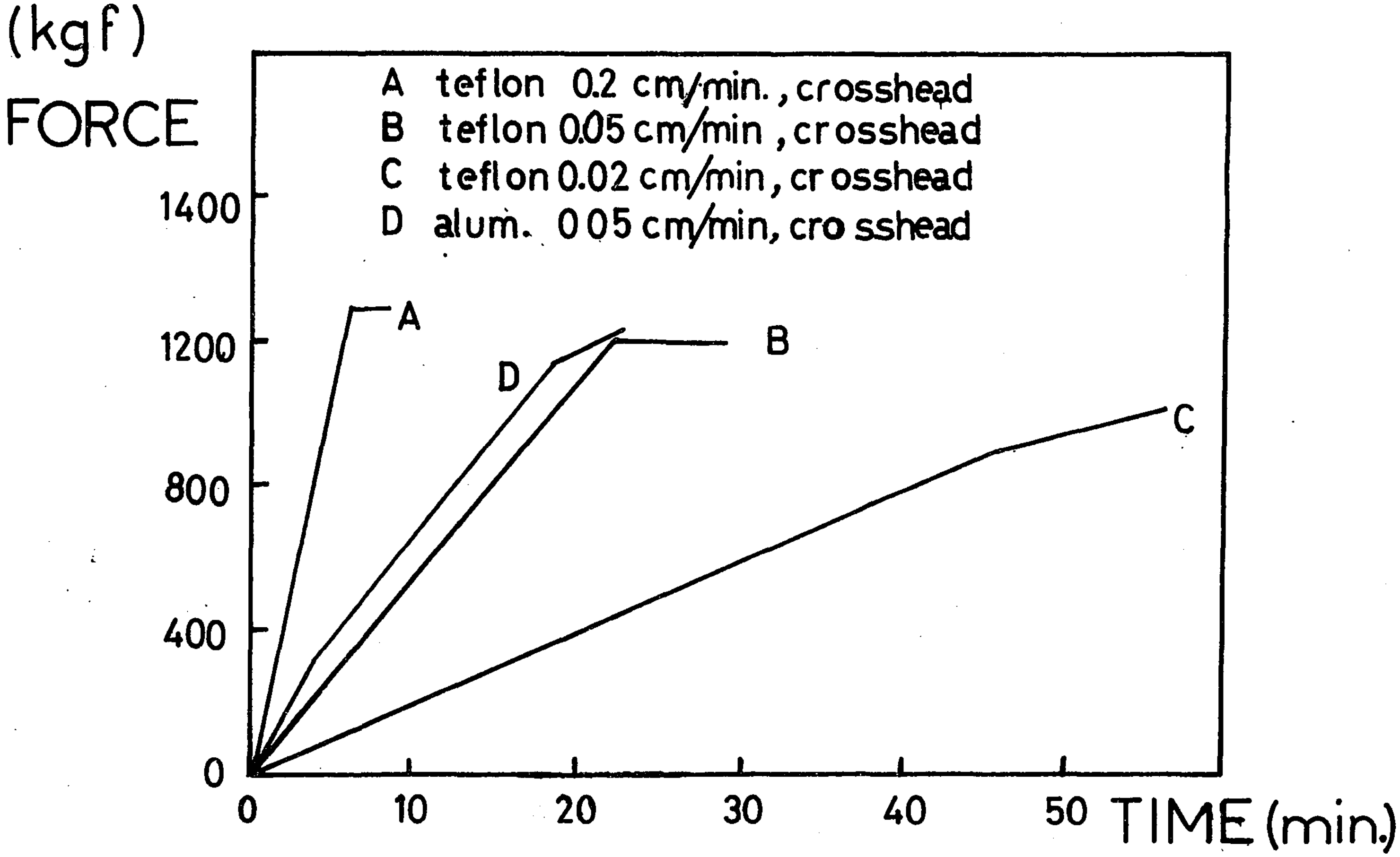

FIGURE 12
FLOW BETWEEN PARALLEL PLATES

TABLE 2

APPARENT VISCOSITIES OF KRATON 1101 IN FLOW IN THE PRESSURE FLOW DEVICE**

Surfaces	Crosshead Speed cm/min	Flowrate cm^3/min	Force Required kgf	Shear Stress at Wall $dynes/cm^2$	Apparent Viscosity poise
aluminum	0.05	1.3	1200	4.5×10^5	1.5×10^6
teflon	0.05	1.3	1180	4.5×10^5	1.5×10^6
teflon	0.02	0.52	850	3.3×10^5	2.7×10^6
teflon	0.2	5.2	1240	4.8×10^5	3.8×10^5

** The gap thickness is 0.08 ± 0.05 inches.

shear stress of 4.5×10^5 $dynes/cm^2$ found by Arnold and Meier (19) where a flow transition occurs. The flow changes from a response characteristic of isolated domains to a power law behaviour similar to PS.

b) Mechanical Behaviour of Sheared Sheets

The Kraton 1101 sheared in the pressure flow device was in the form of sheets 4 x 4 x 0.08 inches. Four samples could be cut from each sheet with the dumbell cutter. Samples cut in the direction of flow will be called longitudinal samples, and samples cut at 90° to the direction of flow will be called transverse samples.

Figure 13 gives the stress-strain curves for sheets sheared between aluminum surfaces sprayed with silicon mold release. Curves are given for the longitudinal and transverse directions, and for two crosshead speeds corresponding to flow rates of 1.3 and 13 cm^3/min. The corresponding shear stresses at the wall were 4.5×10^5 and 7.5×10^5 $dynes/cm^2$ respectively. These curves are shown for comparison with the sheared sheets done between Teflon surfaces. Due to the fact that some prestraining was unavoidable in removing the sheared sheets from the pressure flow device, the curves at the two flow rates cannot be compared quantitatively. Qualitatively, however, the effect of shear stress in the range of flow rates studied is negligible. Doubling the flow rate had little effect on the anisotropy. The ultimate tensile properties could be obtained for the longitudinal direction. For a wall shear stress of 4.5×10^5 $dynes/cm^2$, the nominal tensile strength, f_b, was 140 kgf/cm^2, and the extension ratio at break, λ_b, was 8. For a wall shear stress of 7.5×10^5 $dynes/cm^2$, f_b was 110 kgf/cm^2, and λ_b was 7. The transverse samples had greater tensile strengths and extension ratios than this and slipped from the clamps, as in the case of compression molded samples. The longitudinal samples yielded and necked at a nominal stress of about 25 kgf/cm^2. No such yield stress or necking was observed for the transverse samples. Initial Young's moduli for samples sheared between Teflon surfaces will be discussed later.

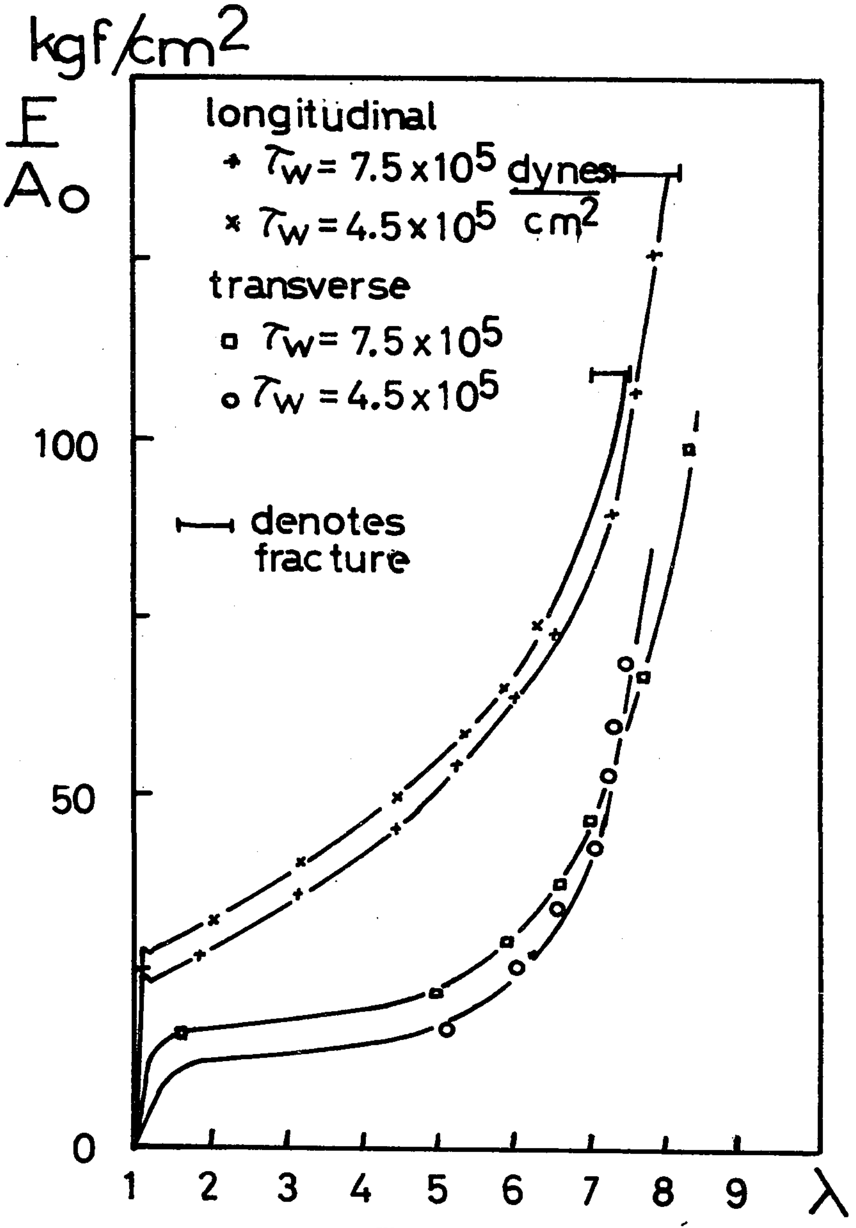

FIGURE 13

STRESS-STRAIN CURVES OF SAMPLES SHEARED IN THE PRESSURE FLOW DEVICE WITH ALUMINUM SURFACES

Shearing in the pressure flow device between Teflon surfaces produced some peculiar results. First, to check the reproducibility of the experiments, three experiments were done at the same flow rate of 1.3 cm^3/min. The longitudinal behaviour was found to vary slightly from sheet to sheet. In the first experiment the stress-strain curve was very similar to that of the longitudinal samples cut from sheets sheared between aluminum surfaces. See Figure 14. For this experiment the tensile properties were quite high and the sample slipped from the clamps before breaking. The second and third sheets sheared had a different stress-strain curve. See Figure 15. Both fractured at relatively low nominal stress and extension ratios. These were f_b's of 50 and 60 kgf/cm^2, and λ_b's of 5 and 6.5 for the two sheets.

Two other flow rates, 0.52 and 5.2 cm^3/min were used to investigate the effects of shear stress on Kraton 1101 sheared between Teflon surfaces. The stress-strain curves for longitudinal samples cut from these sheared sheets are given on Figure 16. Here, as with the sheets sheared between aluminum surfaces, no significant effect of increasing shear stress was found. Comparing all three flow rates used 0.52, 1.3 and 5.2 cm^3/min no trend was evident of increasing or decreasing stress values at the same extension ratio with increasing flow rate. The longitudinal samples of the sheets sheared at flow rates

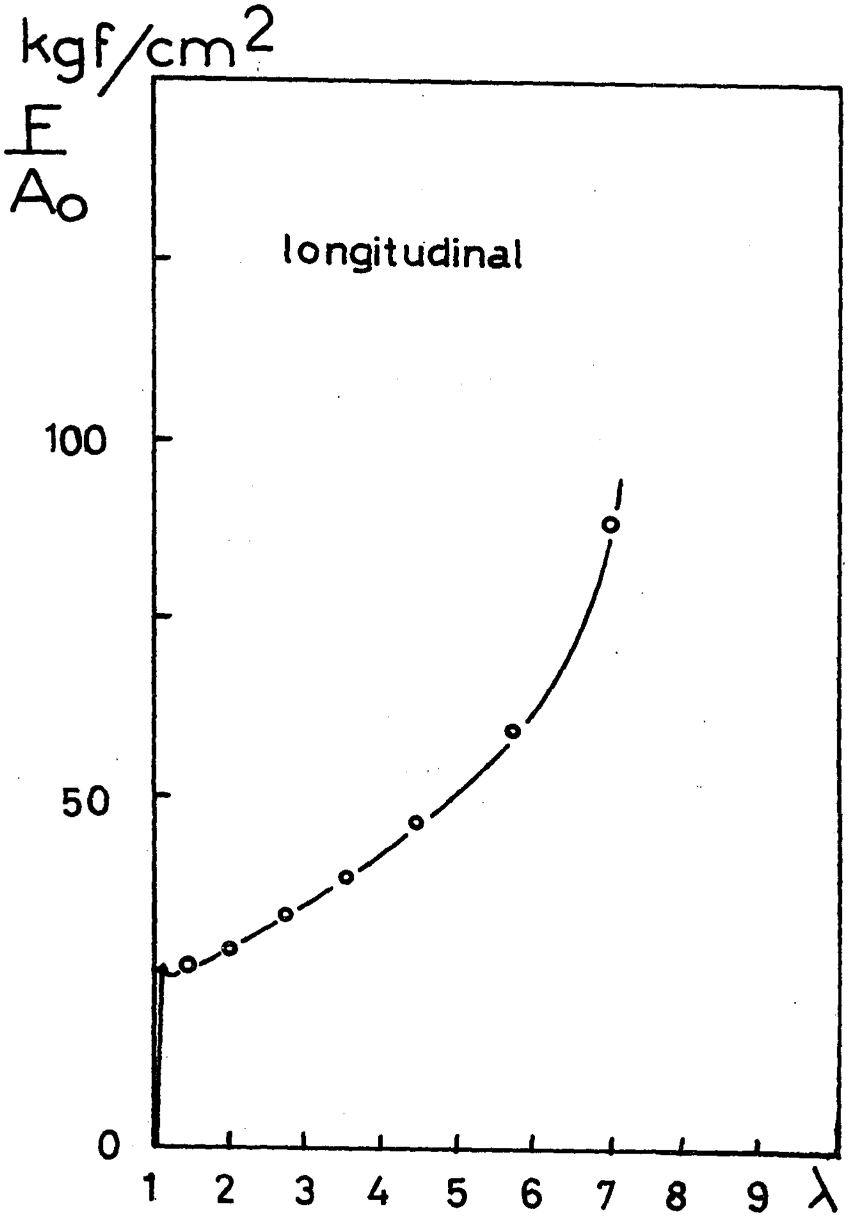

FIGURE 14

1 ST SHEET SHEARED WITH $\tau_W = 4.5 \times 10^5$ DYNES/CM² BETWEEN TEFLON SURFACES

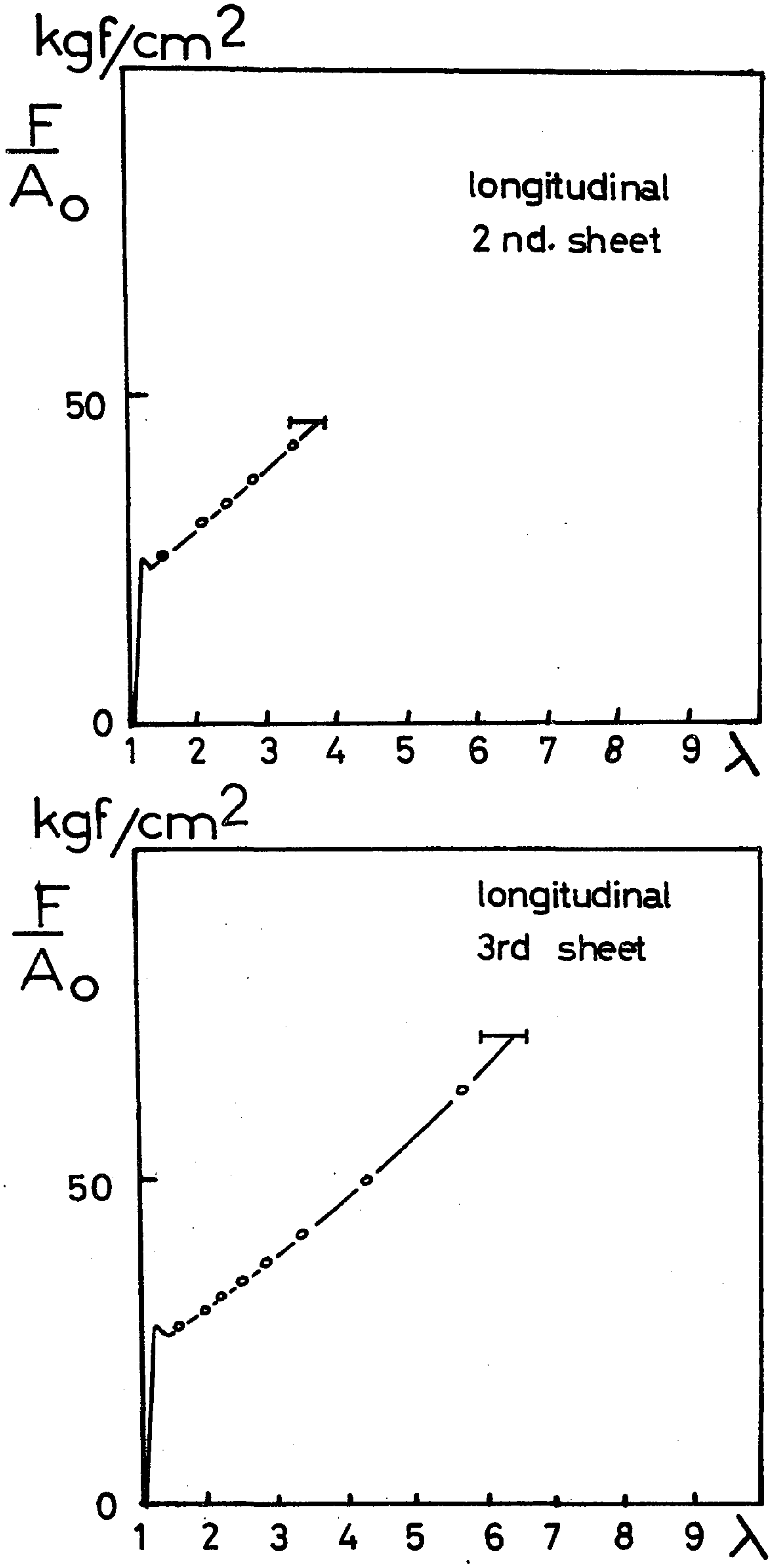

FIGURE 15

2ND & 3RD SHEETS SHEARED WITH $\tau_W =$ 4.5×10^5 DYNES/CM^2 BETWEEN TEFLON SURFACES

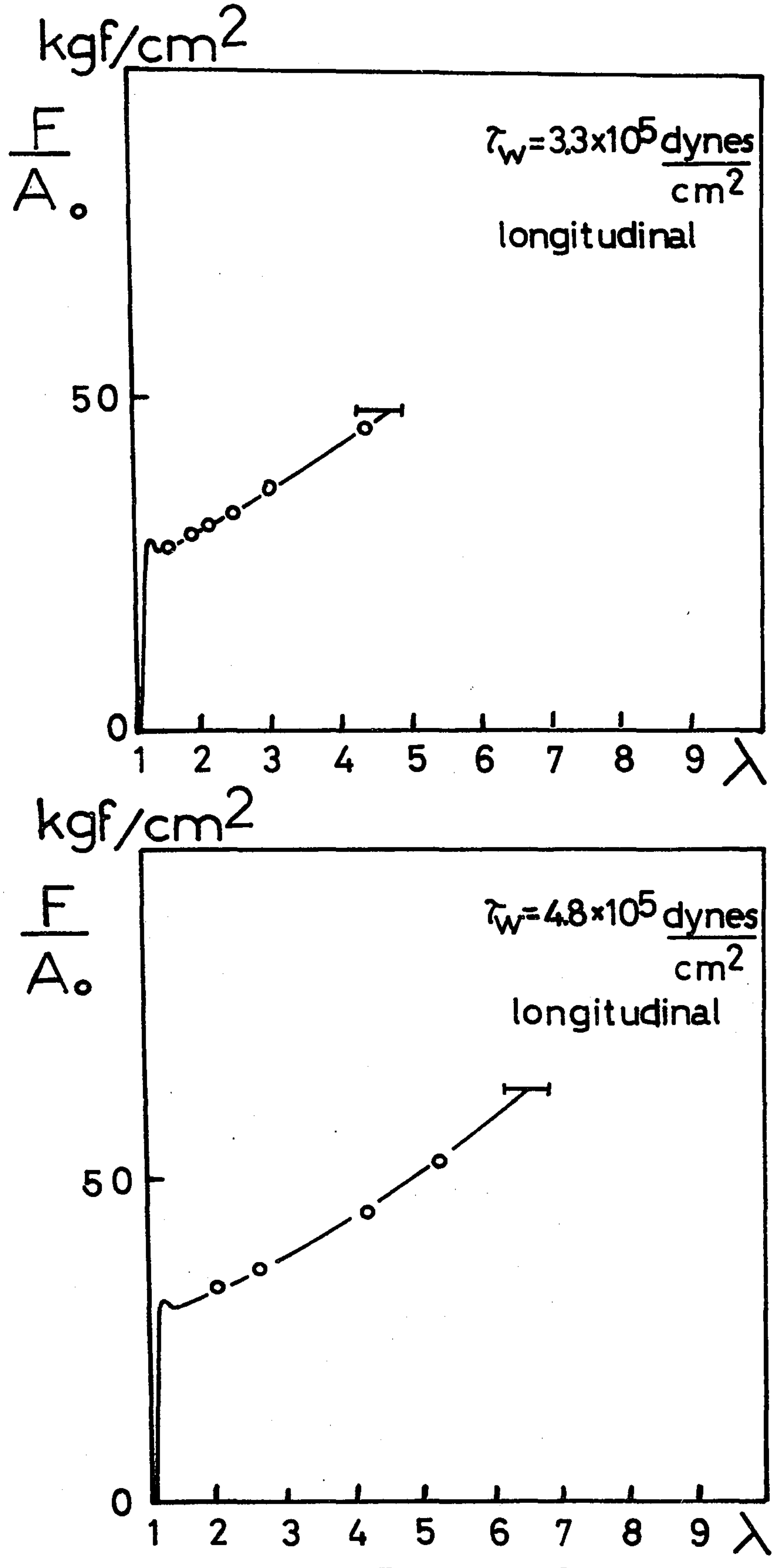

FIGURE 16

SHEETS SHEARED WITH $\tau_W=3.3\times10^5$ AND 4.8×10^5 DYNES/CM^2 BETWEEN TEFLON SURFACES of 0.52 and 5.2 cm^3/min also broke at relatively low nominal stresses and extension ratios. These were f_b's of 50 and 60 kgf/cm^2, and λ_b's of 5 and 6.5 respectively.

The stress-strain behaviour of the transverse samples for all the sheared sheets done between Teflon surfaces were practically the same. The curve is shown on Figure 17. Ultimate properties could not be found as again the samples slipped from the clamps at nominal stresses of approximately 100 kgf/cm^2.

A comparison can be made at this point between the stress-strain properties of the sheared and molded sheets. For this comparison two 4 x 4 x 0.08 inch sheets of Kraton 1101 were compression molded at 200°C for four and six hours respectively. Teflon plates were used in the molding sandwich, which was described earlier, instead of cellophane. Cellophane would have degraded in the long exposure to 200°C. The purpose of the long heating time was to expose the molded samples to temperature for the same length of time as the sheared samples. The results are shown in Figure 17. The molded samples' curve falls in between the stress-strain curves of typical longitudinal and transverse samples. The molded sample is closer in behaviour to the transverse sample except for the yield stress.

One other experiment was performed in the pressure flow device. This experiment was to establish if annealing the sheared sheets, rather than quenching them with cold water immediately after shearing, would affect the anisotropy. A

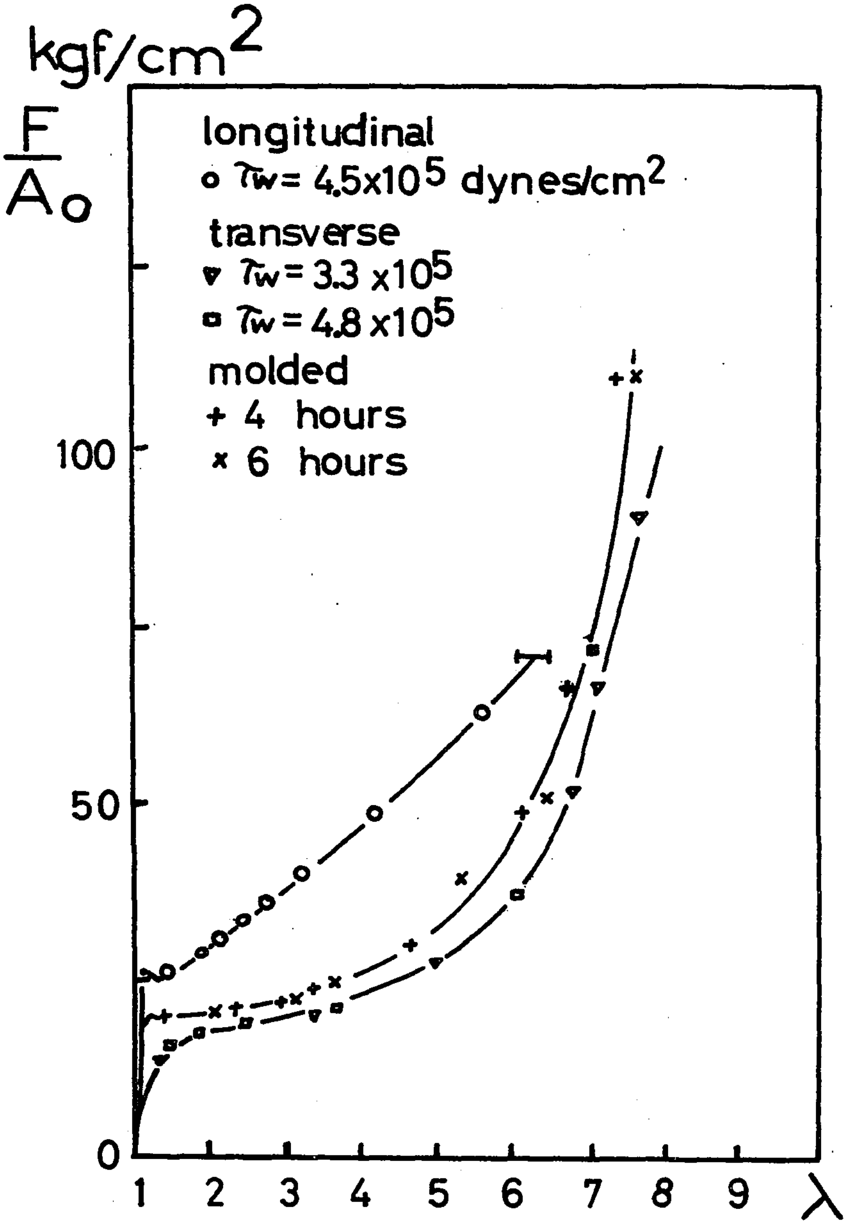

FIGURE 17

COMPARISON OF THE STRESS-STRAIN CURVES OF MOLDED SAMPLES AND SAMPLES SHEARED IN THE PRESSURE FLOW DEVICE BETWEEN TEFLON SURFACES sheet was sheared at 1.3 cm^3/min between Teflon surfaces, but instead of turning on the cooling water after the flow was stopped, the sheet was annealed at 200°C for two hours. Then cooling water was turned on to quench the sheet. The stress-strain behaviour for the longitudinal and transverse directions is shown on Figure 18. The transverse sample is almost the same in behaviour as other unannealed transverse samples. However, the annealed longitudinal sample had lower stress values than all other longitudinal samples tested. The Young's modulus showed the opposite effect. It was greater in both directions for the annealed sheared sheets than for the quenched sheared sheets.

Table 3 below shows the initial Young's moduli of the samples. The moduli shown here are only accurate to about 10%, but the difference between the directions is clear being 10 times greater in the longitudinal direction than in the transverse direction. For their sheared and oriented samples Folkes and Keller (25) found a longitudinal modulus of 4250 kgf/cm^2 and a transverse modulus of 46.5 kgf/cm^2. The differences between this data and the values reported here will be more fully discussed later, but it is obvious from these moduli that the samples studied by Folkes and Keller had a more perfect continuous PS structure. The moduli obtained in this work indicate that a semi-continuous network of polystyrene exists in the transverse as well as the longitudinal

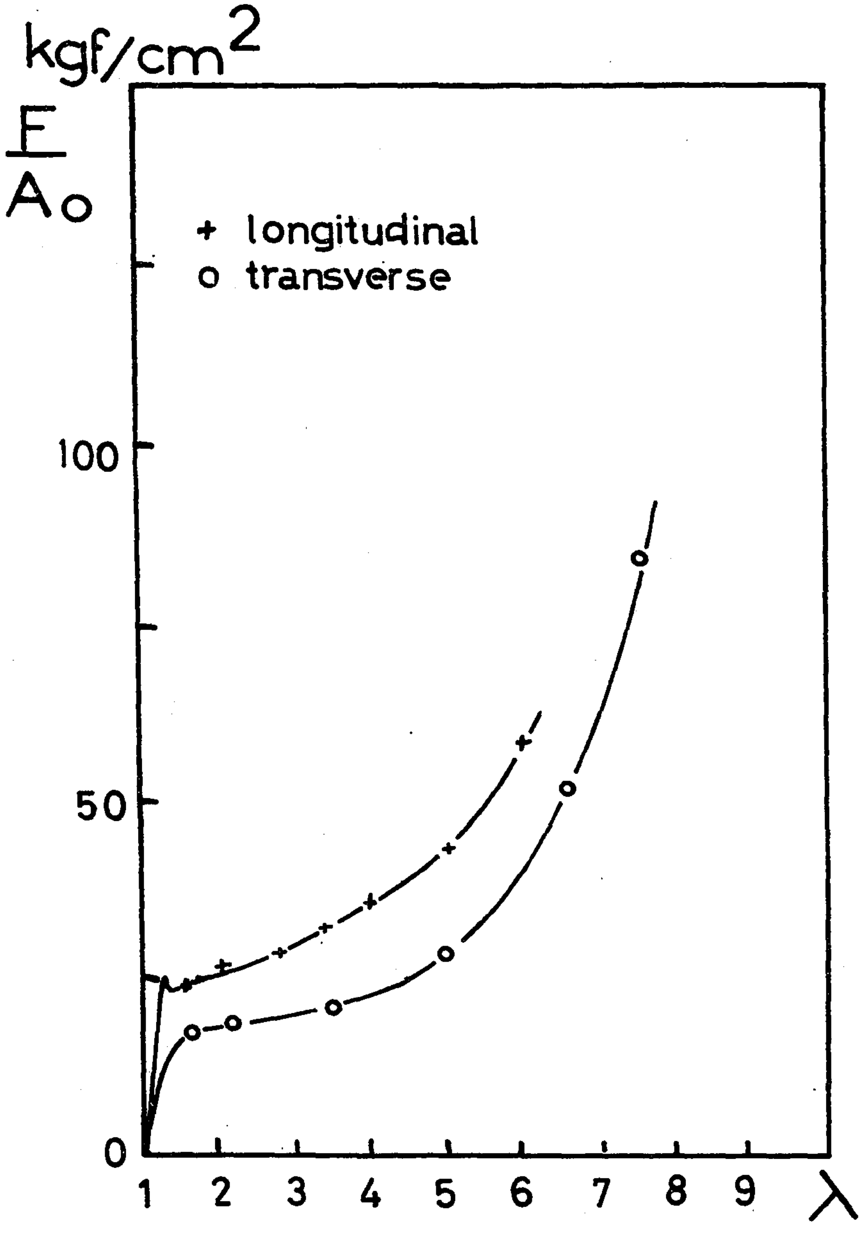

FIGURE 18
EFFECT OF ANNEALING IN THE PRESSURE FLOW DEVICE ON THE STRESS-STRAIN CURVE OF SHEARED SAMPLES

TABLE 3

INITIAL MODULI OF SHEARED SHEETS FROM THE PRESSURE FLOW DEVICE

	FLOW RATE cm^3/min	TRANSVERSE MODULUS kgf/cm^2	LONGITUDINAL MODULUS kgf/cm^2
Rapid Quenching	1.3	85	1000
	1.3	180	1100
	1.3	110	1140
	1.3	---	1200
	1.3	---	1120
	.52	104	1260
	5.2	---	910
		$\overline{E}_t = 120$	$\overline{E}_t = 1100$
Annealed Sheets 200 C for 2 Hours Before Quenching	1.3	145	1960
	1.3	150	1370
		$\overline{E}_t = 148$	$\overline{E}_t = 1600$

direction. Annealing makes this structure more perfect and increases the modulus in both directions. Decreasing anisotropy in the rest of the stress-strain curve due to annealing cannot be easily explained, but a different type of annealing experiment to be discussed later provided a better understanding.

Up until now we have only considered the first stress-strain curve of these sheared samples. A longitudinal and transverse sample were taken from a sheet that had been sheared at a flow rate of 1.3 cm^3/min between Teflon surfaces. The stress-strain curves for the first extension and retraction, and the second extension on these samples were measured. This was done up to an extension ratio of approximately 3. The stress-strain curves are shown in Figure 19. Considerable hysterysis is shown by both the longitudinal and transverse sample. This is attributed to the break down of a semi-continuous network of PS. From the original Instron charts it was found that the set after the first extension was approximately 10% some of which recovered in the few seconds before the second extension was begun.

In an illustrative experiment these previously stretched samples were placed in boiling water for 10 minutes. This was a form of annealing the samples as the temperature is above the T_g of the PS segments. However, the samples

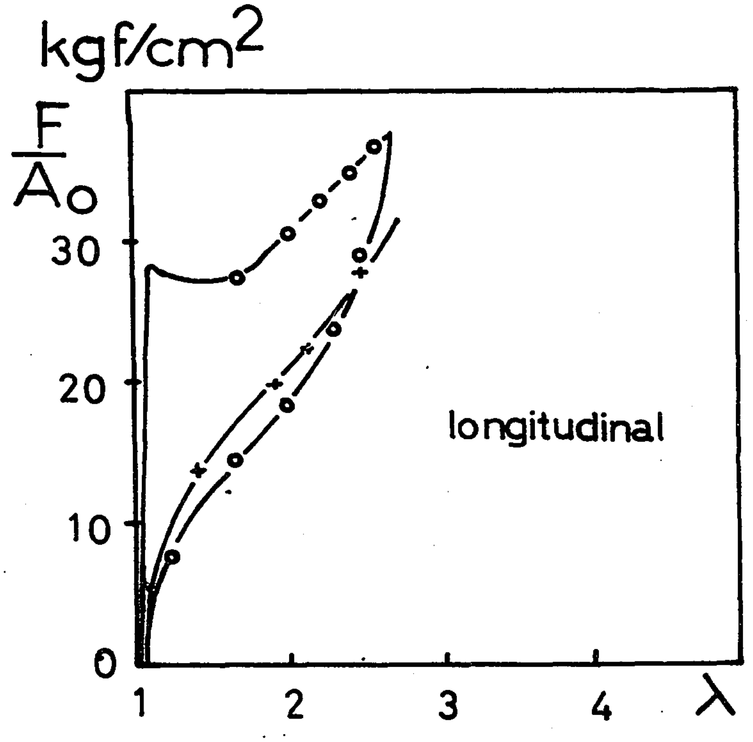

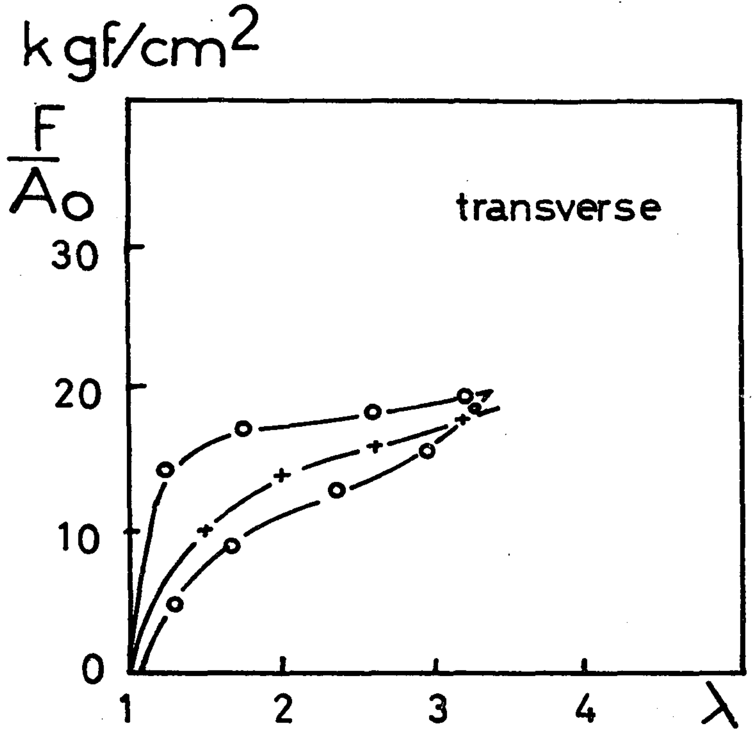

FIGURE 19

MUTIPLE STRESS-STRAIN CURVES OF SAMPLES SHEARED WITH $\tau_w = 4.5 \times 10^5$ DYNES/CM^2

are not constrained in any way by a mold or by the pressure flow device. The viscosity of the Kraton 1101 is high enough so that the samples did not distort, but they were found to shrink along the longitudinal direction and increase in thickness and width. The various dimensions of the samples in the uniform region before extension, after extension, and after being placed in boiling water are summarized in Table 4 below.

TABLE 4

DIMENSIONS OF SAMPLES IN THE RUNIFORM SECTION

	BEFORE EXTENSION	AFTER EXTENSION	AFTER BOILING WATER
LONGITUDINAL			
Length, cm	1.0	1.1	0.9
Width, cm	0.5	0.5	0.52
Thickness, in	0.074	0.071	0.0765
TRANSVERSE			
Length, cm	1.0	1.1	1.1
Width, cm	0.5	0.5	0.467
Thickness, in	0.085	0.081	0.11

The stress-strain curves based on the new initial cross-sectional area for the samples dipped in boiling water are given in Figure 20. The transverse samples recovered almost completely, while for the longitudinal samples the yield point reappeared, but the recovery was not complete, although longer annealing probably would have given almost complete recovery.

The same experiment was performed with previously unstretched samples. They too were found to shrink along the flow direction by about 5%, and to increase in thickness by about 5% as well. The transverse direction was practically unaffected. Stress-strain cruves for longitudinal and transverse samples cut from a sheet sheared at 1.3 cm^3/min and dipped in boiling water for 10 minutes are shown in Figure 21. The same effects are found in this case as for annealing in the pressure flow device. The Young's modulus for the sheared sheet was 1160 kgf/cm^2, in the longitudinal direction, but placing the sheet in boiling water for 10 minutes increased the modulus to 1450 kgf/cm^2.

As a last experiment in this series, a sample was cut from a sheet that had been sheared and annealed in the pressure flow device in the manner previously described. This sample was then placed in boiling water for 10 minutes. It also shrunk in the longitudinal direction 5%, and increased in thickness by 5%. The stress-strain behaviour of a longitudinal

FIGURE 20

RECOVERY OF STRESSED SAMPLES

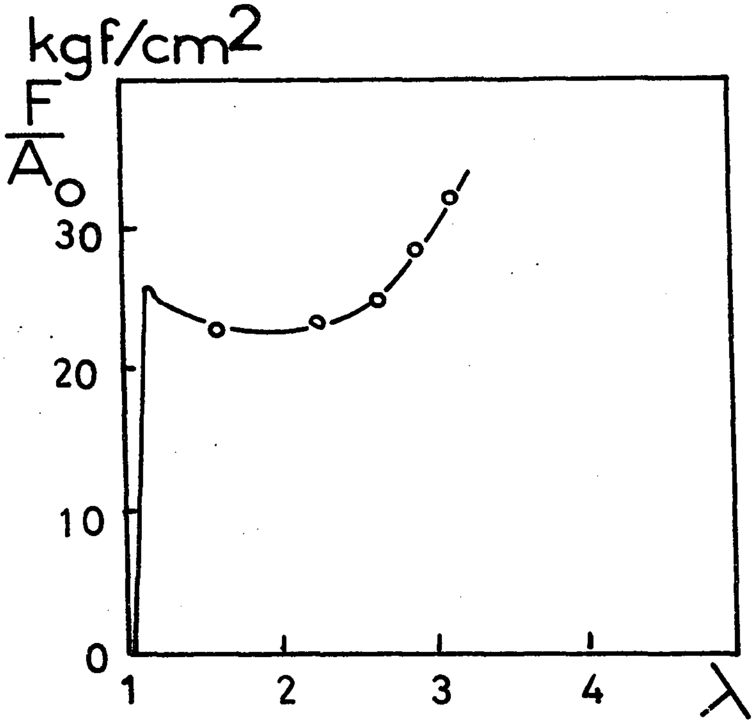

LONGITUDINAL SAMPLE STRETCHED TO λ=3 AND ANNEALED IN BOILING WATER

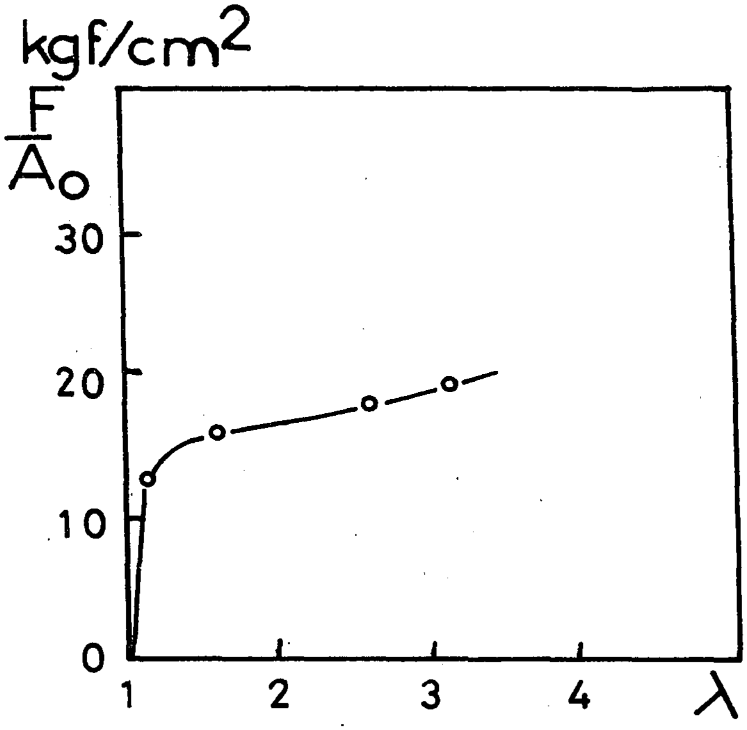

TRANSVERSE SAMPLE STRETCHED TO λ=3 AND ANNEALED IN BOILING WATER

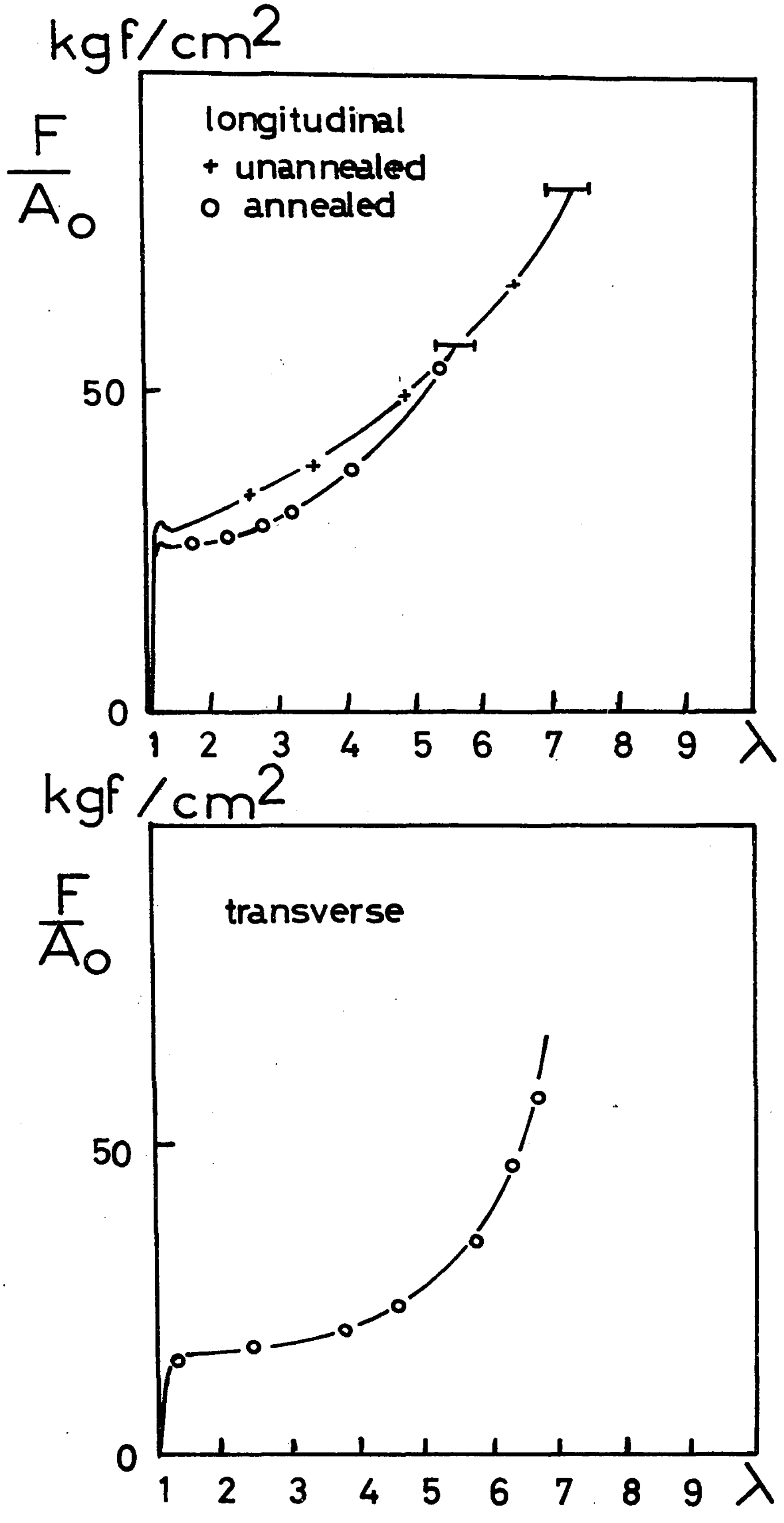

FIGURE 21

SAMPLES FROM A SHEARED SHEET
ANNEALED IN BOILING WATER BEFORE TESTING

sample is shown in Figure 22. It is compared with a longitudinal sample cut from the same sheet, but not placed in boiling water. Here too, dipping in boiling water reduces the stress level at higher elongations.

Now we have a possible explanation for the lower stress levels at higher elongations in longitudinal samples caused by annealing sheared sheets both in the pressure flow device and by dipping samples in boiling water. (In the case where a sheet was first annealed in the pressure flow device, and then sample cut from this given a second annealing by dipping in boiling water, the process of annealing was continued in the second step where the dimensions of the sample were free to change.) In shearing, the molecules are likely extended in the flow direction. When flow is stopped and the sheets quickly quenched the terminal PS segments would return to the glassy state hindering motion. Thus some PB chains are probably left in an extended state. When the sheets are annealed motion of the PS segments again becomes possible, and the PB segments tend to return to a more random state. This would reduce stresses in the sample, and at the same time cause an increase in thickness and a shrinkage in the longitudinal direction. Harpell and Wilkes (22) found the same effects discussed here while annealed samples of Kraton 1101 sheared in a rubber mill, and gave a similar explanation.

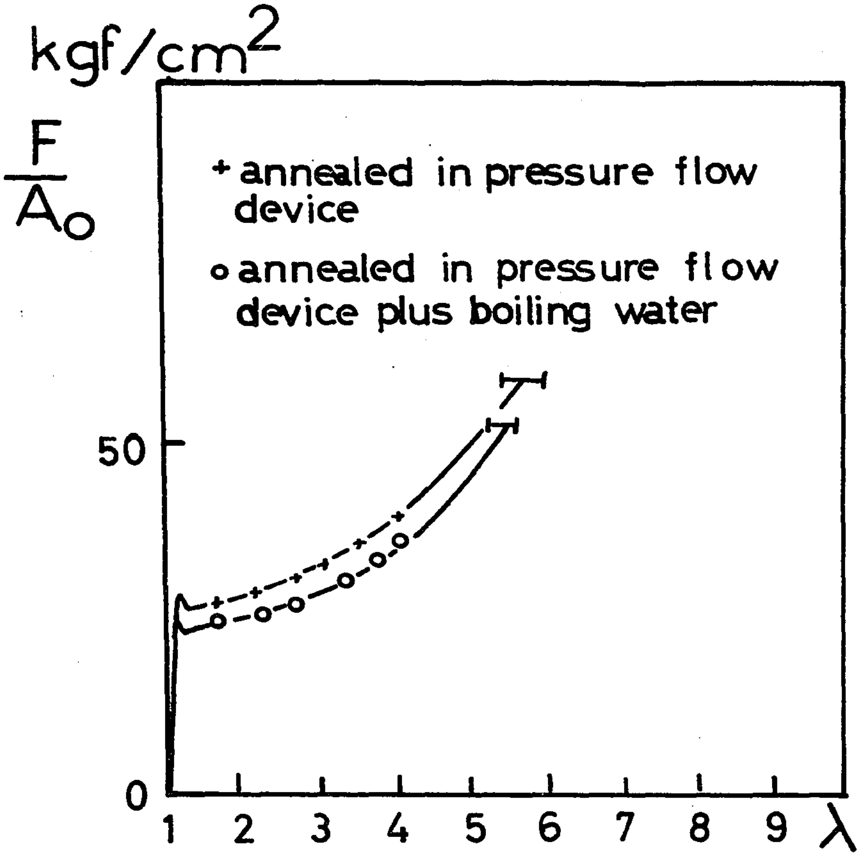

FIGURE 22

STRESS-STRAIN CURVES OF A LONGITUDINAL SAMPLE FROM A SHEET SHEARED AND ANNEALED IN THE PRESSURE FLOW DEVICE AND A SIMILAR SAMPLE ALSO ANNEALED IN BOILING WATER

3. Shearing in the Parallel Plate Plastometer

a) Flow Behaviour

The parallel plate plastometer was shown in Figure 7. The top piston is moved down as slowly as possible on the Instron, 0.02 or 0.05 cm/min, and the force on the top plate is measured by the Instron compression cell and recorded. As the top plate moves down, the polymer is forced to flow along the channel. The flow rate at the centre of the device is 0 and a maximum at the end of the top plate. Thus shear rate and shear stress vary from 0 to the centre of the plastometer to a maximum at the edge. Also the thinner the gap the higher the shear rate. For a material like PS then one could measure the Newtonian viscosity at the start of the experiment, and when the gap got narrower a power law relation for the viscosity. There are two ways to use the plastometer:

1) at constant volume, and
2) at constant length.

These are shown in Figures A2 and A3 of Appendix A.

In Appendix A the following equations are derived for the two cases, assuming a power law behaviour for the material being sheared.

1) Flow at Constant Volume

$$F = \frac{\eta_o}{2H^{3n+3}} \left[\frac{(2n+1)}{n} \frac{dH}{dt} \frac{V_o}{W} \right]^n \frac{V_o^2}{W^2} \qquad \text{........(9)}$$

Here F is the total force on the apparatus, V_o is the initial volume of the sample, W is the width of the flow channel, n is the power law index, η_o is the constant in the equation $\eta = \eta_o \left[\frac{\dot{\gamma}}{\dot{\gamma}_o}\right]^{n-1}$, η is the apparent viscosity, $\dot{\gamma}$ is the shear rate, H is the gap thickness, and dH/dt is the velocity of the top plate.

From a plot of log(f) versus log(H), which should be linear with a slope of -(3n+3) if a power law relation is obeyed by the material being sheared, n can be determined, η_o can be determined from equation 9 once n is known.

2) Flow at Constant Length

In this case L is the length from the centre of the plastometer to the edge of the top plate.

$$F = \frac{2W\eta_o}{H}\Biggl\{\Bigl[\frac{2}{H^2}\,\frac{dH}{dt}\,\frac{2n+1}{n}\,L\Biggr\}^n L^2 \qquad \ldots\ldots\ldots(10)$$

If log (F) is plotted versus log (H) for this case the slope should be -(2n+1) for the power law case, and -3 for the Newtonian case (i.e. n = 1). η_N is the Newtonian viscosity.

$$F = \frac{12W\eta_N L^3}{H^3}\,\frac{dH}{dt} \qquad \ldots\ldots\ldots\ldots(11)$$

The shear stress and the shear rates at the top and bottom plates of the apparatus are given by the following expressions for both cases.

$$\tau_W = \left[\frac{2}{H^2}\ \frac{dH}{dt}\left(\frac{2n+1}{n}\right)\right]^n \eta_o\ y^n \qquad \text{..........(12)}$$

$$\dot{\gamma}_W = \left[\frac{2}{H^2}\ \frac{dH}{dt}\left(\frac{2n+1}{n}\right)\right] y \qquad \text{..........(13)}$$

Here y is the distance from the centre of the apparatus.

i) Calibration with Polystyrene

Before doing experiments with Kraton 1101 the following series of experiments were done with Dow Styron 683 polystyrene at 200°C. The flow properties of the polystyrene used are summarized below in Table 5.**

TABLE 5

FLOW PROPERTIES OF THE POLYSTYRENE USED TO
CALIBRATE THE PLASTOMETER, AT 200°C

$\dot{\gamma}$ sec^{-1}	n —	η_o poise
5	0.58	4.4×10^4
10	0.52	3.3×10^4
15	0.43	2.1×10^4

**The data were determined on an Instron capillary rheometer by Mr. N. Nyun of the Chemical Engineering Department, McGill University.

These experiments were done to find the limitations of the apparatus for viscosity measurement. Prior to the shearing the plastometer containing the sample was heated for two hours at 200°C.

The first experiment performed was at constant length, starting with a molded sheet of PS 2 x 4 x 1/4 inches. This was sheared between the steel plates of the plastometer at an Instron crosshead speed of 0.02 cm/min. The force on the top plate versus time was obtained from the Instron chart, and the thickness corresponding to a particular force was calculated from the final thickness using the velocity of the top plate. A plot of log (F) versus log (H) is shown in Figure 23A. Two regions are obvious, the Newtonian region with slope -3, and a power law region with slope -2. The power law index is calculated as 0.5 from this slope. The deviation from linearity at thicknesses greater than 0.25 cm can be explained by the fact that the gap height to width ratio is too large for the assumptions used in deriving the equations to hold. See Appendix A. From these data and equation 10 and 11 the Newtonian viscosity of the PS was calculated as 2.7×10^5 poise, and the η_o was calculated as 11×10^4 poise. The value of the Newtonian viscosity is in satisfactory agreement with the value given by Middleman (32) of 1.3×10^5 poise for a PS with of similar molecular weight at 295°C. From equation 13 it was calculated that the PS is

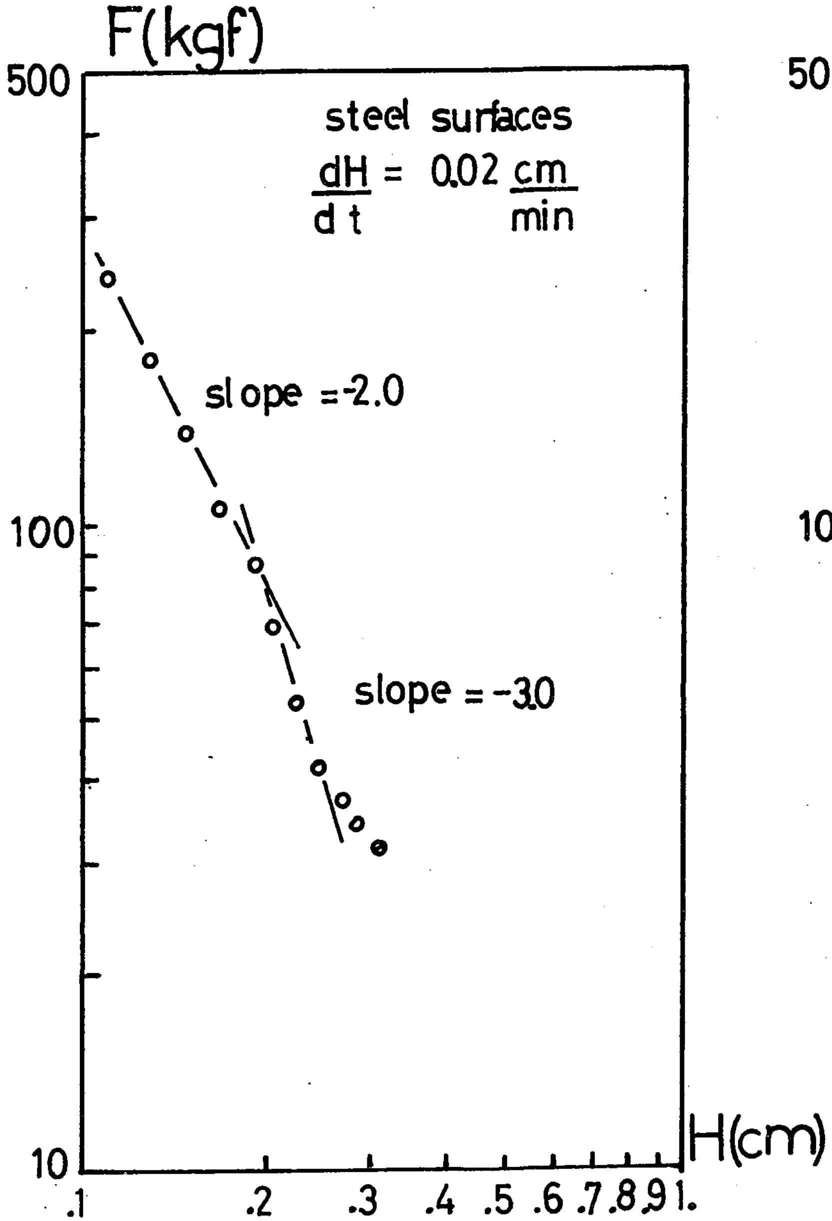

FIGURE 23a-POLYSTYRENE SHEARED AT CONSTANT LENGTH IN THE PLASTOMETER

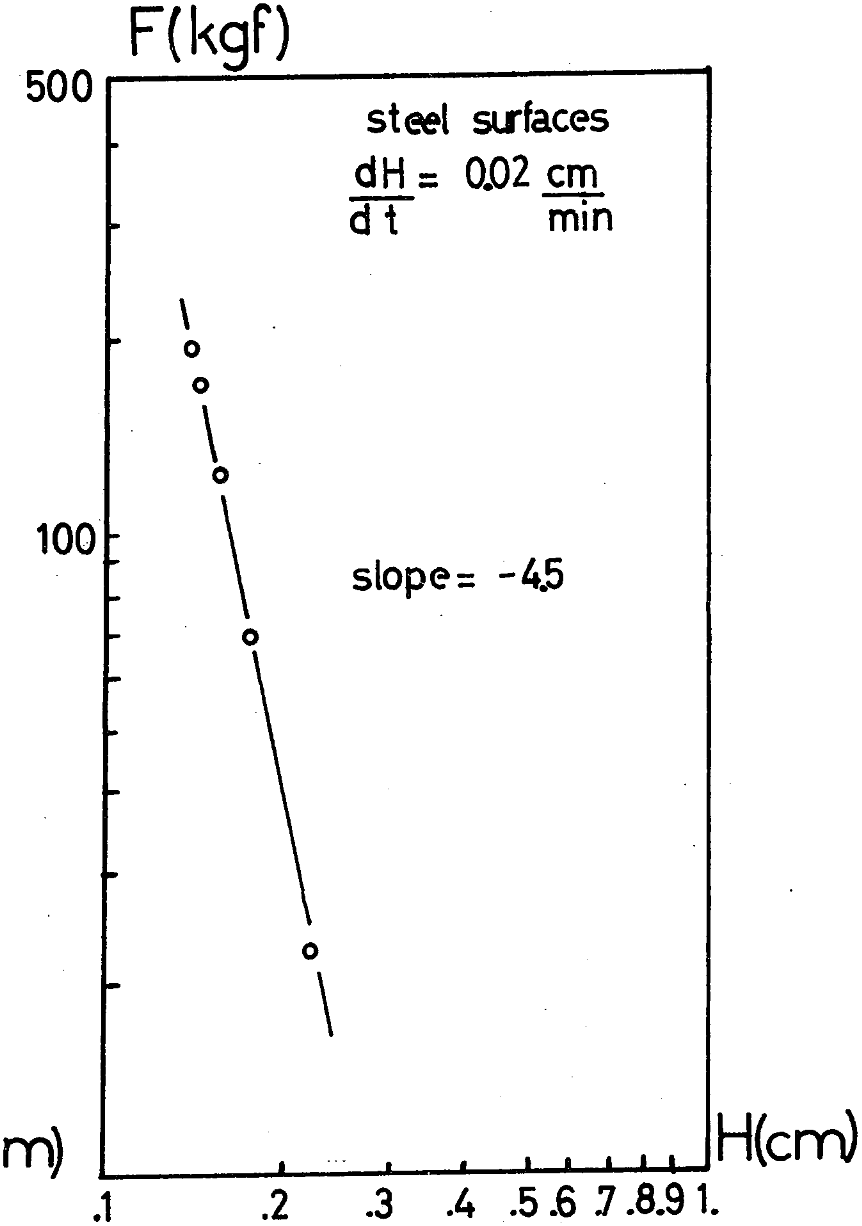

FIGURE 23b-POLYSTYRENE SHEARED AT CONSTANT VOLUME IN THE PLASTOMETER

Newtonian over the range of shear rates from 0 to 0.4 sec^{-1}. The power law relation is valid up to a shear rate of 1.4 sec^{-1}.

Three more experiments were performed with the PS. These were done at constant volume starting with molded samples 2 x 2 x 3/32 inches and shearing them to 4 x 2 x 3/64 inches. To establish the effect of the Instron crosshead speed on the index n determined, two experiments were done at speeds of 0.05 and 0.02 cm/min and at 200°C. These are plotted in Figures 23B and 24A. No Newtonian region was found in these experiments as the shear rates were too high. The power law index was 0.5 in both cases. The η_o was calculated as 16×10^4 poise with a crosshead speed of 0.02 cm/min which is in reasonable agreement with the value found in the constant length experiment.

A final experiment at a 0.02 cm/min crosshead speed, this time with Teflon surfaces, gave a value for n of 0.4. The Kraton 1101 would have to be sheared between Teflon surfaces and it was desirable to see if the Teflon had a great effect on the flow. See Figure 24B. The power law index was slightly affected, but from the figure the flow can still be described by a power law. Thus the equations developed in Appendix A can be applied for flow between Teflon surfaces.

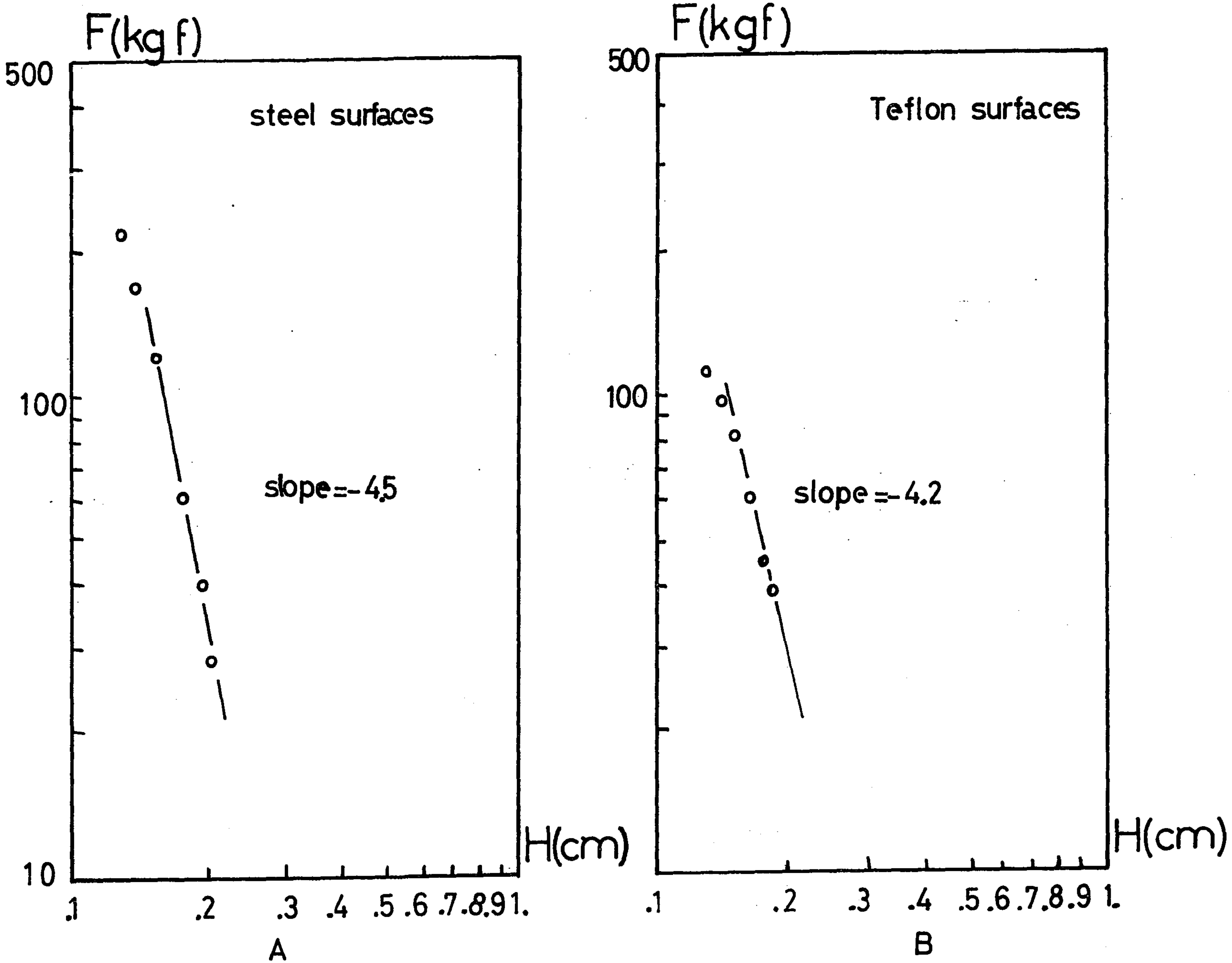

FIGURE 24- POLYSTYRENE SHEARED AT CONSTANT VOLUME IN THE PLASTOMETER

It has been demonstrated that the plastometer, while not suited for precise flow characterizations of polymers, can give reasonable viscosities and power law relations when used in the above manner. Thus while doing shearing experiments to produce anisotropic sheets for mechanical testing, a good idea of the flow properties of Kraton 1101 can be found. It is very hard to find these properties of materials like Kraton 1101 due to their very high viscosities. (Even when heated to 200°C they retain their shape, i.e. do not flow in the usual sense of the word.)

ii) Shearing of Kraton 1101 in the Plastometer

To find the flow characteristics of Kraton 1101, three shearing experiments were done at 200°C with a cross-head speed of 0.02 cm/min. Teflon lined surfaces were used. When shearing was finished, the cooling water was turned on right away.

In the first experiment a molded sheet 2 x 2 x 0.08 inches was sheared at constant volume to 2 x 4 x 0.04 inches. The next two experiments were shearing sheets in the plastometer that had been previously sheared in the pressure flow device at a flow rate of 1.3 cm^3/min. Two sheets 2 x 2 x 0.08 inches were cut from a sheet previously sheared in the pressure flow device. One of these sheets was placed in the plastometer so that it was sheared again in the same direction, and the other was placed so that it was resheared in a direction normal to that of the first shearing. Plots of log (F) versus log (H) for these experiments are given in Figure 25. The curves are linear for thicker gaps heights (lower shear rates) and as the gap height becomes smaller the curves become non-linear. This is because the assumptions made in deriving the equations to describe the flow no longer hold. See Appendix A. The figure also shows a molded sample that was sheared at 0.02 cm/min between steel plates. This made very little difference.

Table 6 below gives the power law constants for the three experiments and the shear stresses in the region where the power law holds. The shear stress under which the experiments were carried out is greater than 1.7×10^5 dynes/cm^2. Thus the stress is close to or above the transition stress discussed earlier. The previously sheared samples show a stronger shear dependence than the molded samples, and the data shows that it is easier to shear in the direction normal to the previous direction of shearing than along it.

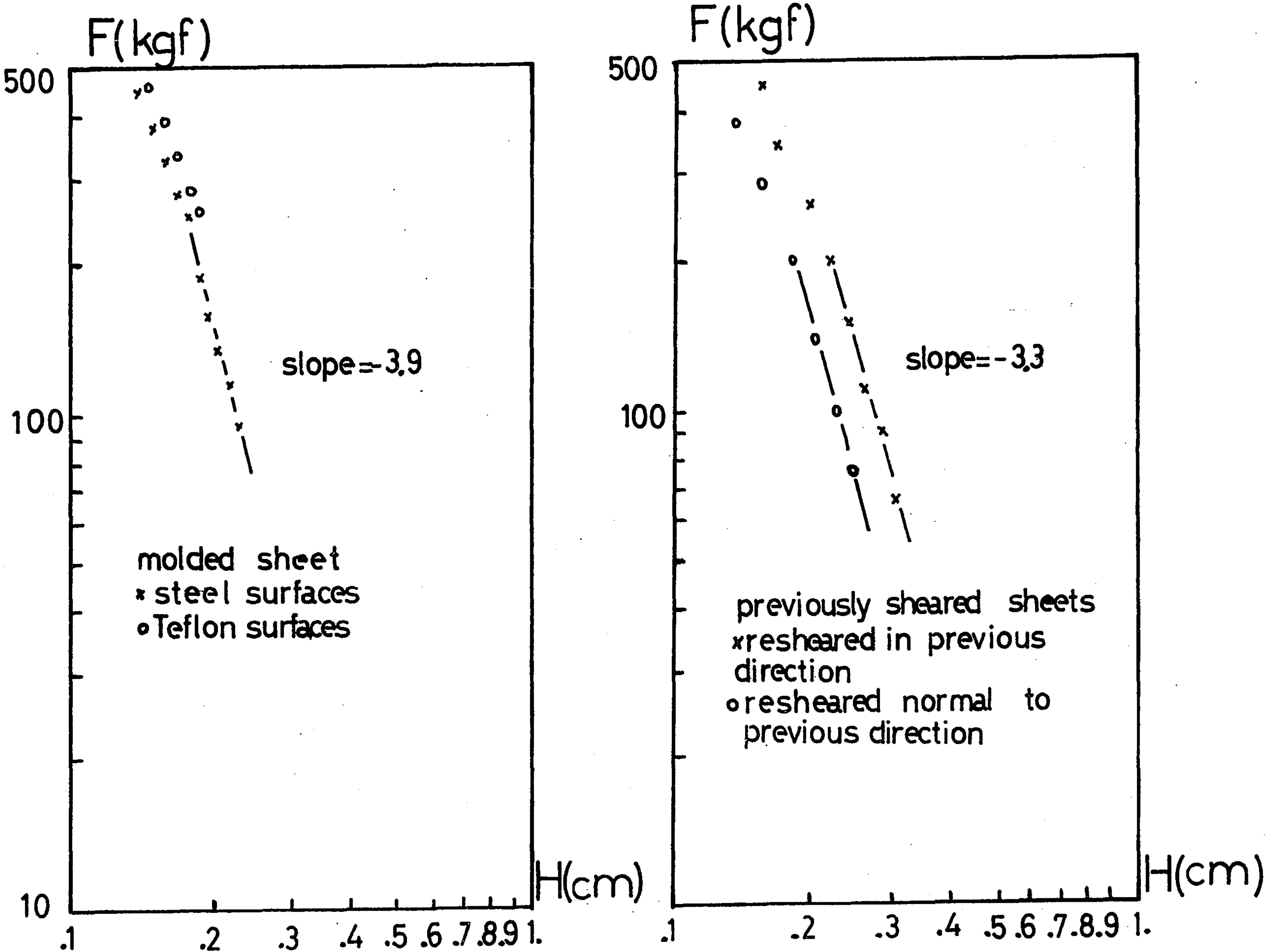

FIGURE 25 - KRATON 1101 SHEARED AT CONSTANT VOLUME IN THE PLASTOMETER

TABLE 6

FLOW PROPERTIES OF KRATON 1101

	η_o poise	n	Limits for τ_W (dynes/cm^2) 1 cm from middle	Limits for τ_W (dynes/cm^2) 5 cm from middle
Moulded Sample	4.5×10^5	0.3	2.4×10^5 1.7×10^5	3.9×10^5 2.8×10^5
Sheared Again Previous Flow Direction	5×10^5	0.1	4.3×10^5 7×10^5	3.9×10^5 6.3×10^5
Sheared Again Normal to Previous Flow Direction	3×10^5	0.1	2.6×10^5 4.2×10^5	2.4×10^5 3.9×10^5

b) Mechanical Behaviour of Sheared Sheets

The experiments performed to study the flow behavior of the Kraton were repeated, but at a crosshead speed of 0.05 cm/min, to prepare sheets for mechanical testing.

First samples were cut from the molded sheet sheared at constant volume. A smaller dumbell sample cutter with a uniform section 0.25 cm wide and 3.0 cm long, and with a 15° taper increasing the width to 0.5 cm at the clamps was used.

This worked well with the smaller sample thickness of 0.04 inches. The work on the pressure flow device showed that small changes in the shear stress around 10^6 dynes/cm^2 did not affect the anisotropy of the sheared sheets to a great extent. Therefore the longitudinal sample was cut near the edge of the sheet, and the reference marks for determining the elongation were put 1 cm apart. The stress-strain curves for the longitudinal and transverse samples are shown in Figure 26. The behaviour is almost identical to the samples tested from sheets sheared in the pressure flow device. This seems to indicate that the mechanism producing the orientation is similar in both devices, shear flow, and the entrance region in the pressure flow device does not have much effect.

The most interesting experiments are those using the previously sheared sheets. Stress-strain curves for samples cut from the sheet resheared perpendicular to the previous flow direction are shown in Figure 27. The anisotropy of the sheet is almost destroyed. The stress-strain curve for both longitudinal and transverse samples falls in between the corresponding curves in the previous case. This seems to indicate that deformation of the polystyrene domains was destroyed, a fact which will be demonstrated when the X-ray scattering is discussed. The behaviour of this

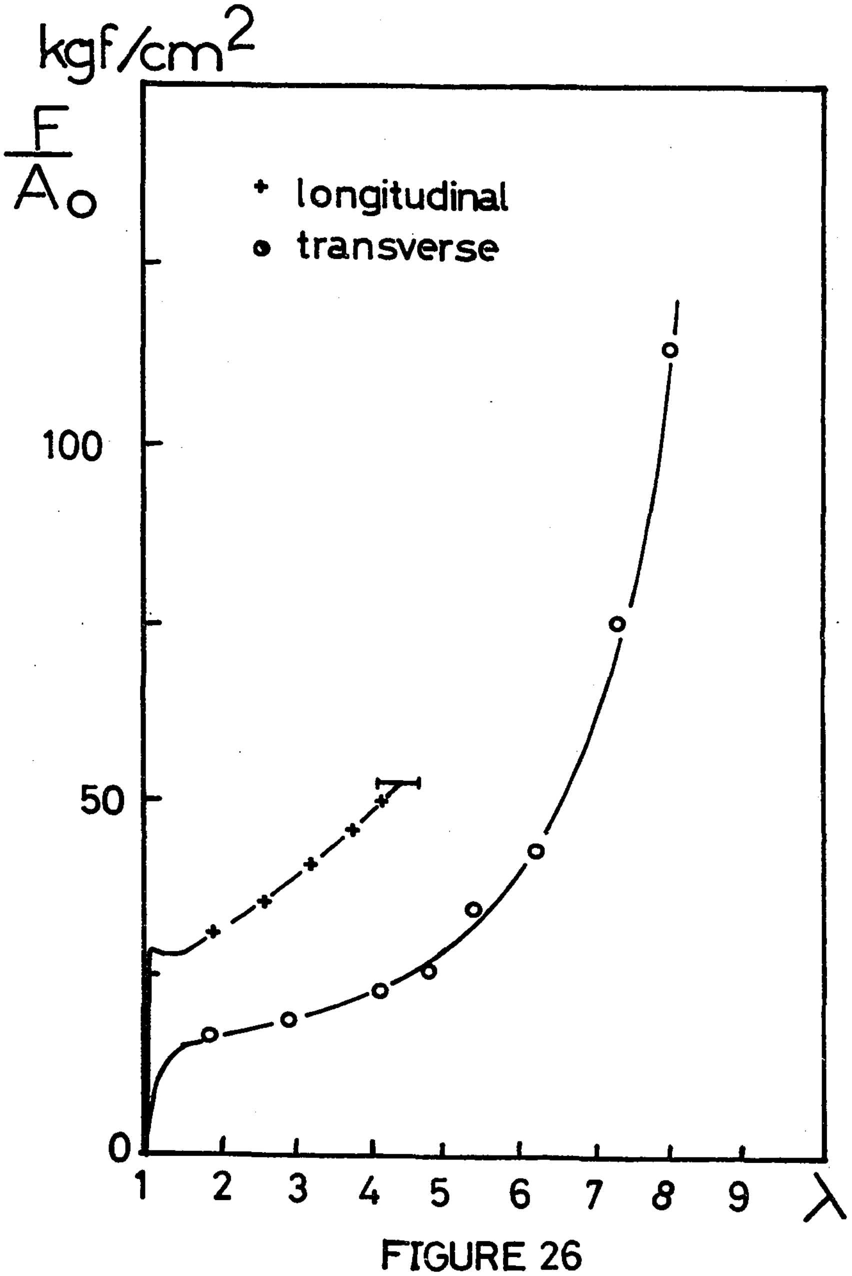

FIGURE 26

STRESS-STRAIN CURVES OF SAMPLES FROM A MOLDED SHEET SHEARED IN THE PLASTOMETER

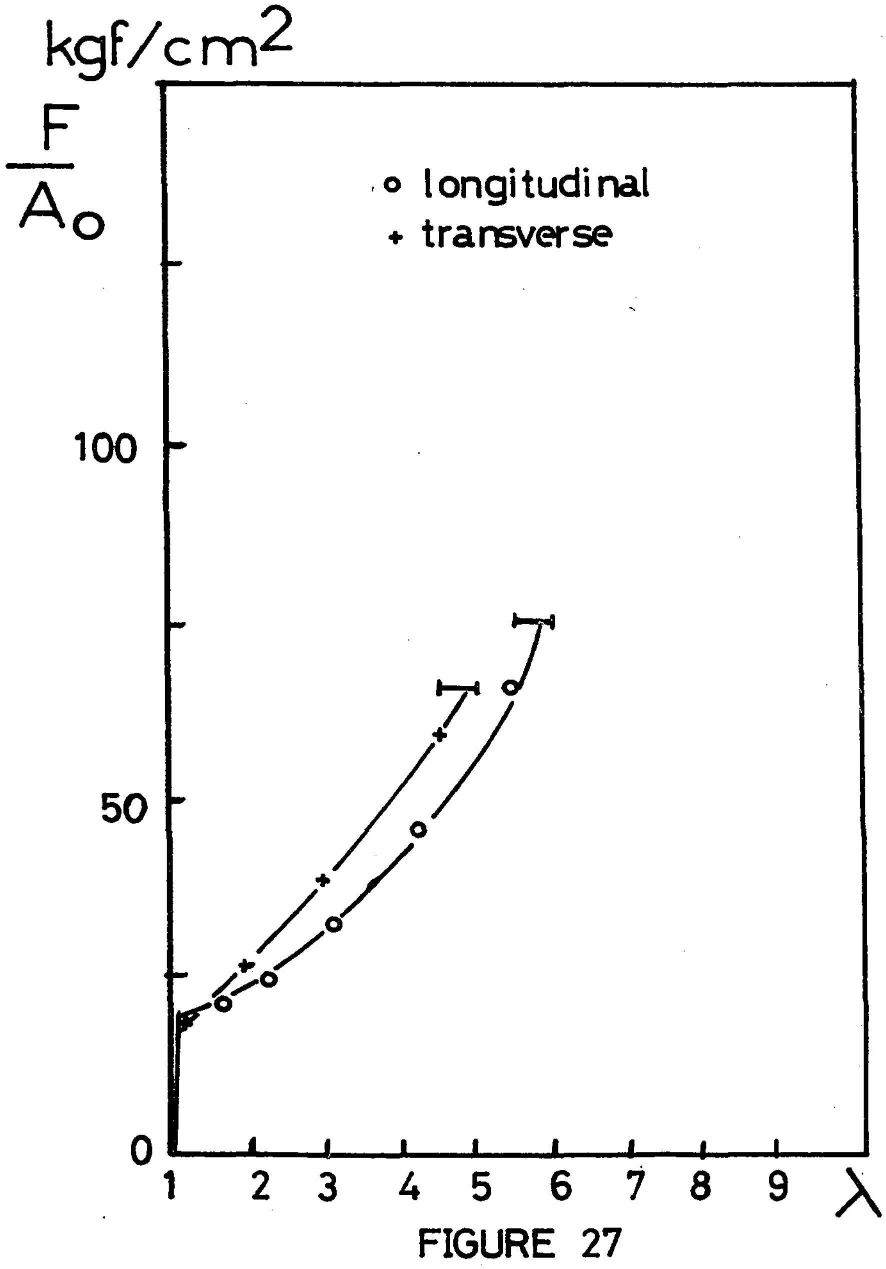

FIGURE 27

STRESS-STRAIN CURVES OF SAMPLES FROM A SHEET SHEARED IN THE PRESSURE FLOW DEVICE AND RESHEARED IN THE PLASTOMETER NORMAL TO THE PREVIOUS DIRECTION OF SHEAR sheet, however, does not correspond to a compression molded sheet. The stress levels are higher in this case. Stress-strain curves for samples cut from the sheet resheared in the direction of the previous shearing are shown in Figure 28. Anisotropy is markedly increased and the longitudinal sample breaks at an extension ratio of 2. The transverse direction is not much affected. This means that the polystyrene domains are so much elongated that fracture occurs almost immediately. It was discussed in the literature survey that fracture of S-B-S block copolymers always occurred by gross deformation of the polystyrene domains.

4. Morphology Investigated by Low Angle X-Ray Scattering

Low angle X-ray scattering was the first method used in this study to establish the morphology of the sheared samples. This method has the advantages of being relatively easy to use and giving information about the bulk material, but the disadvantage of being open to various interpretations.

a) Theory

Small angle X-ray scattering lies in the region where the angle is less than five degrees. In the case of Bragg diffraction where the scattering is produced from a periodicity in the structure, the repeat distance, d, is given by Bragg's relation (33).

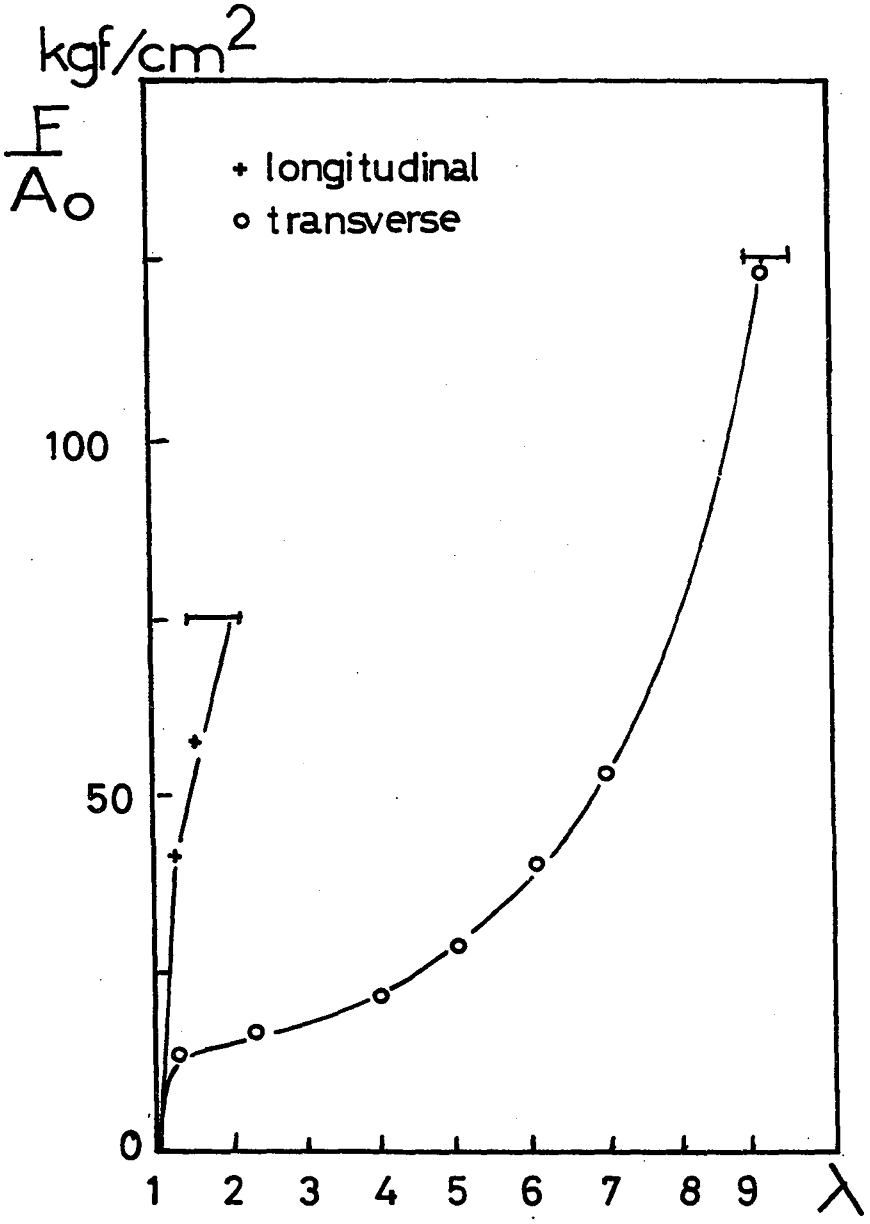

FIGURE 28

STRESS STRAIN CURVES OF SAMPLES FROM A SHEET SHEARED IN THE PRESSURE FLOW DEVICE AND RESHEARED IN THE PLASTOMETER IN THE PREVIOUS DIRECTION OF SHEAR

$$d = \frac{n\lambda}{2\sin\theta} \qquad \ldots\ldots\ldots\ldots\ldots (14)$$

Here λ is the wavelength, n is the order of the scattering peak, and θ is one half of the scattering angle.

However, the scattering produced by an assemblage of small domains or particles is not related to this Bragg scattering. The scattering arises because the domains have a different electron density that the matrix material. Guinier (33) gives the theoretical derivation of the equations describing the scattering. A brief discussion of his theory is necessary so that some quantitative information can be obtained from the photographs taken in this study.

The scattered intensity is composed of two terms. The first depends only on the size and shape of the particles. It has a maximum intensity at a zero angle,and becomes zero at angle of order of magnitude λ/D, where D is the size of the particles under consideration. If the particles are from 10 to 1000 A this central peak is observable.

The second term represents the ordinary diffraction pattern at larger angles. There are three cases here. If the electron density of the sample is periodic, then periodic peaks appear in the diffraction pattern determined by Bragg's relation. If the material is amorphous the electron density is irregular and broad rings appear. If there are faults in the crystal structure the breadth of the Bragg peaks is affected. However, in both of these latter cases the central peak is unaffected. The general expression which describes the scattering is (33):

$$\underline{I}(h) \quad \alpha \quad F^2(h) \quad a(h) \qquad \ldots\ldots\ldots\ldots\ldots(15)$$

$h = 4\pi \sin\theta/\lambda$, $\underline{I}(h)$ is the scattered intensity, $F^2(h)$ is the form factor which depends on the particle size and shape, and $a(h)$ is the interparticle interference function.

Guinier has developed a theory which applies to dilute systems where interactions between particles are negligible. In this case the scattering is the sum of the scattering for each individual particle. For a non-oriented system it is the average of the scattering from one particle over all orientations; for an oriented system the scattering is just an integer times the scattering for one particle. With such a dilute system Guinier describes a method for obtaining particle size information from the central peak of the scattering. However, Kraton 1101 does not contain a dilute quantity of PS domains, so examining the central peak itself would be of little interest in this study.

However, if the shape of the scattering particle is known, the form function $F^2(h)$ can be calculated. Lewis and Price (34) give this function for a system of long parallel cylinders:

$$F^2(h) = 2J_1(hR)/(hR) \qquad \text{..........(16)}$$

where J_1 is the first order Bessel function, and R is the radius of the cylinders. This is an oscillating function.

McIntyre and Campoz-Lopez (10) show how a knowledge of the form factor can be used to obtain the size of the domains in S-B-S copolymers. They show that the interparticle interference function, a(h), becomes 1 at large enough angles, and that in this range the domain size can be obtained by comparing the experimental scattering peaks to the maxima predicted by the form function. In studying the scattering from a solvent cast S-B-S copolymer with block molecular weights 21,000, 63,000 and 21,000 they found a main interference peak at an angle of two degrees. At larger angles the intensity was low enough to observe the scattering due to the form factor, which in their case was for spheres. They measured the low intensities involved with a counter tube. At angles smaller than two degrees several smaller interference peaks were found. In this region the effect of the form factor was assumed small, and interdomain distances were calculated from the angles corresponding to the peaks using Bragg's law. Finally at very small angles of the order of 3 minutes the intensity rose because of the central peak described by Guinier.

Lewis and Price (34) studied the low angle scattering from compression molded Kraton 1101. They measured the scattered intensity from 0.46 to 2.3 degrees. Like McIntyre and Campos-Lopez they assumed that the effect of the form factor, $F^2(h)$, was small for angles in this range, and would only affect the intensity of the interference peaks determined by a(h). For a highly ordered array of domains the maxima in a(h), and hence $\underline{I}(h)$, would be governed by Bragg's law.

The approach taken by Lewis and Price will be used in analyzing the photographs taken in this work. The form factors will be assumed negligible under 3 degrees, and interdomain distances will be calculated from the scattering peaks using Bragg's law. A model of long hexagonally packed cylinders will be assumed. Once the interdomain distance is found the size of the PS cylinders in Kraton 1101 can be calculated from the volume fraction (28%). The choice of the model is of course open to question, but it is the best one based on previous work (23,34). The scattering observed experimentally must confirm the choosen model for it to be accepted.

b) Experimental

Figure 29 shows the scattering from a sample of Kraton 1101 sheared between aluminum surfaces at 1.3 cm^3/min. The scattering from Kraton 1101 sheared between Teflon at 1.3 cm^3/min

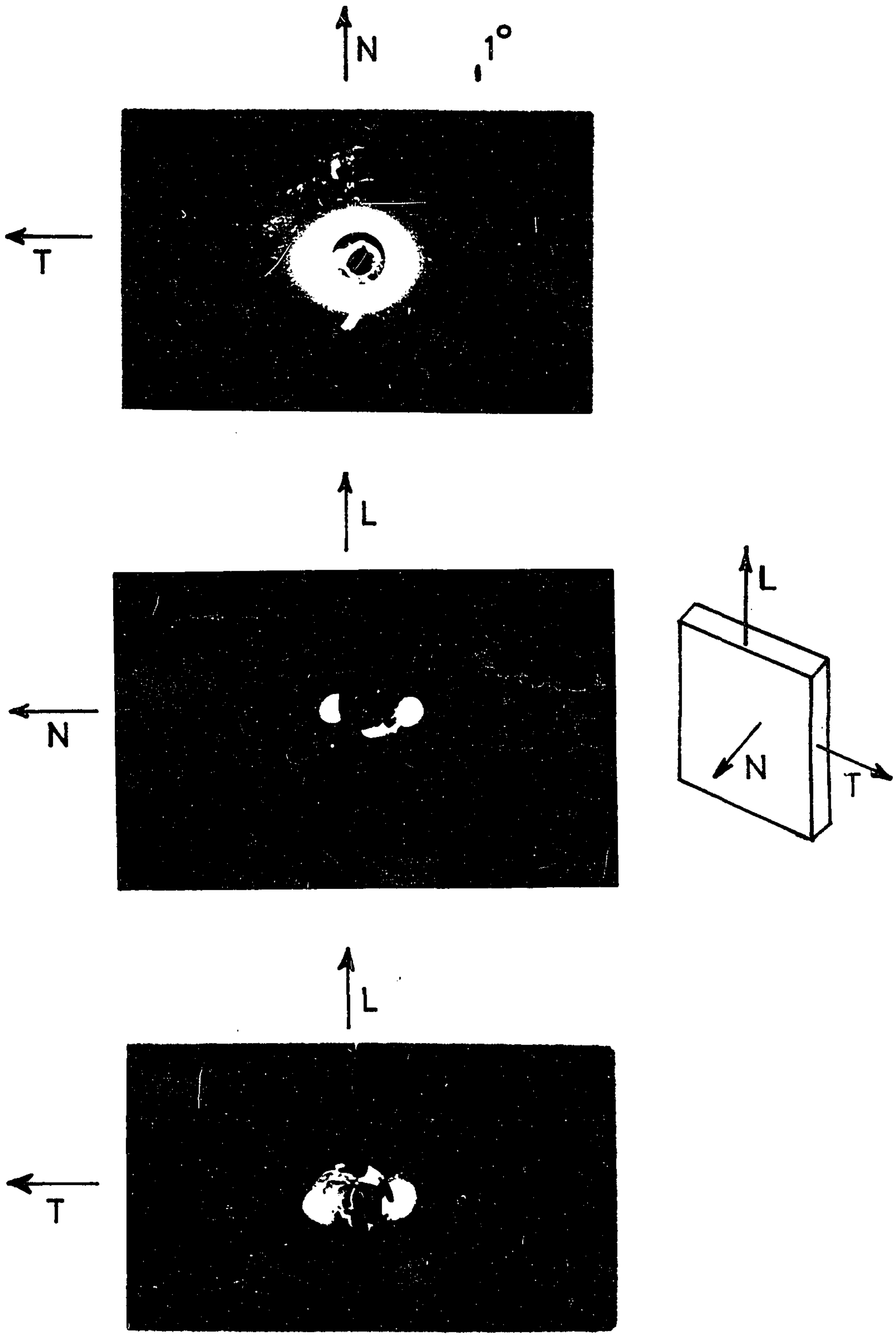

FIGURE 29

LOW ANGLE X RAY SCATTERING FROM A SHEET SHEARED IN THE PRESSURE FLOW DEVICE BETWEEN ALUMINUM SURFACES is shown in Figure 30. Both of these samples were rapidly quenched after the shearing. The X-ray beam was directed through the samples in three directions as shown in Figure 29. Along the sheared direction no preferred orientation is evident, but the other photographs show the orientation along the sheared direction is very marked. There is little difference between the location of the peaks and the shape of the diagram produced by the two samples. On the original negatives three peaks were visible. The central peak described by Guinier appears to be obscured by the beam stop in these photographs.

Table 7 below gives the Bragg angles and distances as determined from the original negatives of the sample sheared between aluminum surfaces. The characteristic ratio di/d1 is the ratio of the interdomain distance corresponding to scattering peak i to the interdomain distance corresponding to the first scattering peak.

TABLE 7

INTERDOMAIN DISTANCES IN KRATON 1101

Peak	2θ radians	di(from Bragg's law) A	di/d1
1	0.2/40	300	1
2	0.35/40	175	0.58
3	0.55/40	110	0.38

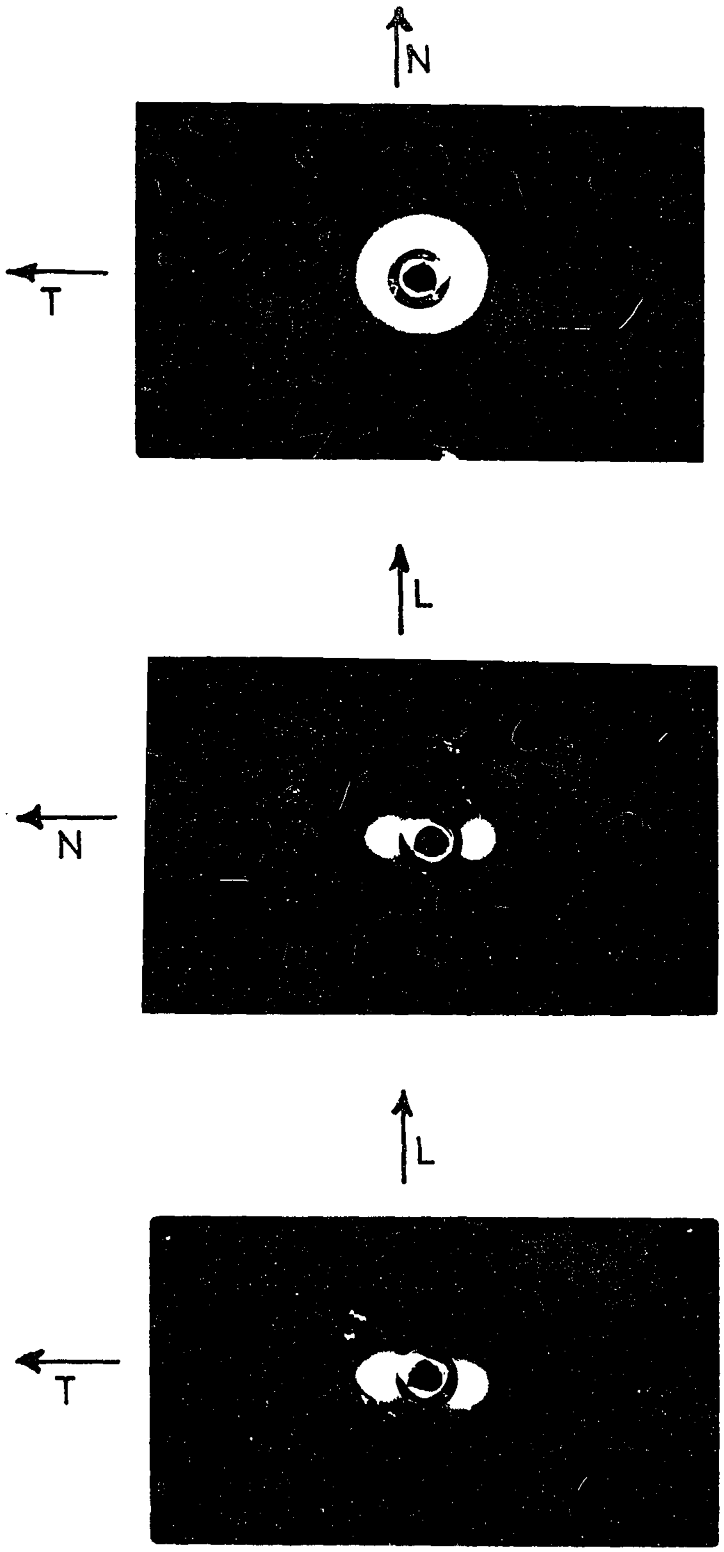

FIGURE 30

LOW ANGLE X RAY SCATTERING FROM A SHEET SHEARED IN THE PRESSURE FLOW DEVICE BETWEEN TEFLON SURFACES

Table 8 gives the theoretical ratios for a hexagonally packed system on long cylinders (34). These are the ratios of the various interplanar distances to the basic one, the centre-to-centre distances of the rods.

TABLE 8

CHARACTERISTIC RATIOS OF A HEXAGONAL SYSTEM OF RODS**

$\frac{dhK}{d_{10}}$	1	0.577	0.500	0.378	0.337
hK (millar indices)	100	110	2000	210	300

$$** \quad \frac{dhK}{d_{10}} = \left[\frac{3}{(h^2 + hK + K^2)}\right]^{\frac{1}{2}}$$

The photographs taken in this study have recorded three peaks at characteristic ratios of 1, 0.58 and 0.38. They agree well with the theoretical values from Table 8, except that the ratio at 0.500 is missing. This can be explained by the effect of the form factor, but first the radius of the cylinders must be calculated.

Based on the centre-to-centre distance of the rods of 300 A given in Table 7, their radius is easily calculated from the volume fraction as 90 A. This distance agrees reasonably well with the value of 75 A found by Keller (23) in X-ray studies of sheared Kraton 102. Kraton 102 has block molecular weights of 10,000, 55,000 and 10,000 compared to 11,000, 53,000 and 11,000 for Kraton 1101. Keller's centre-to-centre distance for the rods was found to be 300 A also. The agreement here is reasonable considering the fact that the scattering was obtained from photographs, and the shearing conditions were quite different in the two experiments.

The missing peak can now be explained. The function $F^2(h)$ for cylinders is calculated to be a minimum (34) when hR = 3.8. This corresponds to $d_{min}/d_{10} = 0.42$. This is approximately the characteristic ratio where the expected peak was missing.

Thus the morphology of the sheared samples can be approximated by long cylinders of PS about 180 A in diameter in a matrix of PB, with a centre-to-centre distance between cylinders of about 300 A. Keller found a hexagonal arrangement of cylinders in his sheared sample. The arrangement of cylinders is probably more random in this study as the X-ray diagram along the extrusion direction is a ring, not hexagonal spots as found by Keller.

The remaining diagrams are shown to provide insight into the effects on morphology of the remaining experiments performed. Figure 31 shows an X-ray diagram of a sample of Kraton 1101 which was sheared between Teflon plates at a flowrate of 1.3 cm^3/min. However, unlike the sample of Figure 30,this sample fractured in the longitudinal direction at an elongation ratio of approximately five. The diagram shows that the orientation is not as perfect in this sample.

An X-ray photograph of the sheet that was annealed in the pressure flow device for two hours before quenching is shown in Figure 32. The shape and arrangement in space of PS domains appears unaffected by the annealing.

Figure 33 shows the X-ray scattering of a sample resulting from the shearing in the plastometer of a molded sheet. The scattering is essentially the same as for samples sheared in the pressure flow device. Figures 34 and 35 confirm that samples previously sheared in the pressure device have their orientation destroyed or reinforced by shearing again in the plastometer in a normal direction and in the same direction respectively.

5. Morphology Investigated by Electron Microscopy

Two pictures were taken on a Philip's microscope using the method described in the section on apparatus. Samples

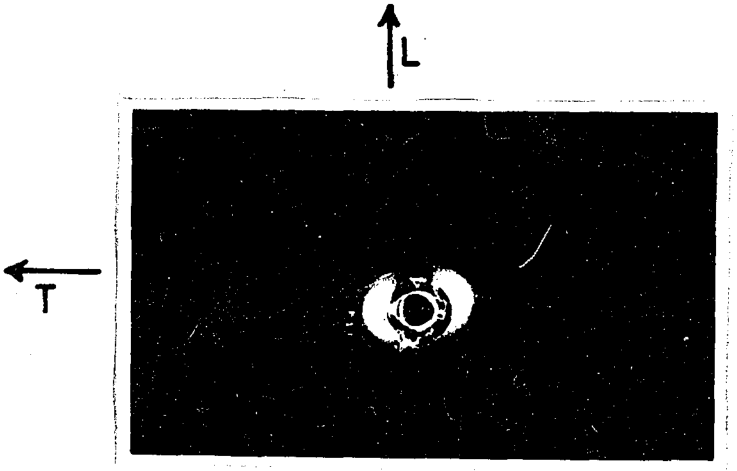

FIGURE 31
SCATTERING FROM A SHEET SHEARED IN THE PRESSURE FLOW DEVICE BETWEEN TEFLON SURFACES WHICH BROKE AT LOW ELONGATIONS

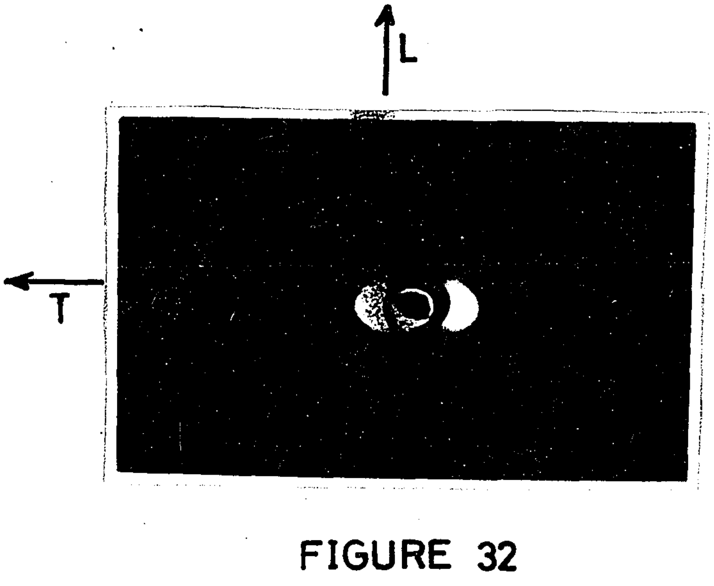

FIGURE 32
SCATTERING FROM A SHEET SHEARED AND ANNEALED IN THE PRESSURE FLOW DEVICE BETWEEN TEFLON SURFACES

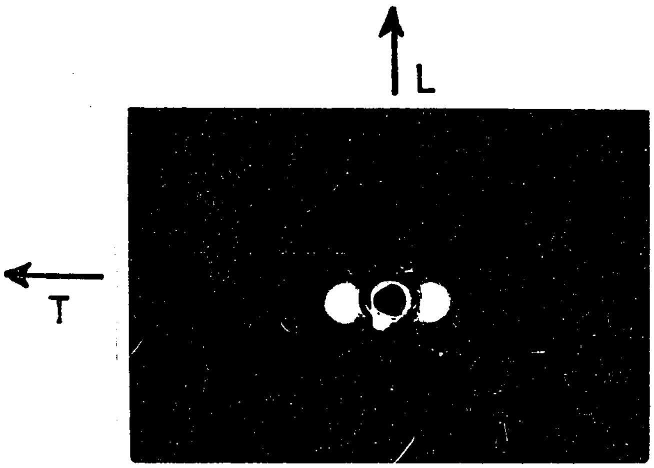

FIGURE 33 -SCATTERING FROM A MOLDED SHEET SHEARED IN THE PLASTOMETER

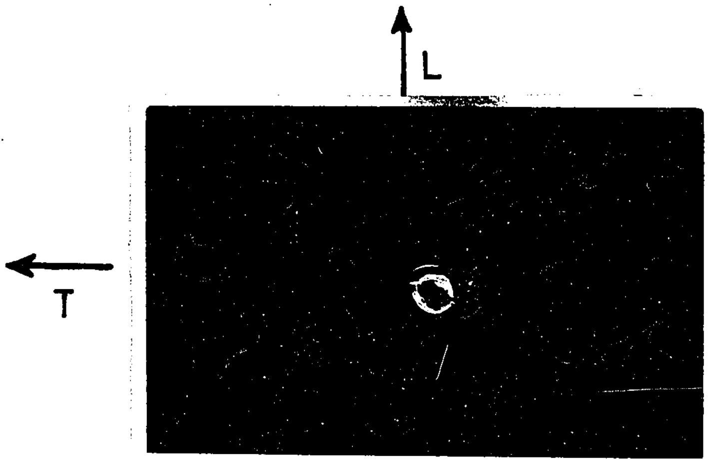

FIGURE 34 - SCATTERING FROM A SHEET SHEARED IN THE PRESSURE FLOW DEVICE AND RESHEARED IN THE PLASTOMETER IN A NORMAL DIRECTION

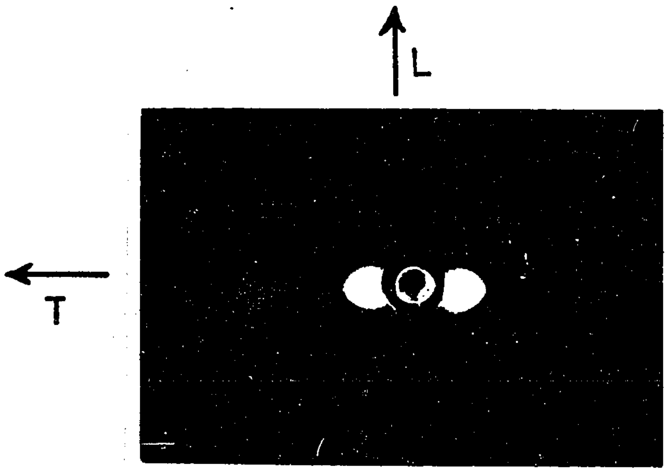

FIGURE 35 - SCATTERING FROM A SHEET SHEARED IN THE PRESSURE FLOW DEVICE AND RESHEARED IN THE PLASTOMETER IN THE SAME DIRECTION

were obtained from a sheet sheared between Teflon surfaces at 1.3 cm^3/min in the pressure flow device. Figure 36(a) shows an electron micrograph taken along the shearing direction. The white spots on the picture are the ends of the polystyrene rods. The rods are generally randomly arranged although some are arranged in a hexagonal fashion. The rods have a radius from 70 to 100A, which agrees with the value found from the X-ray scattering. The interdomain distance is of the order of 300 A, which also agrees with the value found by X-ray scattering. Figure 36(b) shows a picture taken perpendicular to the sheared sheet. The elongated regions of PS are obvious. The structure is wavy, and this probably is similar to the default planes found by Keller in his electron microscope study of sheared Kraton. The length between faults is of the order of 1000 A.

Thus it has been confirmed by X-ray scattering and by electron microscopy that shearing in the pressure flow device changes the morphology of Kraton 1101 from spherical domains of PS suspended in a matrix of PB to long cylinders of PS.

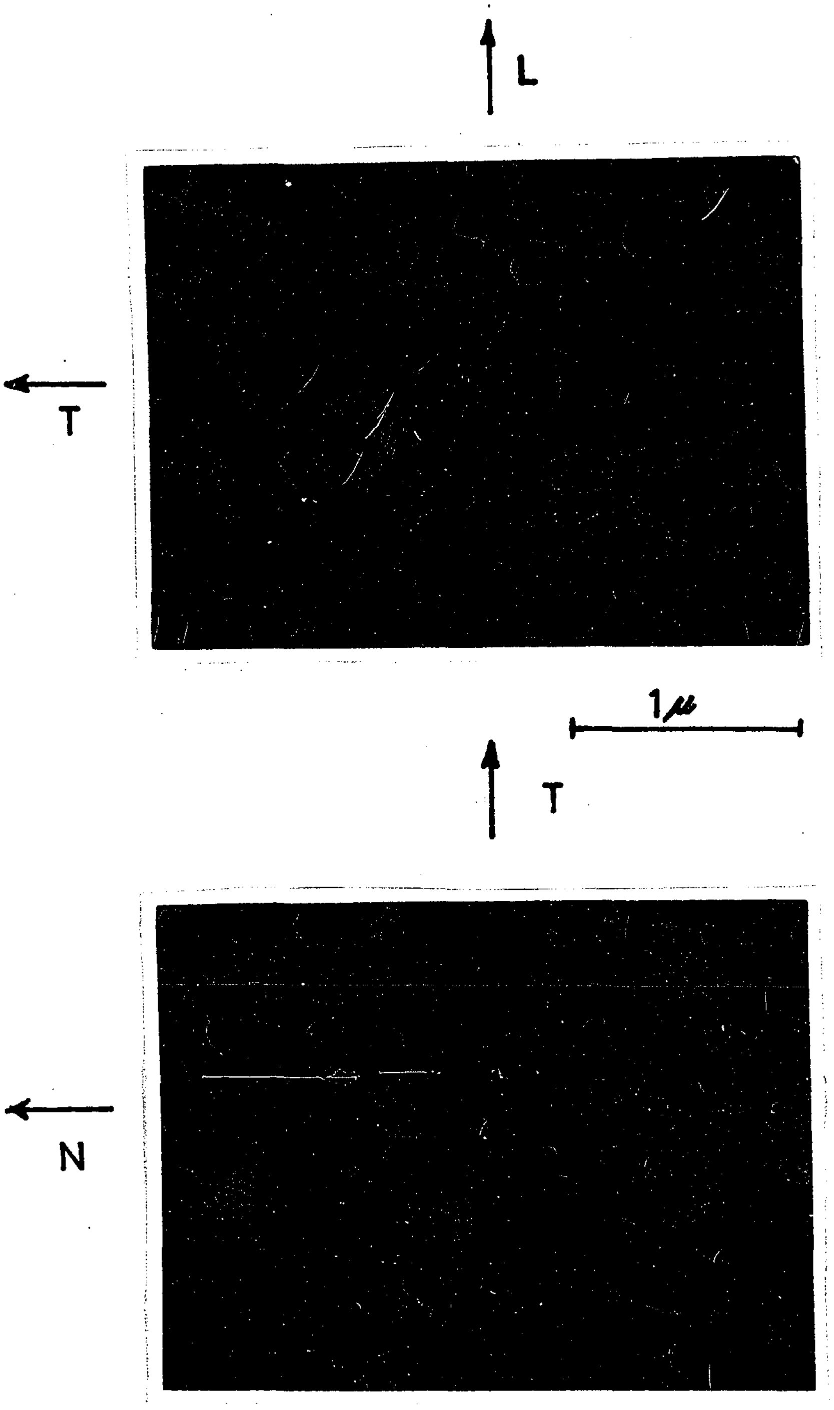

FIGURE 36

ELECTRON MICROGRAPHS OF SHEARED KRATON 1101

V. DISCUSSION

1. Effect of Shearing on the Domains During and Subsequent to Shearing

We have seen how Kraton 1101 PS domains can be changed by shearing from a spherical shape to very long cylinders. Both structures are relatively stable and do not change upon annealing. The mechanism for the change from spheres to cylinders can be better understood if we first look at domain deformation under shear, and then examine domain formation once shearing is stopped.

One can consider three separate regions of flow of molten Kraton 1101. These are shown in Figure 37. The first, at slow small amplitude oscillations, involves a largely elastic deformation of a three dimensional network, the domains of PS being interconnected by chemical bonds; there could be a yield stress associated with the failure of the bonds or pulling out of PS segments from the domains. The second, at low shear rates, involves breaking down of the network, aggregates of PS could remain or would reform from the free PS segments. The third, at high shear rates, would involve the flow of individual molecules, all the PS segments having been pulled from the domains; in this region the material would flow similar to a thermoplastic. These three regions are similar to those proposed by Arnold and Meier (19). At low enough

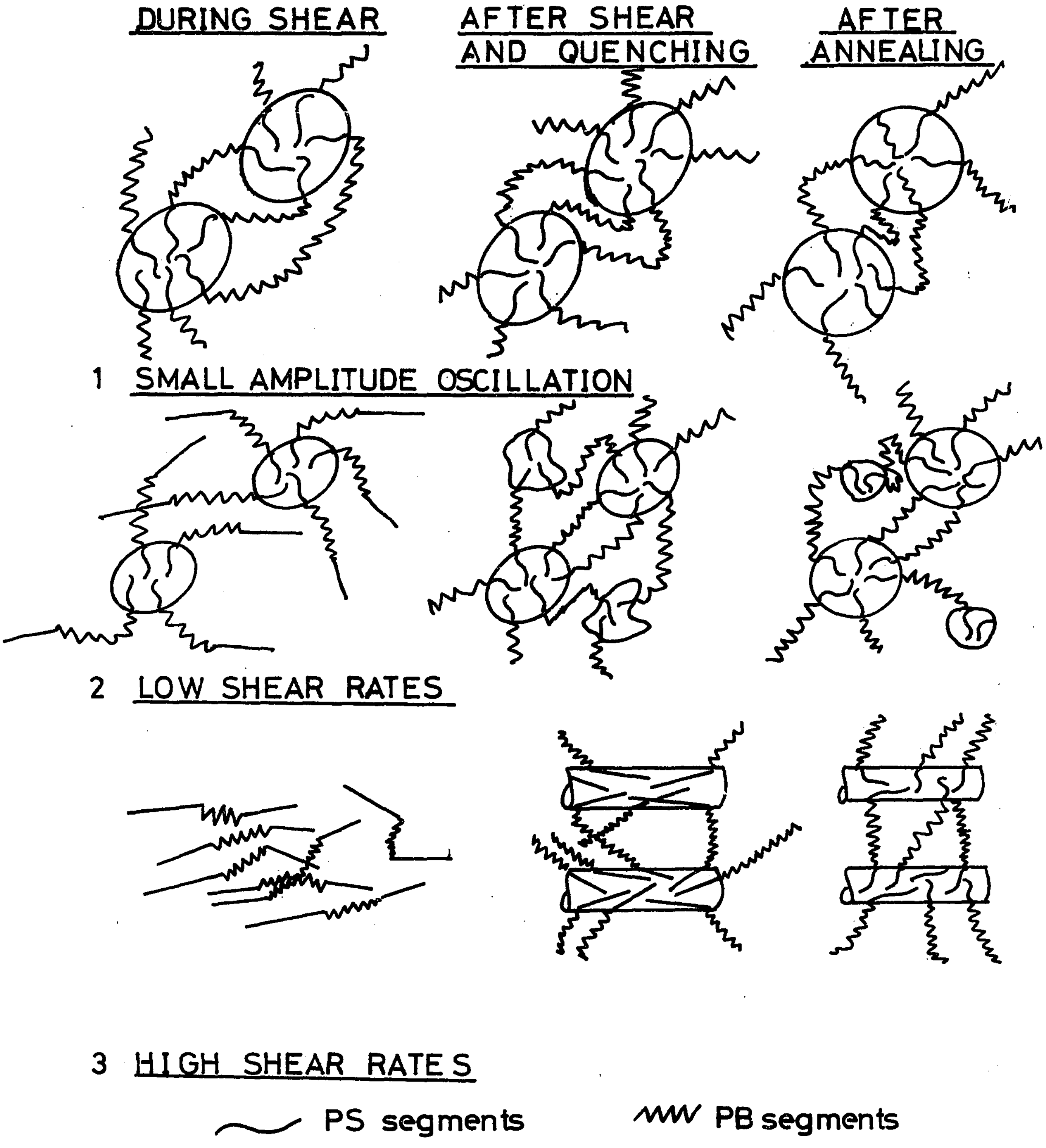

FIGURE 37

EFFECT OF SHEARING AND ANNEALING ON PS DOMAINS IN KRATON 1101 shear rates the stresses are not high enough to overcome the thermodynamic forces leading to domains of PS, but at high shear rates these stresses become great enough to destroy the domains.

The transition to the flow typical of thermoplastic behaviour has been described earlier as taking place at a shear stress of about 4.5×10^5 dynes/cm^2. The shearings in this work were done at a wall sheas stress from 1.7×10^5 to 4.8×10^5 dynes/cm^2. In the apparatus used the shear stress varied from 0 at the center to a maximum at the wall, and thus a variation in the state of disruption of the domains was involved. However over most of the thickness of the samples shear stresses were probably high enough to destroy the domains. The fact that a power law could be used to describe the flow of Kraton in the plastometer shows that the transition to thermoplastic behaviour had likely taken place. This is probably why changes in shear stress in the range studied produced little change in mechanical properties of the sheared sheets. Once destroyed the domains probably reform in the same manner independent of the shear stress applied.

The type of domain reformed once the shear stress was removed was found to be long parallel cylinders in this work. In Appendix D calculations are given which show that the formation of such cylindrical domains is thermodynamically favoured over the formation of spherical domains. The free energy change turns out to be positive for the formation of spherical domains from sheared material, and negative for cylindrical domains. The calculations assume that shearing at high rates extends the PS segments to their fully extended length.

After shearing is ceased and the plates of Kraton 1101 rapidly quenched the PS ends are probably still left to some extent in an extended state. Some PB chains are likely extended from the equilibrium state as well, held by the frozen PS segments. As we have seen annealing at the T_g of the PS or above reduced stress levels in stress-strain measurements. It was postulated that this was because the PB segments were free to return to a more random position because motion of the PS segments was possible within the domains above the T_g of the PS. At the same time the PS segments probably return, too, to a more random state within the domains. The gross shrinkage observed in the longitudinal direction while annealing samples in boiling water was evidence for this rearrangement. As discussed previously, annealing probably also increases the purity of the PS, and by doing so increases the initial modulus of the sheared material. Changes taking place after shearing at high rates and during annealing are also shown in Figure 37.

The Figure also shows some postulated effects on the domains when shearing is removed and when the material is annealed after shearing at low rates and after slow small amplitude oscillations. During shearing at low rates the aggregates could be deformed to ellipsoids inclined to the direction of shearing. When the shearing is stopped the lose PS segments might tend to form smaller irregular domains. Annealing might permit the PS segments in these smaller domains to diffuse to the larger ellipsoids, and also to return the ellipsoids to a more spherical shape. Slow small amplitude oscillations probably would only distort the domains slightly to ellipsoids, which would return to a spherical shape upon annealing.

2. Young's Modulus of Compression Molded and Sheared Kraton 1101

The initial Young's modulus reveals much about the structure of the material. In Appendix C a cubic model is developed which can describe the modulus of compression molded and sheared Kraton 1101. The model assumes for simplicity a cubic arrangement of parallelepipeds. The possibility exists for interconnections between these particles in three perpendicular directions. See Figure C1. Two formulas for the modulus are derived, and these correspond to reasonable bounds for the predicted modulus. These are given below. The various symbols are defined in Figure C1.

$$K_a = \frac{A}{A + \Delta} \qquad K_b = \frac{B}{B + \Delta} \qquad K_c = \frac{C}{C + \Delta}$$

$$K_a' = \frac{A'}{A} \qquad K_b' = \frac{B'}{B} \qquad K_c' = \frac{C'}{C}$$

K_a, K_b and K_c indicate the relative size of the particle in each direction. K_a', K_b', K_c' indicate the relative size of the interconnections between particles.

E_p = modulus of particulate material, PS,(E_s)

E_m = modulus of the matrix material, PB, (E_b)

E_c = modulus of two phase material

V_p = volume fraction of particulate material (V_s)

$$\frac{E_c}{E_m} = K_a\ K_b\ K_a'\ K_b'\ \frac{E_p}{E_m} + \frac{K_a\ K_b\ (1 - K_a'\ K_b')}{K_c\ \frac{E_m}{E_p} + (1 - K_c)}$$

$$+ \frac{K_a'\ K_a\ (1 - K_b) + K_b'\ K_b\ (1 - K_a)}{K_c'\ K_c\ \frac{E_m}{E_p} + 1 - K_c'\ K_c}$$

$$+\ 1 - K_a\ K_b - K_a\ K_a'\ (1 - K_b) - K_b'\ K_b\ (1 - K_a)$$

............(17)

$$\left(\frac{E_c}{E_m}\right)^{-1} = K_c\,K'_c\,\left(K_a\,K_b + K'_a\,K_a(1-K_b) + K_b\,K'_b(1-K_a)\,\frac{E_p}{E_m}\right.$$

$$\left. + \; 1 - K_aK_b - K_aK'_a\,(1 - K_b) - K_bK'_b\,(1 - K_a)\right)^{-1}$$

$$+ \; (K_c - K_cK'_c)\left(K_aK_b\,\frac{E_p}{E_m} + 1 - K_aK_b\right)^{-1}$$

$$+ \; (1 - K_c)\left(K_aK_bK'_aK'_b\,\frac{E_p}{E_m} + 1 - K_aK_b\,K'_aK'_b\right)^{-1}$$

$$\dots\dots\dots(18)$$

$$V_p = K_aK_bK_c + K'_aK_aK_b(1 - K_c)K'_b + K'_aK_aK_c(1 - K_b)K'_c + K'_bK_bK_c(1 - K_a)K'_c$$

$$\dots\dots\dots(19)$$

For compression molded samples $K_a = K_b = K_c$ so that the model is a cubic arrangement of interconnected cubes, and K'_a, K'_b and K'_c are chosen so that $K'_a = WK_a$, $K'_b = WK_b$ and $K'_c = WK_c$. W is a constant that can have a value from 0, corresponding to no interconnections, to 1 corresponding to $K'_a = K_a$ etc. The choice of the model to represent the interconnections is an arbitrary one. There may be ways to calculate K'_a, K'_b and K'_c based on the geometry of the system, but this is not the purpose of this work. The purpose is to show that the modulus of compression molded samples is too high to be achieved with no interconnections. The function chosen to represent K_a', K_b' and K_c' will work well for this. E_c/E_m is 30 using the experimental modulus of 6×10^8 dynes/cm^2 (600 kgf/cm^2) for compression molded samples, and 2×10^7 dynes/cm^2 for the modulus of PB. This is a good estimate given by Dlugosz et al (24). E_p/E_m is 1000 using 2×10^{10} dynes/cm^2 for the modulus of the PS.

In Figure 38 the pairs of E_c/E_m predicted by the model are plotted as functions of V_p and W. In reading the curves the average of the two predictions is used. To obtain $E_c/E_m = 30$ at a volume fraction of 0.28 corresponding to Kraton 1101, W must be approximately 0.2. This corresponds to $K_a' = K_b' = K_c' = 0.13$ indicating that the PS domains should be well interconnected. Beecher et al (6) observed that the ratio of the interconnection size to the domains' size was about 0.1 in Kraton 1101 using electron microscopy.

Data from the literature (20) gave an initial modulus of 4×10^7 dynes/cm^2 for a compression molded S-B-S block copolymer with 25% by volume PS. Here $E_c/E_m = 2$, and by reading Figure 38 it appears that there should be no interconnections between domains in this polymer. This could be due to the lower volume fraction, and to less mixing during the molding process.

The initial Young's modulus can tell us too about the structure of sheared Kraton 1101. The X-ray data and electron micrographs really gave no information about the length of

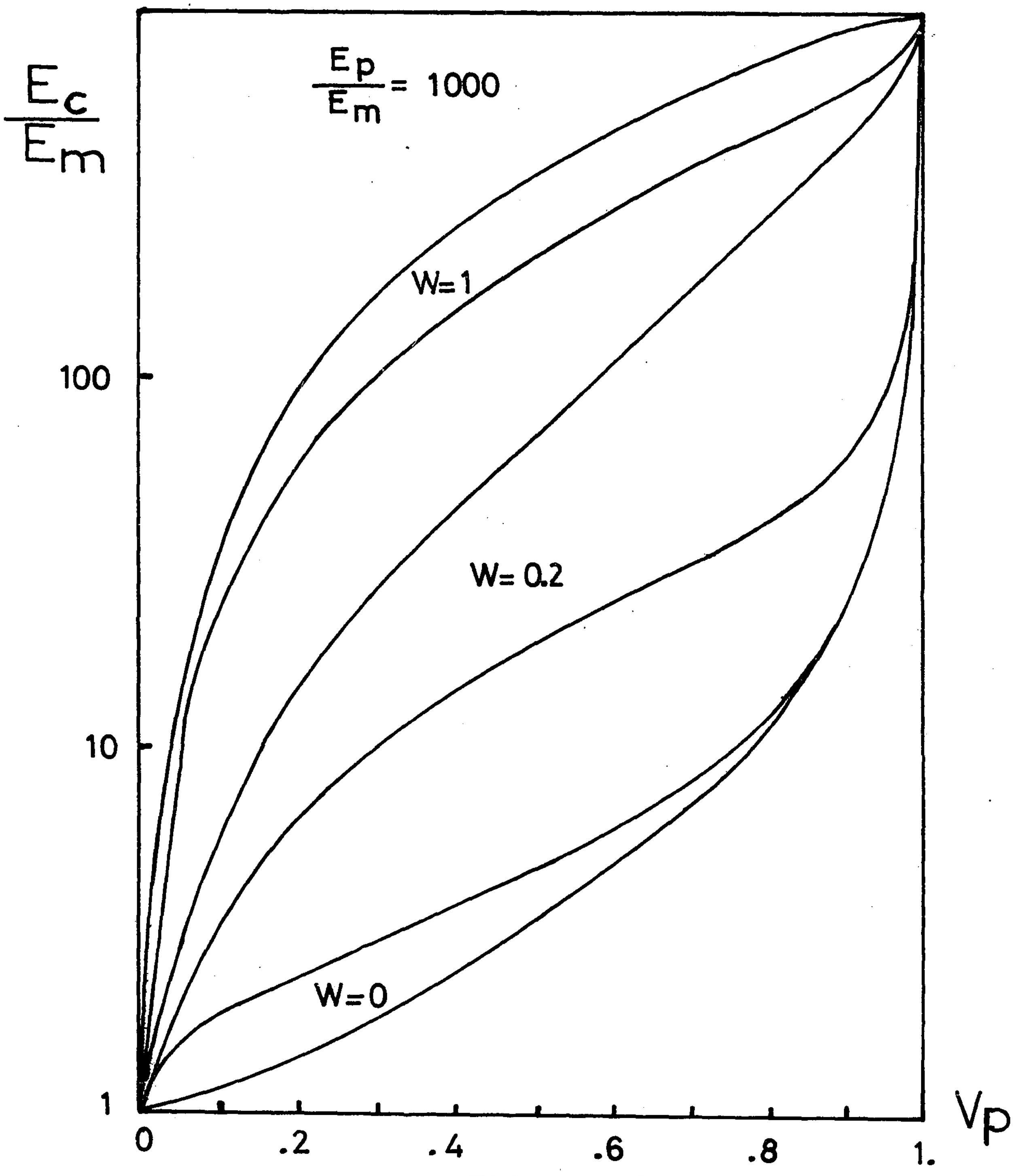

FIGURE 38
PREDICTED MODULI OF COMPRESSION MOLDED SAMPLES

the PS cylinders of the size or interconnections between the cylinders in the transverse direction. What can the initial moduli reveal.

It is first interesting to calculate the moduli in the longitudinal and transverse direction assuming that the PS cylinders are infinitely long. Then the modulus in the longitudinal direction is given by the parallel law.

$$E_\ell = E_b (1 - V_s) + E_s V_s \qquad \text{..........(20)}$$

The modulus in the transverse direction may be calculated by the following relation (37):

$$E_t = \frac{V_s\, E_b(1 - E_b/E_s) + E_b(1 + E_b/E_s)}{(1 + E_b/E_s) - V_s\,(1 - E_b/E_s)} \qquad \text{....(21)}$$

This formula is theoretically valid as long as the particulate phase is dilute enough so that the cylinders do not interfere with one another. It can also be derived for other particle shapes: spheres, ellipsoids etc.

Taking $E_s = 2 \times 10^{10}$ dynes/cm^2, and $E_b = 2 \times 10^7$ dynes/cm^2 as before, E_ℓ is calculated as 5.6×10^9 dynes/cm^2 from Equation 20, and E_t as 3.5×10^7 dynes/cm^2 from Equation 21. Experimentally it was found that $E_\ell = 1.1 \times 10^9$ dynes/cm^2 (1,100 kgf/cm^2) for unannealed Kraton 1101 and $E_\ell = 1.4 \times 10^9$ dynes/cm^2 (1,400 kgf/cm^2) for annealed Kraton 1101,and

$E_t = 1.2 \times 10^8$ dynes/cm^2 (120 kgf/cm^2). Comparing the theoretical predictions and the experimental results it appears that the PS cylinders should not be infinitely long, and that there should be a few PS connections in the transverse directions.

To get an estimate of the length of the PS cylinders the cubic model is again useful. This time it is assumed that there are no interconnections in any direction (W = 0), and the length of the parallelepipeds is longer in the sheared direction. The dimensions in the other two directions are made equal. X = C/A = C/B is the aspect ratio of the cylinders. Figure 39 shows the moduli calculated from Equations 17, 18 and 19 for X = 100 and 1000 for the longitudinal and transverse directions. Also shown are the moduli predicted by the parallel law in the longitudinal direction, and by the series law in the transverse direction. The series law is not expected to give as good a prediction as Equation 21.

From Figure 39 it appears that an aspect ratio of about 100 could be used to predict the E_c/E_m of 55 to 70 observed experimentally in the longitudinal direction. The cubic model without interconnections predicts $E_c/E_m = 1.8$ in the transverse direction, about the same as predicted by Equation 21. The experimental value is 6, which seems to indicate as we have seen that some connections between PS domains should be present in the transverse direction.

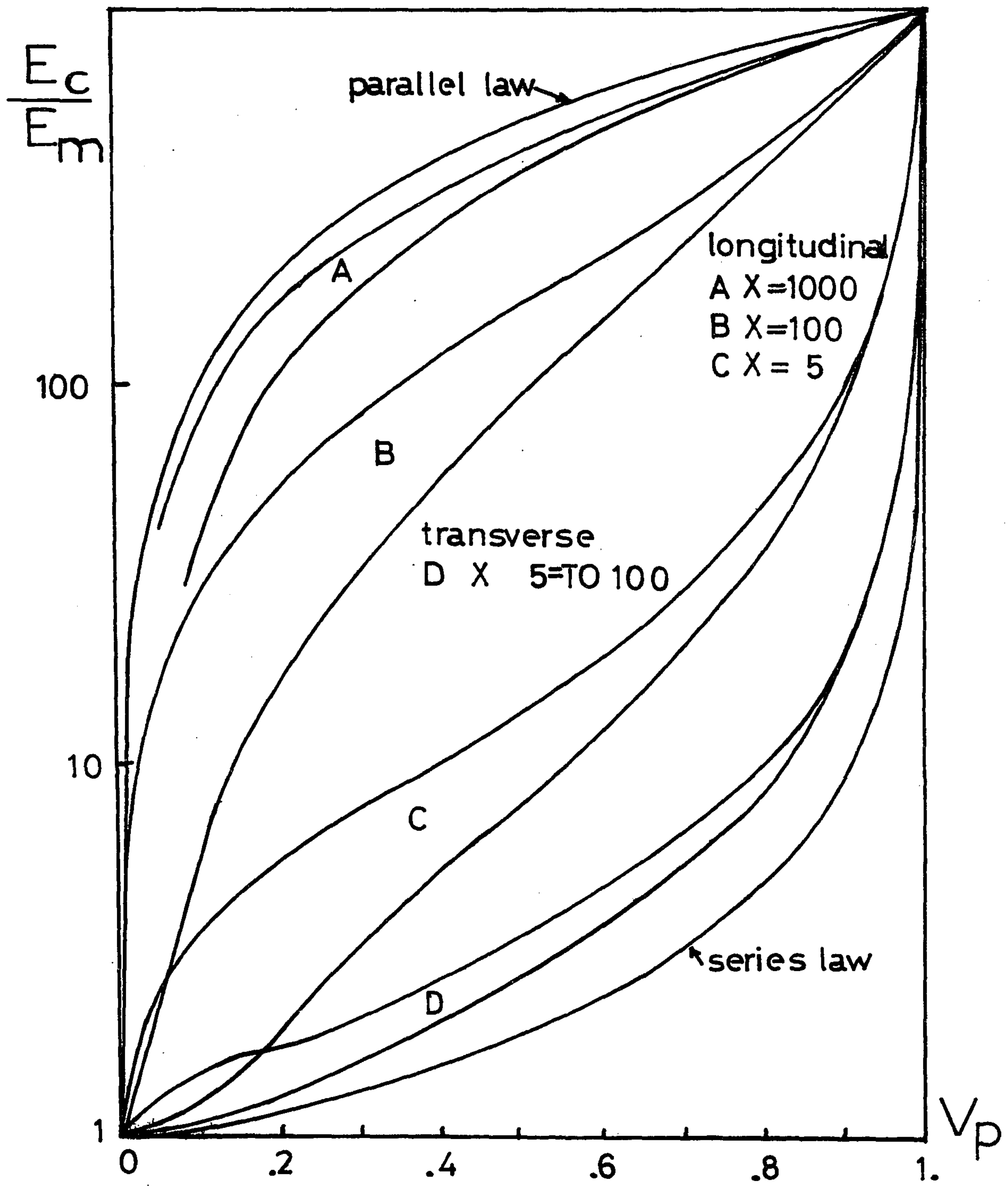

FIGURE 39

PREDICTED MODULI OF SHEARED SAMPLES

The electron micrographs in this study seem to indicate an aspect ratio lower than 100, but this is not easy to assess. Using the same technique Dlugosz et al (24) find aspect ratios from 60 to 1000 in sheared samples of an S-B-S block copolymer with 25% by volume PS. From Figure 39 it appears that an aspect ratio of 1000 corresponds mechanically to almost infinitely long rods. This is what Dlugosz et al observed as discussed previously.

3. Stress-Strain Behaviour of Sheared Kraton 1101

A yield point occurs at about 25 kgf/cm^2 when longitudinal samples are tested. At this point PS connections between cylinders are probably breaking allowing the structure to deform more. No such yield point was found in the transverse direction, but fewer connections may be present here. Once the yield point was passed, stress levels were greater in the longitudinal direction that in the transverse direction. The PS cylinders must be supporting most of the load in the longitudinal direction. In multiple extensions samples corresponding to both directions were softer on the second extension because of broken connections between domains. This softening effect was greatest in the longitudinal direction because of the greater number of connections broken. From the multiple stress-strain curves, see Figure 19, the percent energy loss to an extension ratio of 2.7 between the first and second extensions is about 40% for the longitudinal direction and 23% for the transverse direction. If connections are broken they seem to be easily reformed by annealing the sample in boiling water. A long enough period of heating will restore the original mechanical behaviour completely.

A few tensile strength measurements were made in this study. To obtain accurate values for this property would require many tests, but due to the method of obtaining samples only a few tests could be performed in this work. It was found however, that shearing reduces the tensile strength in the sheared direction. Other workers (20) have found a nominal tensile strength of 250 kgf/cm^2 and an extension ratio at break of 10 for molded Kraton 1101. Shearing reduced these to 50 to 60 kgf/cm^2 and 5 to 6 respectively. There was some variability in the reduction of the ultimate properties, some samples did not show the effect as strongly. The variability might have been due to subtle changes in the semi-continuous structure of the PS. As discussed previously in the text the gross deformation of the PS phase is responsible for the fracture of Kraton 1101. The sheared sheets already have their domains deformed in the flow direction, so it is reasonable that fracture should occur earlier in this case. By the same reasoning one would expect ultimate properties to be greater in the transverse direction. This remains to be shown.

4. Effect of Reshearing Kraton 1101 in the Plastometer

It was found that reshearing sheets in the plastometer in a direction normal to the previous direction of shearing could make the mechanical behaviour almost identical in the longitudinal and transverse directions. Stress values were higher than for molded samples, however, indicating a different domain structure. It could be more lamellar in nature, but this remains to be confirmed. The X-rays scattered confirmed only that the structure was isotropic in a plane around the normal direction.

When Kraton 1101 was resheared in the plastometer in the same direction as previously sheared,a relatively brittle material was formed. It broke at an extension ratio of about 2. It was first thought that the PS cylinders might be almost infinitely long in this case, but the Young's modulus in the longitudinal direction showed this not to be the case. It was the same order of magnitude as for other sheared sheets prepared in this work. One possible explanation is that the PS domains had become fairly oriented and therefore less deformable.

5. Suggestions for Future Work

1. It would be very interesting to study the effect of shearing on Kraton 1101 at low rates, where the network is disrupted to aggregates of PS with free segments. For this a different type of apparatus would have to be constructed.
2. More work should be done using the plastometer, reshearing in both a normal direction to and in the same direction as a previous shearing. This would further investigate the unusual behaviour found in such resheared sheets.
3. An X-ray study in biaxial and simple tension would tell more about the behaviour of PS domains under deformation.
4. It would be interesting to do the same studies as in this work using S-B-S block copolymers of different volume fractions PS. The cubic model for the initial modulus could then be investigated for a wider range of volume fractions.
5. Electron micrographs could be obtained on more samples sheared in the work.

VI. CONCLUSIONS

1. It was found that shearing in the melt with a stress close to the value where the flow becomes similar to a thermoplastic and subsequent quenching change the morphology of Kraton 1101 from PS spheres about 250 A in diameter in a matrix of PB to long cylinders of PS about 180 A in diameter.
2. Annealing did not destroy the new domain structure formed by the shearing, but only improved the purity of the domains.
3. Annealing temperature or rate of quenching was found not to affect to any extent the initial modulus and stress-strain properties of molded Kraton 1101.
4. It was shown that shearing creates a marked anisotropy, stiffness and stress-level being much higher in the longitudinal than in the transverse direction. It was also found that shearing can significantly reduce the tensile strength and ultimate elongation in the shearing direction, but not in the transverse direction. During the course of the work a dumbell sample was designed which made it possible to obtain the initial modulus and the stress-strain curve to high elongations with a single test.

5. The plastometer proved to be a useful tool for obtaining the flow properties of Kraton 1101. During the work it was found that once sheared, Kraton 1101 is harder to shear in the same direction again, and easier to shear in a direction normal to that previous shearing.
6. A good method was found for preparing samples from sheared sheets for examination under the electron microscope. The method was found not to destroy the domains structure of interest, and is quite easy to use. The method used for interpreting the X-ray scattering photographs proved quite good, and gave dimensions for the PS cylinders in good agreement with those found by electron microscopy.
7. The model developed to describe the initial modulus of compression molded and sheared Kraton 1101 provided a good insight into interconnections in molded samples, and the aspect ratio of the PS cylinders in sheared samples.
8. A reasonable thermodynamic reason for the formation of cylindrical rather than spherical PS domains from sheared Kraton 1101 was given.

NOMENCLATURE

A	Avogadro's number
a_T	shift factor
d	interdomain distance
d_i/d_1	characteristic ratio, ratio of the interdomain distance corresponding to peak i to the interdomain distance corresponding to peak 1
E_B	modulus of PB
E_S	modulus of PS
E_ℓ	longitudinal modulus
E_t	transverse modulus
ΔE	energy of activation
F/A_o	nominal stress
f_b	nominal stress at break
k	Boltzmann constant
K	constant in relation $(r_o^2)^{1/2} = KM_{PS}^{\frac{1}{2}}$
M_{PS}, M_{PB}	molecular weight
R_s	domain radius
R	gas constant
V_s	volume fraction of PS

α	chain expansion parameter
γ	interfacial energy
ρ	density
η	viscosity
λ	extension ratio, wavelength
2θ	scattering angle
$\dot{\gamma}_W$	shear rate at wall
τ_W	shear stress at wall

BIBLIOGRAPHY

1. L.R.G. Treloar, "The Physics of Rubber Elasticity", Oxford, New York (1958).
2. R. Zelinksi and C.W. Childers, Rubber Chem. Technol., 41, 161 (1968).
3. L. Bohn, Rubber Chem. Tech., 41, 495 (1968).
4. G. Kraus, C.W. Childers and J.T. Gruver, J. Appl. Polym. Sci., 11, 1581 (1967).
5. M. Morton, J.E. McGrath and P.C. Juliano, J. Polym. Sci., C, 26, 99 (1969).
6. J.F. Beecher, L. Marker, R.D. Bradford, S.L. Aggarwal, J. Polym. Sci., C, 26, 117 (1969).
7. J.M. Charrier and R.J.P. Ranchoux, Polym. Eng. Sci., 11, 381 (1971).
8. T. Miyamoto, K. Kodama and K. Shibayama, J. Polym. Sci., A-2, 8, 2095 (1970).
9. D.S. Brown, K.U. Fulcher, and R.E. Wetton, J. Polym. Sci., B, 8, 659 (1970).
10. D. McIntyre and E. Campos-Lopez, Macromolecules, 3, 322 (1970).
11. E. Fischer, J. Macromol. Sci.-Chem., A2(6), 1285 (1968).
12. R.F. Fedors, J. Polym. Sci., C, 26, 189 (1969).
13. P.J. Flory, "Principles of Polymer Chemistry", Cornell Univ. Press, New York, 1953, ch. 13.
14. D.J. Meier, J. Polym. Sci. C, 26, 81 (1969).

15. U. Bianchi, E. Pedemonte and A. Tunturro, Polymer Lond., 11, 268 (1970).

16. D.M. Brunwin, E. Fischer and J.F. Henderson, J. Polym. Sci. C, 26, 135 (1969).

17. T.L. Smith and R.A. Dickie, J. Polym. Sci. C, 26, 163 (1969).

18. M. Shen and D.H. Kaelble, Polymer Letters, 8, 149 (1970).

19. K.R. Arnold and D.J. Meier, J. Appl. Polym. Sci., 14, 427 (1970).

20. G. Holden, E.T. Bishop and N.R. Legge, J. Polym. Sci. C, 26, 37 (1969).

21. P.F. Erdhart, J.J. O'Malley and R.G. Crystal, "Block Copolymers", S.L. Aggarwal (ed.), Plenum Press, New York, London (1970).

22. G.A. Harpell and C.E. Wilkes, "Block Copolymers", S.L. Aggarwal (ed.), Plenum Press, New York, London (1970).

23. A. Keller, E. Pedemonte and F.M. Willmouth, Kolloid-Z, 238, 1-2, 385 (1970).

24. D. Dlugosz, A. Keller and E. Pedemonte, Kolloid-Z, 242, 1125 (1970).

25. M.J. Folkes and A. Keller, Polymer Lond., 12, 222 (1971).

26. M. Takayanagi, Mem. Fac. Eng. Kyushu Univ., 23, 50 (1963).

27. M. Outa, J. of Materials, 4, 437 (1968).

28. H. Keissig, Kolloid-Z, 152, 62 (1957).

29. K. Kato, Polym. Eng. Sci., 39, (1967).

30. E.B. Bradford and J.W. Vanderhoff, J. Polym. Sci. C, 3, 41 (1963).

31. J.A. Koutsky, N.V. Hein and S.L. Cooper, J. of Polym. Sci. B, 8, 353 (1970).

32. S. Middleman, "The Flow of High Polymers", Interscience (1968).

33. A. Guinier, "X-Ray Diffraction", W.H. Freeman and Company, San Francisco and London (1963).

34. P.R. Lewis and C. Price, Polymer Lond., 12, 258 (1971).

35. J.A. Reynolds and J.M. Hough, Proc. Phys. Soc., 70 769 (1957).

36. J.A. McKelvey, "Polymer Processing", John Wiley and Sons Inc., New York, (1962).

37. J.M. Charrier, A.G. Dickson and L. Mok, to be published.

APPENDIX A

Theory for the Parallel Plate Plastometer

The theory developed here assumes that Kraton 1101 behaves as a power law fluid. As we have seen (19), if the stress is above about 4.5×10^5 dynes/cm^2 this is the case. In the derivation it is assumed that the distance between the top and bottom plates of the plastometer is much less than the length and width, and that the top plate moves down with a very small velocity. A sketch of the co-ordinates used is given in Figure A1. The symbols used are defined in a listing at the end of the Appendices.

The volumetric flowrate of a power law fluid between parallel plates is given by (36):

$$Q = -\frac{n\ WH^2}{2(2n+1)} \left\{\frac{H}{2\eta_o} \frac{dP}{dy}\right\}^{\frac{1}{n}} \qquad \ldots\ldots\ldots\ldots\ldots A1$$

The volumetric flow rate in the plastometer may also be calculated from the velocity of the top plate.

$$Q = -L'\ W \frac{dH}{dt} \qquad \ldots\ldots\ldots\ldots\ldots A2$$

Comparing equations A1 and A2 and using the boundary condition that pressure is zero when y = L', the pressure may be solved for:

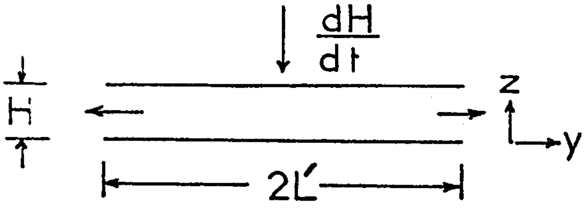

FIGURE A1 - COORDINATES FOR THE PLASTOMETER

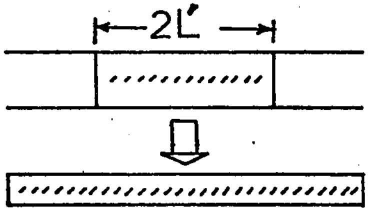

FIGURE A2 - PLASTOMETER USED AT CONSTANT VOLUME

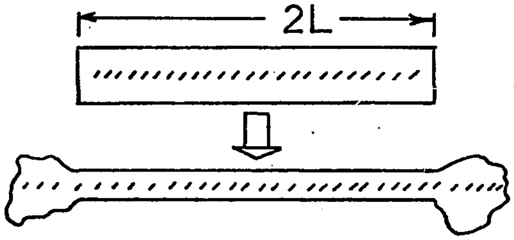

FIGURE A3 - PLASTOMETER USED AT CONSTANT LENGTH

$$P = \left\{\frac{2}{H^2}\,\frac{dH}{dt}\,\frac{2n+1}{n}\right\}^n \frac{2\eta_o}{H}\,(L'y - L'^{\,n+1}) \qquad .....A3$$

There are two ways to use the apparatus, at constant length and at constant volume. They are illustrated in Figures A2 and A3.

1. Constant Length

In this case L' = L the length of the top plate of the plastometer. The total force on the upper plate is calculated by integrating the following expression, substituting equation A3 for the pressure.

$$F = 2W \int_o^L P dz = -\,\frac{2\ \eta_o W L^2}{H} \left\{\frac{2L}{H^2}\,\frac{dH}{dt}\,\frac{(2n+1)}{n}\right\}^n \qquad ....A4$$

If n = 1, the viscosity is Newtonian and the formula simplifies to:

$$F = \frac{12\ \eta_N\ W L^3}{H^3}\ \frac{dH}{dt} \qquad ....A5$$

Here η_o has been replaced by η_N to indicate the viscosity is Newtonian.

2. Constant Volume

In this case L' can be calculated from the volume of the sample, $L' = V_o/(2WH)$. In this case, the total force on the upper plate is calculated, to be:

$$F = 2W \int_{o}^{L'} P\,dz = - \frac{\eta_o V_o^2}{2\ WH^3} \left\{ \frac{V_o}{WH^3} \frac{dH}{dt} \frac{(2n+1)}{n} \right\}^n \quad .....A6$$

The shear stress and shear rate at the top and bottom plates can be shown to be given by the following expressions:

$$\tau_W = \frac{dP}{dy} \frac{H}{2} = \left\{ \frac{2}{H^2} \frac{dH}{dt} \frac{2n+1}{n} \right\}^n \eta_o\ y^n \quad .....A7$$

$$\dot{\gamma}_W = \frac{(2n+1)}{n} \frac{2Q}{WH^2} = \left\{ \frac{2}{H^2} \frac{dH}{dt} \frac{2n+1}{n} \right\} y \quad .....A8$$

In the above calculations it is assumed that $\dot{\gamma}_o$ in the power law expression is equal to 1 sec^{-1}.

APPENDIX B

Initial Young's Modulus of a Dumbell Sample

a) Strain of a Triangular Shaped Section

The triangular shaped section and co-ordinates are shown in Figure B1. The symbols used are defined in a listing at the end of the Appendices.

Hookes's law valid for small deformations of a material is:

$$F/A = E\varepsilon \qquad \text{...............B1}$$

For the triangular section $A = t_o\ (W_o + 2x \tan \alpha)$, the strain at any length x is given by:

$$\varepsilon_x = F/(Et_oW_o(1 + \frac{2x \tan \alpha}{W_o})) \qquad \text{..........B2}$$

However, for a small element dx in the triangular section:

$$\varepsilon_x = \frac{dl - dx}{dx} = \frac{dl}{dx} - 1 \qquad \text{..........B3}$$

By equating equations B2 and B3 and integrating from x = 0 to $x = l_o$, the total strain of the triangular section can be shown to be

$$\varepsilon_T = \frac{l - l_o}{l_o} = \frac{F}{Et_oW_ol_o} \frac{\ell n(1 + 2l_o \tan\alpha/W_o)}{2 \tan \alpha/W_o} \qquad \text{.....B4}$$

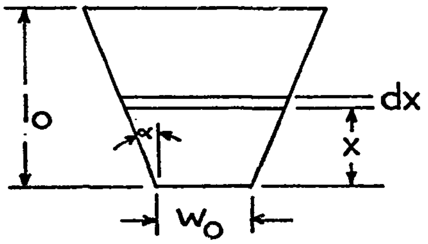

FIGURE B1 - STRAIN OF A TRIANGULAR SECTION

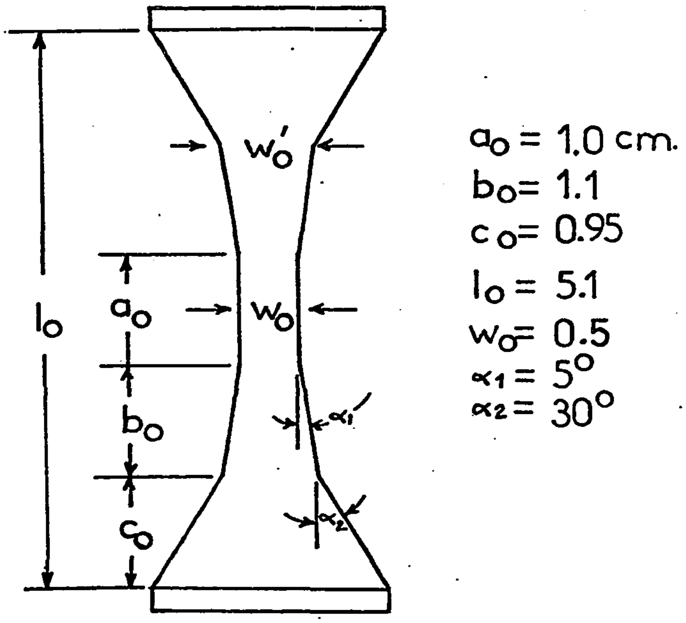

FIGURE B2 - DUMBELL SAMPLE

b) Modulus of the Dumbell Samples Used in this Work

Figure B2 shows a sketch with the dimensions of the dumbell sample used in this work. By computing the strain of each section of the sample using equation B4 the Young's modulus E of the material was calculated as:

$$E = \frac{F}{A_o \varepsilon_T} \left\{ \frac{a_o}{l_o} + \frac{\ell n\,(1 + 2\,b_o \tan \alpha_1/W_o)}{l_o \tan \alpha_1/W_o} \right.$$

$$\left. + \frac{(W_o/W_o'\ \ell n(1 + 2\,c_o \tan \alpha_2/W_o'))}{l_o \tan \alpha_2/W_o'} \right\} \qquad ..B5$$

or $E = E^* \beta$

But $F/A_o\varepsilon_T = E^*$ is the apparent Young's modulus assuming the sample was of uniform cross section A_o. This can be calculated from the initial slope of the Instron chart in an experiment. The factor β depends on the geometry of the sample. For the dimensions given in Figure B2, β is equal to 0.7, and

$$E = 0.7\ E^* \qquad ....B6$$

APPENDIX C

Model to Calculate the Initial Young's Modulus of Compression Molded and Sheared Kraton 1101

The model assumes that the domains of Kraton 1101 are arranged as a cubic arrangement of parallel epipeds with the distance between domains the same in all directions. The possibility exists for interconnections between the domains. See Figure C1. The parallel and series laws can describe the Young's modulus of a two phase material considered in parallel and series. (See for example (26)).

Series law $1/E_c = (1-v_p)/E_m + V_p/E_p$ C1

Parallel law $E_c = (1-v_p)E_m + V_pE_p$ C2

Symbols are defined in a listing after the Appendices. These laws can be applied to the model shown in Figure C1, and this can be done in two different ways. One way is to consider columns of material, and the other way is to consider rows of material. The two answers are different and are equivalent to assuming (if a heat flow analogue is used) to vertical flux lines in one case, and horizontal isothermal lines in the other case. The calculations are best shown in Figures C2 for rows and C3 for columns. The formulas are written on the figure in terms of actual distances used, but are written in the text in terms of the ratios, K_i, K_i' defined in the nomenclature.

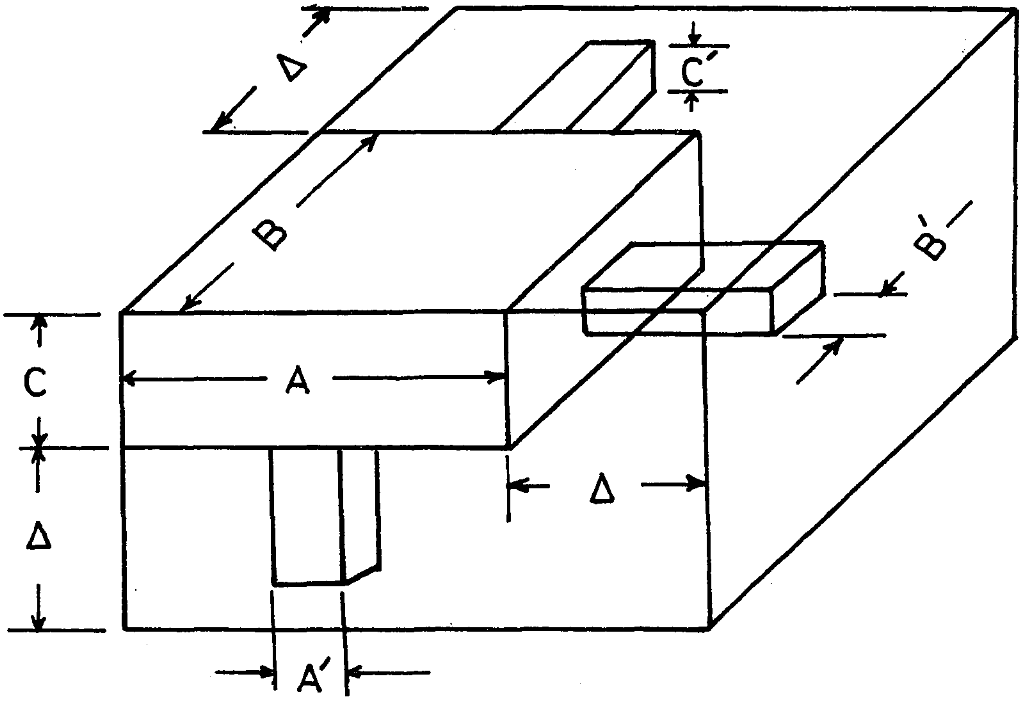

FIGURE C1 - MODEL TO PREDICT MODULUS

APPLY PARALLEL LAW

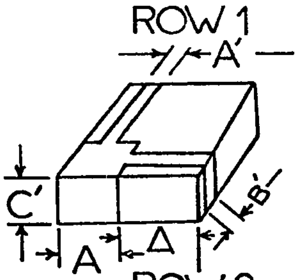

$$E_1 = \frac{AB + A'\Delta + B'\Delta}{(A+\Delta)(B+\Delta)} E_p + \left(1 - \frac{AB + A'\Delta + B'\Delta}{(A+\Delta)(B+\Delta)}\right) E_m$$

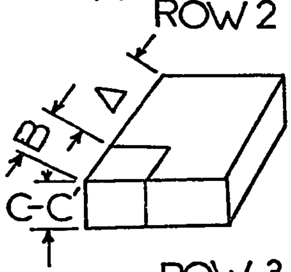

$$E_2 = \frac{AB}{(A+\Delta)(B+\Delta)} E_p + \left(1 - \frac{AB}{(A+\Delta)(B+\Delta)}\right) E_m$$

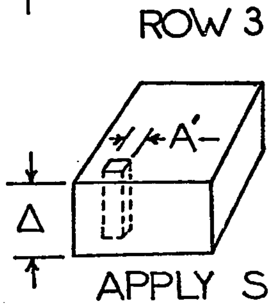

$$E_3 = \frac{A'B'}{(A+\Delta)(B+\Delta)} E_p + \left(1 - \frac{A'B'}{(A+\Delta)(B+\Delta)}\right) E_m$$

APPLY SERIES LAW TO THE ROWS

$$\frac{1}{E_c} = \frac{C'}{C+\Delta}\frac{1}{E_1} + \frac{C-C'}{C+\Delta}\frac{1}{E_2} + \frac{1-C}{C+\Delta}\frac{1}{E_3}$$

FIGURE C2- MODULUS OF THE MODEL USING ROWS

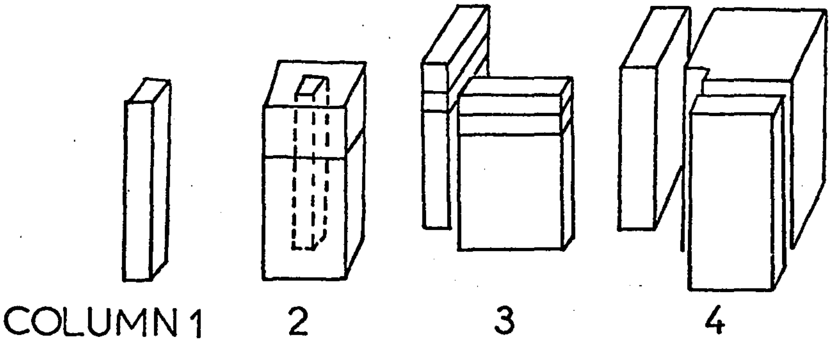

APPLY SERIES LAW

$$E_1 = E_p \quad , \quad E_4 = E_m$$

$$\frac{1}{E_2} = \frac{C}{C+\Delta}\,\frac{1}{E_p} + \left(1 - \frac{C}{C+\Delta}\right)\frac{1}{E_m}$$

$$\frac{1}{E_3} = \frac{C'}{C+\Delta}\,\frac{1}{E_p} + \left(1 - \frac{C'}{C+\Delta}\right)\frac{1}{E_m}$$

APPLY PARALLEL LAW TO THE COLUMNS

$$E_c = \frac{A'B'}{(A+\Delta)(B+\Delta)}E_1 + \frac{AB - A'B'}{(A+\Delta)(B+\Delta)}E_2 + \frac{A\Delta + B\Delta}{(A+\Delta)(B+\Delta)}E_3 + \left(1 - \frac{AB + A\Delta + B\Delta}{(A+\Delta)(B+\Delta)}\right)E_4$$

FIGURE C3-MODULUS OF THE MODEL USING COLUMNS

APPENDIX D

Prediction of Favoured Type of Polystyrene Domain In Kraton 1101

Bianchi et al (15) derive the free energy change occurring when ν copolymer chains are changed from a state of complete mixing to a state in which the 2ν PS ends are grouped into n domains. The entropy change for this transformation to a domain system is given by the following equation, independent of domain shape.

$$\Delta S = -R\,\ell n(i) \qquad \text{...............D1}$$

R is the gas constant and i is the number of PS ends per island. Taking as a reference one mole of PS chain ends, i = NA/n, where NA is Avogadro's number.

The energy change occurring is given by the change in surface area times the interfacial energy, γ. Bianchi et al assumed the PS ends were initially coiled into spheres, and then aggregated to form spherical domains. It then can be shown that the energy change, ΔE, occurring per mole of PS chains is

$$\Delta E = B((i)^{-1/3} - 1) \qquad \text{...............D2}$$

where $B = (4\pi)^{1/3}\,(3V_s)^{2/3}\,(NA)^{1/3}\,\gamma$, and V_s is the molar volume of PS.

Then the free energy change, ΔF, per mole is

$$\Delta F = B((i)^{-1/3} - 1) + RT\,\ell n(i)$$

where T is the absolute temperature. By equating $d\Delta F/di$ to zero the equilibrium value of i can be found as:

$$i_{eq} = \left(\frac{B}{3RT}\right)^3 \quad \ldots\ldots\ldots\ldots\ldots\ldots\ldots D3$$

R_s the equilibrium value of the polystyrene spheres is given by:

$$R_s = \left\{\frac{3V_s}{4\pi} \quad \frac{i}{NA}\right\}^{1/3} = \frac{V_s \gamma}{RT} \quad \ldots\ldots\ldots\ldots D4$$

This same type of derivation can be done assuming the shape of the domains of aggregation to be infinite cylinders. The initial shape of the PS ends can be choosen as either coiled into spheres or stretched out to their fully extended length. The latter case is likely to apply after shearing. The formulas have been derived for both these cases using the method described above. Calculations are done per unit length. Table D1 shows the derivation of the formulas.

TABLE D1

DERIVATION OF FORMULAS TO PREDICT FREE ENERGY CHANGE UPON FORMING CYLINDRICAL DOMAINS IN KRATON 1101

Initial state - spherical coils of PS ends	Initial state - fully extended PS ends
$\Delta S = -R \ln(i)$ $S_o = (3V_s)^{2/3} (4\pi)^{1/3} NA^{1/3}$ $S_f/\text{unit length} = (4\pi)^{1/2}(V_s)^{1/2}(\frac{NA}{i})^{1/2}$ $\Delta E = (S_f - S_o)\ \gamma$	$\Delta S = -R \ln(i)$ $S_o/\text{unit length} = (4\pi)^{1/2}(V_s)^{1/2}(NA)^{1/2}$ $S_f/\text{unit length} = (4\pi)^{1/2}(V_s)^{1/2}(\frac{NA}{i})^{1/2}$ $\Delta E = (S_f - S_o)\ \gamma$
$B = (3V_s)^{2/3}(4\pi)^{1/3}(NA)^{1/3}\ \gamma$	$B' = (4\pi)^{1/2}(V_s)^{1/2}(NA)^{1/2}\ \gamma$
$\Delta E = \frac{B'}{(i)^{1/2}} - B$ $\Delta F = \Delta E - T\Delta S$ $\Delta F = (\frac{B'}{(i)^{1/2}} - B) + RT \ln(i)$ $i_{equi} = (\frac{B'}{2RT})^2$ $R_c = \frac{\gamma V_s}{RT}$	$\Delta E = B'(\frac{1}{(i)^{1/2}} - 1)$ $\Delta F = \Delta E - T\Delta S$ $\Delta F = B'\ (\frac{1}{(i)^{1/2}} - 1) + RT \ln(i)$ $i_{equil} = (\frac{B'}{2RT})^2$ $R_c = \frac{\gamma V_s}{RT}$

Shown below are the equilibrium domain sizes, and free energy changes at 200°C and 100°C for the 3 cases discussed above. γ is choosen as 3 ergs/cm^2 as calculated by Bianchi et al, and the molar volume of the PS ends, V_s, is taken as 10^4 cm^3/gmole assuming a density of 1 gm/cm^3.

TABLE D2

Predicted Free Energy Changes on Formation of Spherical and Cylindrical Polystyrene Domains in Kraton 1101

	Radius Å	ΔF ergs/mole	
		initial state coiled PS ends	initial state fully extended PS ends
Spherical Domains			
T = 200°C	100	$- 2.5 \times 10^{11}$	---
T = 100°C	75	$- 2.9 \times 10^{11}$	
Cylindrical Domains			
T = 200°C	100	$+ 3.0 \times 10^{11}$	$- 1.4 \times 10^5$
T = 100°C	75	$+ 0.7 \times 10^{11}$	$- 1.4 \times 10^5$

These calculations show that unoriented PS ends would form spherical domains, while extended PS ends would form cylindrical domains. This would be an explanation for the fact that cylindrical domains are formed in sheared Kraton 1101. Annealing would allow the PS to return to a random arrangement within the domains. It was found experimentally that such annealing does not change the shape of the domains.

The calculated domain radius turns out to be the same for cylinders and spheres, but both are in reasonable agreement with experimental values.

The calculations performed above are not absolute, there are many assumptions involved (see Bianchi et al's original paper). However, they are useful as they provide predictions of the domain type formed in Kraton 1101, which agree with experimental findings.

APPENDIX A - NOMENCLATURE

F	total force on the upper plate of the plastometer
dH/dt	downward velocity of the top plate
H	gap thickness
L'	one half the length of the plastometer flow channel full of material
L	one half the length of the plastometer top plate
n	index of the power law
P	pressure
Q	volumetric flow rate
W	width of the plastometer flow channel
η_N	Newtonian viscosity
η_o	viscosity at the reference shear rate in the power law which is taken as 1 $\sec^{-1}$ in these calculations
τ_W	shear stress at the flow surfaces
$\dot{\gamma}_W$	shear rate at the flow surfaces

APPENDIX B - NOMENCLATURE

A	cross-sectional area
A_o	cross-sectional area of the uniform section of the dumbell sample
E	Young's modulus of the material
E^*	apparent Young's modulus determined from the Instron chart
ϵ	strain
ℓ_o	length of triangular section before strain
ℓ	length of triangular section after strain

α	angle of the triangular section
α_1, α_2	two angles in the dumbell sample
a_o	length of the uniform region of the dumbell sample
b_o, c_o	length of triangular sections of the dumbell sample
t_o	thickness of the sample
W_o'	width of the dumbell sample at the start of the triangular section
W_o	width of the dumbell sample in the uniform region
l_o	initial length of the dumbell sample

APPENDIX C - NOMENCLATURE

A, B, C	dimensions of the PS domain
A', B', C'	dimensions of the connections
E_p	modulus of dispersed phase
E_m	modulus of matrix phase
E_c	modulus of composite material
K_a,K_b,K_c	ratio of domain dimension to domain dimension plus spacing between domains
K_a',K_b',K_c'	ratio of interconnection to domain dimension
Δ	the distance between the boundaries of the domains

APPENDIX D - NOMENCLATURE

ΔE	change in internal energy on domain formation
ΔF	change in free energy on domain formation
i	number of PS ends per domain
NA	Avagadro's number
n	number of domains
R	gas constant
R_c	radius of cylindrical domains
R_s	radius of the spherical domains
S_o	initial surface area of PS ends
S_f	final surface area of domains
ΔS	entropy change on domain formation
T	absolute temperature
V_s	molar volume of polystyrene
Y	interfacial energy
ν	number of copolymer chains